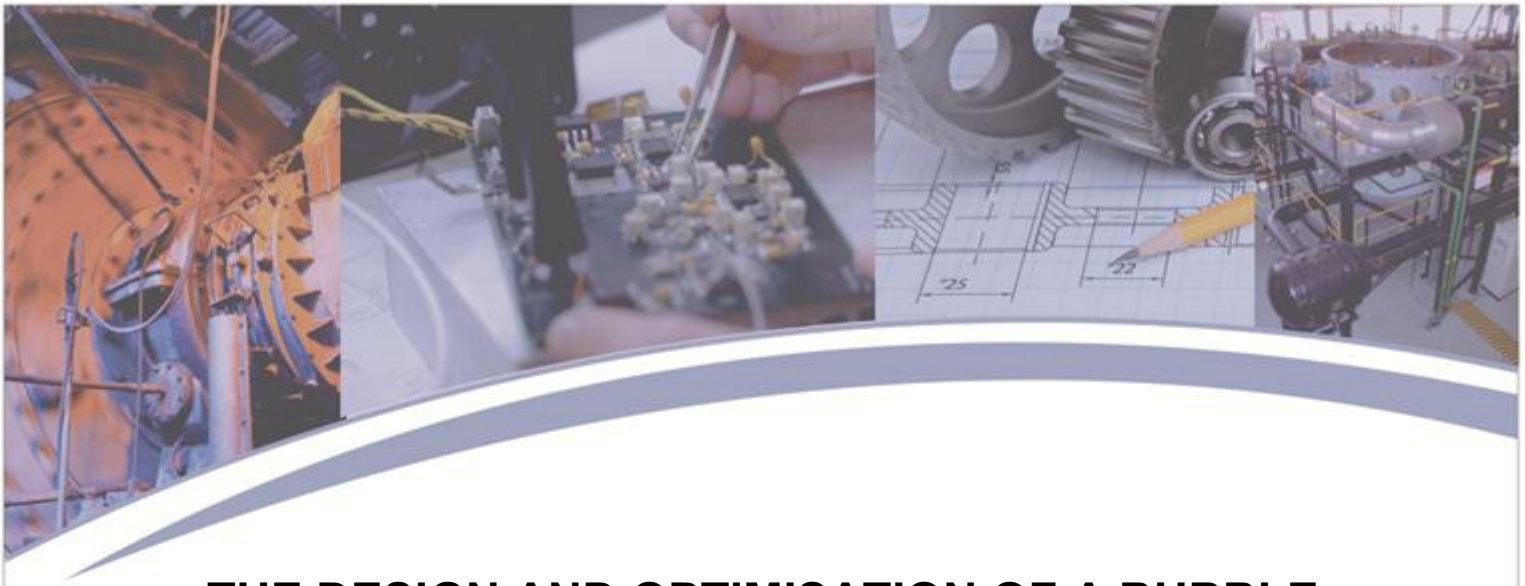

THE DESIGN AND OPTIMISATION OF A BUBBLE PUMP FOR AN AQUA-AMMONIA DIFFUSION ABSORPTION HEAT PUMP

Stefan van der Walt

Dissertation submitted in fulfilment of the requirements for the degree

Master of Engineering

North-West University Potchefstroom Campus

Student number: 20399782

Supervisor: Prof. C.P. Storm

Potchefstroom

November 2012

It all starts here

NORTH-WEST UNIVERSITY
YUNIBESITI YA BOKONE-BOPHIRIMA
NOORDWES-UNIVERSITEIT
POTCHEFSTROOM CAMPUS

Abstract

Energy shortages around the world necessitated research into alternative energy sources especially for domestic applications to reduce the load on conventional energy sources. This resulted in research done on the possibility of integrating solar energy with an aqua-ammonia diffusion absorption cycle specifically for domestic applications.

The bubble pump can be seen as the heart of the diffusion absorption cycle, since it is responsible, in the absence of a mechanical pump, to circulate the fluid and to desorb the refrigerant (ammonia) from the mixture. It is thus of paramount importance to ensure that the bubble pump is designed efficiently.

Various bubble pump simulation models have been developed over the years, but it was found that none of the existing models served as a good basis for application-specific design. Most of the models constrained too many parameters from the outset which made the investigation of the effects of certain parameters on the bubble pump's performance impossible. According to the research, no bubble pump model investigated the effect of such a wide variety of factors including tube diameter, heat flux, mass flux, generator heat input and system pressure on the bubble pump's lift height.

A simulation model for a bubble pump for integration with a solar-driven aqua-ammonia diffusion absorption cycle was developed. It serves as a versatile design model to optimise the bubble pump for a large variety of conditions as well as changes in parameters. It was achieved by constraining the bubble pump dimensions and parameters as little as possible. A unique feature of this model was the fact that the bubble pump tube was divided into segments of known quality which made the length of the pipe completely dependent on the flow inside the pipe. It also made the demarcation of the flow development inside the tube easier.

The model attempted to incorporate the most appropriate correlations for pressurised two-phase aqua-ammonia flow. The most appropriate void fraction correlation was found to be

the Rouhani-Axelsson (Rouhani I) correlation. It was mainly due to its exclusive use of thermophysical properties and the vapour quality.

The most appropriate heat transfer coefficient that predicted the most realistic wall temperature, was the correlation from Riviera and Best (1999) which was the only correlation found in the literature developed with aqua-ammonia in mind. It was found that the published correlation could not reproduce their experimental results, and a modification of their correlation was made after which the simulation model's results correlated well with the experimental values of Riviera and Best (1999).

The main goal of the simulation model was to determine the height that the bubble pump was capable of lifting at the slug to churn flow transition under various conditions. The effect of varying a variety of parameters on the bubble pump lift height was also investigated.

The results from Shelton & White Stewart (2002) were compared to the outputs of the simulation model, and it was found that their constraining of the submergence ratio limited their outputs, and that their heat inputs under different conditions was a bit optimistic. The simulation model's outputs correlated well at higher tube diameters with the results from Shelton & White Stewart (2002), but at the lower diameters which was used in their study it was impossible to compare data, since their diameters was already in mini flow and micro flow regions. The temperatures also correlated well, all within 2% of the results from Shelton & White Stewart (2002).

It was found that there couldn't be just one set of optimised conditions and values for the bubble pump, but that each cycle with differing specifications and operating conditions would yield a unique set of optimised parameters. It was for that reason very important not to constrain parameters beforehand without investigating its effect on the bubble pump first.

Keywords: Bubble pump, two-phase flow, aqua-ammonia, ammonia water, diffusion absorption, two-phase heat transfer

Opsomming

Wêreldwye energie tekorte het genoodsaak dat alternietewe energiebronne ondersoek word veral vir huishoudelike gebruik, om sodoende die las op konvensionele kragstasies te verlig. Dit het meegebring dat daar navorsing gedoen is op die moontlikheid van die integrasie van sonenergie op aqua-ammoniak diffusie absorpsie siklusse spesifiek vir huishoudelike gebruik.

Die borrelpomp is beskou as die hart van die diffusie absorpsie siklus, waar dit in die afwesigheid van ‘n meganiese pomp verantwoordelik was om die vloeier te sirkuleer deur die stelsel en om die ammoniak gas (wat die werksvloeier is) uit die aqua-ammoniak mengsel te kook vir gebruik in die siklus. Dit was dus van kardinale belang om die borrelpomp ontwerp so effektief moontlik te maak.

Verskeie simulasie modelle van die borrelpomp is ontwikkel, maar daar is gevind dat geen van die bestaande modelle as ‘n goeie basis kan dien vir ‘n ontwerp met sekere spesifikasies en onder verskeie werkstoestande nie. Meeste van die modelle het te veel parameters vasgemaak van die staanspoor af wat die ondersoek van die effek van die parameters op die borrelpomp se uitsette onmoontlik maak. Volgens die navorsing het geen borrelpomp model die effek van so veel faktore op die borrelpomp se pomphoogte ondersoek nie.

‘n Simulasie model van ‘n borrelpomp vir integrasie met ‘n son-aangedrewe aqua-ammoniak diffusie absorpsie siklus is opgestel. Dit dien as ‘n veelsydige ontwerpsmodel om die borrelpomp te optimiseer vir ‘n groot verkseidenheid toestande asook veranderinge in sekere parameters. Dit is bereik deur so min as moontlik beperkings te stel op die borrelpomp dimensies en parameters. ‘n Unieke eienskap van die model was dat die borrelpomp pyp in segmente van bekende kwaliteit (i.p.v. onbekende lengte) ingedeel is, wat die lengte van die pyp ten volle afhandlik gemaak het van die vloei in die pyp. Dit het ook gemaak dat die vloei-ontwikkeling in die pyp makliker afgebaken kon word.

Die model het gepoog om die mees gepasde korrelasies vir aqua-ammoniak twee-fase vloei onder druk te gebruik. Die mees gepasde korrelasie vir die volumetriese fraksie van die gas

(*void fraction*), is gevind om die Rouhani-Axelsson (Rouhani I) korrelasie te wees. Dit was hoofsaaklik weens sy gebruik van slegs termofisiese eienskappe asook kwalieit.

Die hitte-oordrag koëffisiënt wat geblyk het om die mees realistiese voorspelling van die wand temperatuur te gee, was die korrelasie van Riviera en Best (1999) wat die enigste korrelasie gevind is in die literatuur wat spesiaal ontwikkel is met die oog op aqua-ammoniak. Dit was gevind dat die oorspronklike gepubliseerde korrelasie nie die eksperimentele resultate van Riviera en Best (1999) kon reproduseer nie, en ‘n aanpassing van die korrelasie was nodig waarna die gesimuleerde waardes die eksperimentele waardes perfek weergegee het.

Die hoofdoel van die simulasie model was om die hoogte wat die borrelpomp kon pomp te bepaal by die koeëlvloei na bruisvloei oorgang (*slug to churn transition*), en dit is ondersoek onder verskeie toestande. Die effek van die verandering van verskeie parameters op die borrelpomp hoogte is ook ondersoek.

Die resultate van Shelton & White Stewart (2002) is vergelyk met die uitsette van die simulasie model, en is gevind dat die vasmaak van die onderdompelingsverhouding (*submergence ratio*) hulle uitsette beperk het, en dat die hitte-inset vir die borrelpomp ‘n bietjie optimisties was. By hoër buisdiameters het die simulasie se uitsetwaardes goed gekorreleer met Shelton & White Stewart (2002), maar die laer diameters wat in hul studie gebruik is het getoon om onbruikbaar te wees weens die feit dat dit mini- en mikrovloei betree. Die temperature het wel redelik ooreengestem, als binne 2% van die resultate van Shelton & White Stewart (2002).

Dit is gevind dat daar nie slegs een stel geoptimiseerde waardes as ‘n uitset vir die borrelpomp betsaan nie, maar dat dit eerder uniek sal wees gegee die spesifikasies van elke siklus waarvoor dit gebruik sal word. Daarom is dit belangrik om nie parameters voor die tyd vas te maak sonder om hul effek op die borrelpomp ten volle te ondersoek nie.

Acknowledgements

I would like to thank our supervisor, Professor C.P. Storm for his guidance, willingness and eagerness to help, even in the wee hours of the morning.

I would also like to thank my colleague, Marinus Potgieter, for his help in almost every aspect of this project.

And a final acknowledgement to my saviour Jesus Christ for providing me with perseverance and patience to finish this project.

Table of contents

1. INTRODUCTION AND BACKGROUND 1

1.1 Introduction 1

1.2 Background 1

1.3 Energy comparison 4

1.4 Problem statement 7

1.5 Objective 7

1.6 Issues to be addressed 7

1.7 Research methodology for the simulation model 8

2. LITERATURE SURVEY 9

2.1 Basic Cycle operation 9

2.1.1 Mechanical pump-driven absorption cycle (two-pressure cycle) 9

2.1.2 Bubble pump-driven absorption cycle (single-pressure cycle) 10

2.2 Purpose of the bubble pump 11

2.3 Basic operation of the bubble pump 12

2.4 Previous research done on the bubble pump 13

2.4.1 Research done on physical modifications of the bubble pump 13

2.4.2 Research done on the mathematical modelling of the bubble pump 16

2.4.3 Concluding remarks 17

3. TWO-PHASE FLOW THEORY 19

3.1 Two-phase flow regimes 19

3.2 Two-phase flow parameters 20

3.2.1 Void fraction 20

3.2.2 Slip 24

3.3 Two-phase pressure drop 25

3.3.1 Homogeneous two-phase flow pressure drop 25

3.3.2 Separated two-phase flow pressure drop 27

3.4 Boiling heat transfer 30

3.5 Flow regime map for a vertical pipe 31

3.6 Conclusion 32

4. MATHEMATICAL MODEL 33

4.1 Conservation equations 33

4.1.2 Conservation of mass 35

4.1.3 Conservation of momentum 35

4.1.4 Conservation of energy *37*
4.2 VOID FRACTION 37
4.3 TWO-PHASE VELOCITY AND MASS FLOW 38
4.4 TWO-PHASE HEAT TRANSFER COEFFICIENT 39
4.4.1 Gungor-Winterton correlation *40*
4.4.2 Shah correlation *40*
4.4.3 Riviera and Best correlation *42*
4.4.4 Critical wall superheat *42*
4.5 FLOW REGIME TRANSITIONS 43
4.6 PRESSURE GRADIENT ALONG THE LIFT TUBE HEIGHT 44

5. RESULTS AND DISCUSSION 47

5.1 RANGE OF PRESSURES FOR THE TEST 47
5.2 SELECTION OF VOID FRACTION CORRELATION 48
5.3 DISCUSSION AND MODIFICATION OF TWO-PHASE HEAT TRANSFER CORRELATION 51
5.4 HEAT TRANSFER COEFFICIENT CORRELATIONS 55
5.5 LENGTH OF BUBBLE PUMP 58
5.5.1 Effect of tube diameter on bubble pump length *58*
5.5.2 Effect of heat flux on bubble pump length *60*
5.5.3 Effect of mass flux on bubble pump length *62*
5.6 BUBBLE PUMP HEAT INPUT 63
5.7 SYSTEM PRESSURE INFLUENCE 65
5.8 COMPARISON OF RESULTS TO SHELTON & WHITE-STEWART (2002) 67
5.9 SUMMARY 70

6. CONCLUSIONS AND RECOMMENDATIONS 73

6.1 INTRODUCTION 73
6.2 THE MODEL IN GENERAL 73
6.3 COMPARISON WITH OTHER MODELS 74
6.4 RESULTS AND GENERAL REMARKS FROM THE SIMULATION MODEL 75
6.5 RECOMMENDATIONS FOR FURTHER STUDY 76

7. BIBLIOGRAPHY 79

8. APPENDIX A – SIMUATION MODEL 83

List of figures

Figure 1.1 Energy input comparison between a vapour compression cycle and a diffusion-absorption cycle. 2

Figure 1.2 Type I Heat pump. 4

Figure 1.3 Type II heat pump. 5

Figure 1.4 Heat pump cycle as Carnot cycle. 5

Figure 2.1 Sketch of a basic dual-pressure aqua-ammonia cycle, showing the basic components of the cycle. 10

Figure 2.2 The original von Platen and Munters patent application sketch for the diffusion absorption cycle (von Platen & Munters, 1928). 11

Figure 2.3 A simplified representation of the bubble pump with slug flow (Zohar *et al.*, 2008). 13

Figure 2.4 The original Platen and Munters patent application sketch showing the generator and absorber configuration (von Platen & Munters, 1928). 14

Figure 2.5 Current bubble pump configuration in use by the Dometic absorption refrigerators (Zohar *et al.*, 2007). 14

Figure 2.6 The improved partially attached bubble pump configuration as developed by Zohar *et al.* (2008). 15

Figure 2.7 The generator with heat exchanger as developed by Chen et al (1996). 16

Figure 3.1 The five basic flow regimes of two-phase flow. 20

Figure 3.2 Flow regime map showing void fraction as a function of the gas superficial velocity (Samaras & Margaris, 2005). 32

Figure 4.1 Generator tube segment showing arbitrary divisions of known quality. 33

Figure 4.2 Basic representation of the bubble pump setup. 35

Figure 5.1 Comparison between the Rouhani-Axelsson (Rouhani I) void fraction correlation and the Toshiba void fraction correlation for a system pressure of 8 [bar], mass flux of 20 [kg/m^{2}s] and a tube diameter of 10 [mm]. 49

Figure 5.2 Rouhani-Axelsson void fraction correlation for massfluxes ranging from 10 – 120 [kg/m^2], system pressure of 8[bar] and a tube diameter of 20[mm]. 50

Figure 5.3 Toshiba void fraction correlation for massfluxes ranging from 10 – 120 [kg/m^2], system pressure of 8[bar] and a tube diameter of 20[mm]. 50

Figure 5.4 Results from the modified equation (in red) superimposed on the experimental results from Riviera & Best (1999).....53
Figure 5.5 Comparison between the different heat transfer coefficient correlations, including the modified Riviera and Best (1999) correlation, and the critical heat flux needed for nucleation. Mass flux of 10 [kg/m^{2}s], a system pressure of 8 [bar] and a tube diameter of 10 [mm]. 54
Figure 5.6 Comparison between the different heat transfer coefficient correlations, including the modified Riviera and Best (1999) correlation, and the critical heat flux needed for nucleation. Mass flux of 50 [kg/m^{2}s], a system pressure of 8 [bar] and a tube diameter of 10 [mm]. 54
Figure 5.7 Comparison of the achieved wall superheat ($T_{wall} - T_{sat}$) against the critical wall superheat at different heat flux values, for a massflux of 10 kg/m^{2}s, a system pressure of 8 [bar] and a tube diameter of 10 [mm]. 55
Figure 5.8 Comparison of the achieved wall superheat ($T_{wall} - T_{sat}$) against the critical wall at different heat flux values, for a massflux of 50 kg/m^{2}s, a system pressure of 8 [bar] and a tube diameter of 10 [mm]. 56
Figure 5.9 Comparison of heat transfer correlations for the achieved wall temperature against the minimum required temperature to achieve nucleation for the values in Benhmidene *et al.* (2011).....57
Figure 5.10 Influence of different tube diameters on the maximum lift height of the bubble pump and the generator height for a system pressure of 8 [bar], mass flux of 20 [kg/m^{2}s] and a heat flux of 10 [kW/m^2].....59
Figure 5.11 The influence of the mass flux on lift height and on the optimum diameter, for a system pressure of 8 [bar] and a heat flux of 10 [kW/m^2]. 60
Figure 5.12 Effect of heat flux on the bubble pump length for a mass flux of 20 [kg/m^{2}s] and a system pressure of 8 [bar]. 61
Figure 5.13 Influence of heat flux on the pressure drop at the slug-churn transition, for a mass flux of 10, 20, 50 and 100 [kg/m^{2}s], tube diameter of 10 [mm] and a system pressure of 8 [bar]. 62
Figure 5.14 Heat input, generator length and total length of the bubble pump at various mass flux values at the slug-churn transition, for a tube diameter of 10 [mm], at a pressure of 8 [bar]. 63

Figure 5.15 Influence of different tube diameters on the maximum lift height of the bubble pump, the generator height and the generator heat input required for a system pressure of 8 [bar], mass flux of 20 [kg/m^{2}s] and a heat flux of 10 [kW/m^2]..64

Figure 5.16 Influence of different tube diameters on the total fluid pumped and the ammonia vapour at the outlet of the pump tube for a system pressure of 8 [bar], mass flux of 20 [kg/m^{2}s] and a heat flux of 10 [kW/m^2]. 65

Figure 5.17 System pressure influence on the bubble pump height with varying tube diameter, for a mass flux of 20 [kg/m^{2}s] and a heat flux of 20 [kW/m^2].....66

Figure 5.18 System pressure influence on the bubble pump heat input required with varying tube diameter, for a mass flux of 20 [kg/m^{2}s] and a heat flux of 20 [kW/m^2].....66

Figure 5.19 System pressure influence on the ammonia vapour produced with varying tube diameter, for a mass flux of 20 [kg/m^{2}s] and a heat flux of 20 [kW/m^2].....67

Figure 5.20 Results for the bubble pump efficiency of Shelton & White-Stewart (2002) for a ratio of 0.4, with a mixture concentration of 15.5% ammonia and a system pressure of 4 [bar]. 68

List of Tables

Table 3.1 Comparison of various drift-flux models in a wide variety of experimental data as done by Coddington & Macian (2002). 24

Table 4.1 Example of data retrieved from REFPROP, with the quality varied at a constant pressure of 1MPa 34

Table 5.1 Table illustrating the effect of system pressure on the fluid and vapour saturation temperatures 48

Table 5.2 Comparison of results obtained using the original published equation and the modified equation. Results are for a mass flux of 5 [kg/m^{2}s], a system pressure of 10 [bar] and a concentration of 40% ammonia. 52

Table 5.3 Comparison of results obtained using the original published equation and the modified equation. Results are for a mass flux of 8 [kg/m^{2}s], a system pressure of 10 [bar] and a concentration of 40% ammonia. 52

Table 5.4 Comparison of current model to Shelton & White-Stewart (2002). 69

Table 5.5 Percentage differences between the current model and the model of Shelton & White-Stewart (2002) 69

Nomenclature

A	Cross-sectional area	m^2
Bo	Boiling number	
C_0	Distribution factor used in the drift flux model	
d	Diameter	m
f	Friction factor	
F_s	Shah constant	
g	Gravitational acceleration	m/s^2
H	Height	m
h	Enthalpy	kJ/kg
h_{LG}	Latent heat of vaporisation	kJ/kg
h_{htc}	Heat transfer coefficient	kW/m^2K
j	Superficial velocity	m/s
k	Conductivity	kW/mK
L	Length	m
$\dot{M}$	Mass flux	kg/m^2s
m	Mass	kg
$\dot{m}$	Mass flow	kg/s
P	Pressure	Pa
P_k	Phase of fluid / presence of vapour	
Pr	Prandtl number	
Q_{flux}	Heat flux	kW/m^2
$\dot{Q}$	Energy input	kW
R	Resistance, heat exchanger	
Re	Reynolds number	
T	Temperature	K
V	Velocity	m/s
v	Specific volume	kg/m^3
$\dot{v}$	Volumetric flow rate	m^3/s
x	vapour quality	kg/kg

X_{tt}	Lockhard-Martinelli parameter	
z	Height of generator	m

Greek symbols

Δ	Difference	
ε	Gas void fraction	
μ	Dynamic viscosity	kg/m-s
ρ	Density	kg/m^3
σ	Surface tension	N/m

Subscripts

c	Condenser
crit	Critical
c-b	Convective boiling
c-s	Cross-sectional
e	Evaporator
H	Homogeneous
h	Driving heat input
i	Inner, internal
mix	Mixture
NH_3	Ammonia
sat	Saturation
tp	Two-phase

List of abbreviations

COP	Coefficient of performance
DAHP	Diffusion absorption heat pump

1. Introduction and Background

1.1 Introduction

As the country's population and their level of lifestyle increases, so does the demand for more electricity, which is mostly generated by non-renewable fossil fuel in South Africa (Menyah & Wolde-Rufael, 2010). This continuous pressure on the electricity grid gets worse as the population uses luxury items such as air-conditioning (Jakob *et al.*, 2008). As the country's (and the world's) non-renewable energy reserves is shrinking, other alternative energy resources need to be explored.

One of the most reliable renewable energy sources is the sun, which is also a free source of energy. Thus one of the most promising fields of development in alternative energy research is solar energy. If this energy can be coupled to a heat pump, it would become a very usable and energy-saving domestic device.

The aqua-ammonia diffusion absorption heat pump (DAHP) is such a cycle which can be used in conjunction with a low-heat energy source such as a solar-heated fluid. The DAHP doesn't have any moving parts which allows the cycle to run virtually silent, minimises maintenance costs and improves the cycle's reliability (Zohar *et al.*, 2007).

1.2 Background

The diffusion absorption cycle was invented by von Platen and Munters in 1928, and uses at least three fluids to create the saturation temperature difference between the condenser and evaporator (von Platen & Munters, 1928).

An aqua-ammonia absorption system is generally used for air-conditioning or refrigeration purposes, although it can also be used simultaneously for heating. There are two cycles that can be used namely the intermittent cycle and the continuous cycle.

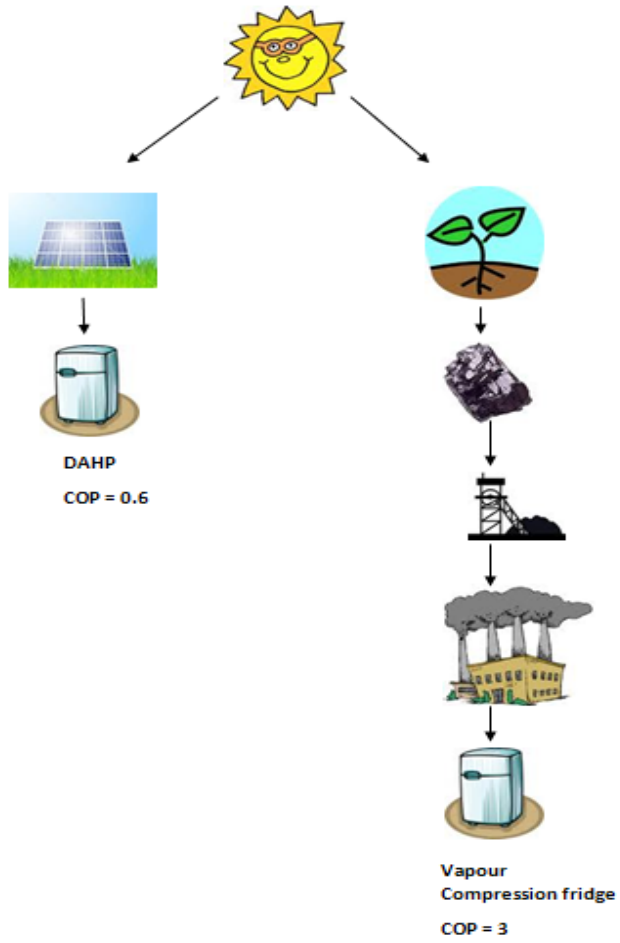

Figure 1.1 Energy input comparison between a vapour compression cycle and a diffusion-absorption cycle.

The intermittent cycle has just enough fuel or energy input to complete one cycle, which means that you design the system per cycle and not for continuous operation. This cycle is used when there is only a limited amount of fuel (usually kerosene) available. This restricts the generation of ammonia vapour to about 20 to 40 minutes.

The continuous cycle has enough fuel or energy input to complete multiple cycles so that the system runs continuously without stopping. This system is designed to run for weeks on end, or even permanently. The system has no moving parts and uses thermal siphoning to circulate the working fluid. The positioning and height of the individual components is critical to effectively circulate the fluids.

There are basically two types of continuous cycles: 1) the pump-driven absorption cycle; and 2) the diffusion absorption cycle. The difference between the two cycles is that the pump-driven absorption cycle uses a mechanical pump to circulate the refrigerant, while the diffusion absorption cycle uses a third non-reactive gas such as helium or hydrogen to lower the pressure of the refrigerant in order to circulate it without a pump (Dalton's law of partial pressures). Consequently there are no moving parts in the diffusion absorption cycle and the result is that it runs virtually silent.

Dalton's law of partial pressures states that the total pressure of a confined mixture of gases is the sum of the pressures of each of the gases in the mixtures. For example the total pressure of the air in a compressed air cylinder is the sum of the oxygen, nitrogen and carbon dioxide gases, and the water vapour pressure. This means that if the total system pressure is constant, and the partial pressure of a non-reactive gas like hydrogen is used in the evaporator, the partial pressure of the working fluid will lower accordingly and the sum of the hydrogen and working fluid gases will be the total system pressure (Herold *et al.*, 1996).

The absorption system requires five essential parts: 1) the generator or still; 2) the condenser; 3) the expansion valve; 4) the absorber and 5) the pump (or pressure-reducing part in the case of the diffusion absorption cycle). The current patent on the diffusion absorption heat pump is held on the Electrolux-Servel process from 1943 (Marks, 1944).

Since the DAHP has no moving parts and runs virtually silent, its main use is in the hotel industry, in offices and with recreation vehicles if operated with alternative energy (Jakob *et al.*, 2008). There was no DAHP that was specifically designed for the common household that was cost-effective, energy efficient, integrated with common household appliances and used solar energy together with phase changing materials (PCM's) to ensure non-reliance on the local electricity supplier found in the literature surveyed. If this could be achieved, it will result in the DAHP to be capable of operating even on remote locations like game farms and lodges.

1.3 Energy comparison

Since the cycle in question is a type of heat pump, it would be wise to define it first. According to Herold *et al.* (1996) a heat pump transfers heat from a low temperature source to a high temperature sink, which requires either heat or work as a thermodynamic input. This is supported by the Claussius statement of the second law of thermodynamics, which can be paraphrased as: "It is impossible for heat to be transported from a colder to a hotter body as the only result of the system" (Herold *et al.*, 1996).

There are two types of heat pumps, which can be designated as type I (figure 1.2) and type II (figure 1.3). The first type requires a driving heat input at the highest temperature level, which results in either refrigeration at the lowest temperature or heating at the intermediate temperature. Type II heat pumps require a driving heat input at the intermediate temperature level, which results in a heat output at the highest temperature level. Type II heat pumps require that a portion of the heat input be sacrificed at the low temperature output in order to heat the waste heat stream input at the intermediate level. The dissertation will be mainly concerned with a type I heat pump.

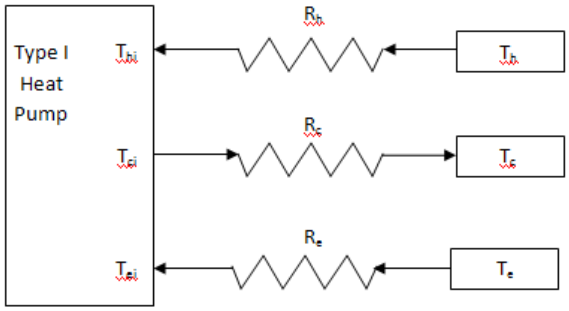

Figure 1.2 Type I Heat pump.

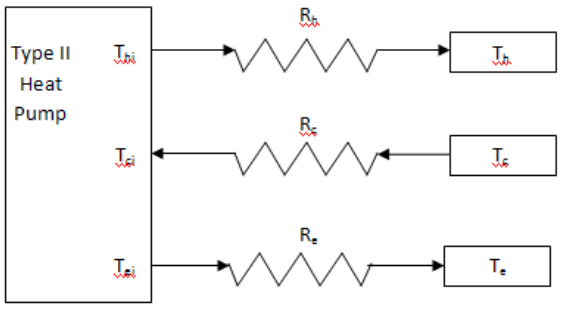

Figure 1.3 Type II heat pump.

The highest temperature is at the top of figure 1.2 and figure 1.3 while the lowest temperature is at the bottom thereof. The temperatures indicated as T_h, T_c and T_e represent the thermal boundary conditions that the absorption machine must interact with. The resistances in between the boundary conditions and the absorption machine represent heat-exchangers that are necessary for the interaction between the absorption machine and the surroundings. The temperatures designated with a subscript 'i' represent the internal temperature of the absorption machine.

The Carnot cycle can be used to simulate an ideal heat pump cycle as shown in figure 1.4. The heat Q_0 is added to the working fluid at T_0 along the isothermal line GH; the fluid is then compressed isentropically with W_{input} along HI; heat Q_1 is rejected isothermally along lines IJ while work W_{output} is done along the isentropic lines JG by expansion. The net work input is represented by the area GHIJ; the heat absorbed by the cycle is represented by the area GHKL and the heat rejected is represented by the sum of the two areas, IJLK.

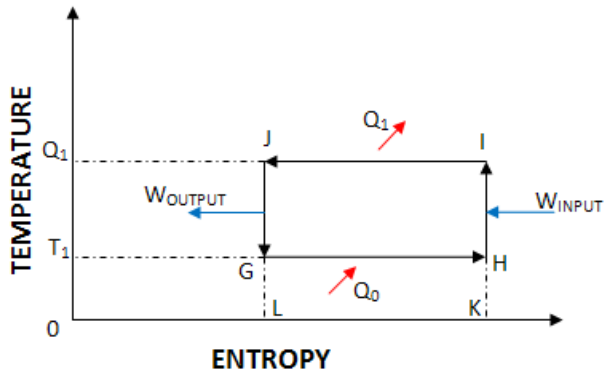

Figure 1.4 Heat pump cycle as Carnot cycle.

Vapour compression cycles (like a refrigerator) typically have a COP of 3 to 4, while a DAHP have a COP of around 0.5 (Herold *et al.*, 1996). This looks less than ideal since the DAHP produces only about 25% of the refrigeration of the vapour compression cycle. Why should one then bother with a DAHP system that can perhaps be optimised to produce a COP of 0.6 or 0.7 after years of research and monetary investment, while current vapour compression technology is visibly so much better? The answer is not necessarily the most obvious.

By viewing figure 1.1 it can be reasoned that, even with a much lower coefficient of performance (COP), the renewable energy as used in the diffusion absorption cycle is more efficient than a vapour compression cycle which uses high-grade energy. This high grade energy is extracted from fossil fuels which formed during a non-reversible cataclysmic event, with high grade energy needed to mine or extract the fossil fuel from its natural location, to process it and to transfer it to the intended location. It's thus much more efficient to harness the sun's renewable energy on-site, and to implement it directly into the cycle.

According to Chen *et al.* (1996) the COP of a diffusion absorption cycle is so low mainly due to the following three reasons:

(a) The heat input to the generator is at a low temperature, and the evaporator temperature is very low, which yields a low Carnot efficiency.

(b) The auxiliary gas requires some of the cooling load.

(c) The rectifier gives off heat to the environment.

Zhang *et al.* (2006) stated that the diffusion absorption cycle's efficiency is directly linked to the bubble pump since it is responsible for pumping the strong aqua-ammonia solution from the generator to the rectifier, and for desorbing the ammonia vapour (the refrigerant used in the cycle). It is because of the integral part that the bubble pump play in the diffusion absorption cycle that it is of the utmost importance to ensure that it operates at its optimum.

1.4 Problem statement

Various models have been presented for the bubble pump, but none has fully explored the effects of varying a wide variety of parameters on the bubble pump's performance. These parameters include tube diameter, maximum pump height, system pressure and temperature, etc. Most studies have also been performed with e.g. a water-lift pump with air bubbles injected under open ambient conditions. The main concern will be the optimum lift height possible of the bubble pump under certain operating conditions with a solar-driven absorption cycle in mind.

1.5 Objective

Few models have approached the design with a minimum number of inputs not influenced by ungrounded assumptions. Careful consideration will be given to choose the least amount of input parameters to maximise the amount of calculated and optimised parameters. Of these known models none have approached the problem with the methodology of developing the simulation by dividing the tube into segments of a known quality rather than a fixed length.

1.6 Issues to be addressed

The purpose of the research is to incorporate accurate thermophysical properties for aqua-ammonia, two-phase flow models with current boiling heat transfer theory in modelling the bubble pump. If possible the correlations must be developed especially for aqua-ammonia as the fluid. As little as possible inputs need to be used in order to maximise the optimisation of each aspect of the bubble pump. A separate design team need to be able to incorporate the outputs from the model. If the bubble pump is optimised it will improve the efficiency of the cycle as a whole.

The study will focus on the development of a mathematical simulation model for the generator and bubble pump which uses two-phase flow models as well as boiling heat transfer equations to accurately model the flow in the aforementioned components of a diffusion absorption cycle for maximum efficiency.

1.7 Research methodology for the simulation model

- The two-phase flow parameters inside the bubble pump need to be analysed first to understand the basic flow inside the pump pipe.
- The boiling heat transfer models need to be applied to the bubble pump setup to predict the setup's heat transfer characteristics, especially the wall temperature.
- The flow map for the flow parameters and pipe dimensions chosen needs to be set up to determine the flow regime inside the bubble pump tube.
- Different void fraction correlations need to be investigated to ensure that the most accurate one is used.
- The mathematical model needs to be programmed in the computer program Engineering Equation Solver (EES) to solve the model.
- Thermophysical properties need to be integrated for aqua-ammonia to accurately predict the flow characteristics inside the tube.
- Correlation for determining the maximum lift height of the tube need to be integrated into the model.
- Various iterations of a variety of parameters must be applied to investigate its effect on the bubble pump performance.
- Meaningful discussions on and possible conclusions from the results need to be made afterwards in order to ascertain the optimum operating point for the given parameters.

2. Literature survey

In this chapter the basic operation of a diffusion absorption cycle as well as a bubble pump will be discussed. The importance of the bubble pump will also be highlighted. Various bubble pump designs, modifications and simulation models will be discussed.

2.1 Basic Cycle operation

2.1.1 Mechanical pump-driven absorption cycle (two-pressure cycle)

The basic pump-driven absorption cycle, as shown in figure 2.1, is made up of an absorber, pump, generator, condenser, expansion valves and evaporator (Sözen *et al.*, 2002). As in the vapour compression cycle, there is both a low pressure and high pressure region. The low pressure region consists of the evaporator and absorber, while the high pressure region consists of the generator and condenser.

The pump is used to drive the strong solution from the low pressure of the absorber to the high pressure of the generator. In the generator, heat is added to the strong solution, consisting of a fluid and an absorbent, to separate the fluid from the absorbent. The fluid requires a lower boiling temperature than the absorbent. The fluid usually contains small amounts of absorbent bubbles traveling to the condenser, so it is necessary to purify the fluid before it reaches the condenser by using a rectifier.

The weak solution (weak in fluid) travels from the generator directly to the absorber, to absorb the fluid exiting the evaporator. The fluid leaving the generator and rectifier travels to the condenser where it is cooled by surrendering heat to the heat sink to form liquid. The liquid fluid leaves the condenser and travels to the evaporator, where it passes through expansion valves to lower its pressure. This causes the fluid to evaporate and by doing so absorbs energy from the surrounding environment causing it to cool down. The fluid then travels to the absorber where it is absorbed back into the weak solution, transforming it into the strong solution once more and the cycle is repeated (Ziegler, 1999).

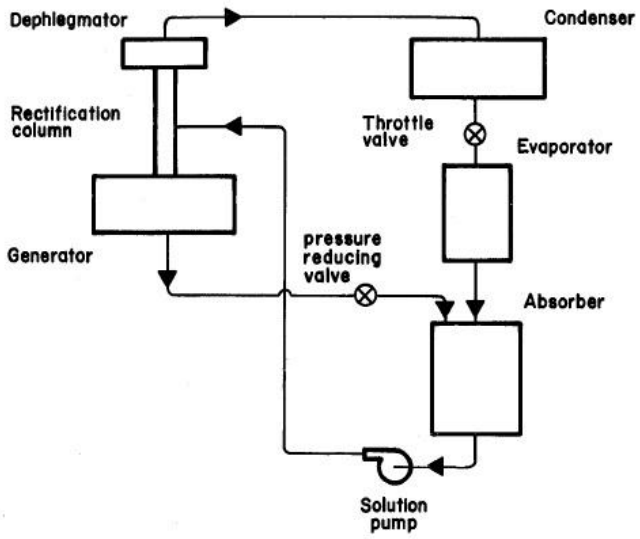

Figure 2.1 Sketch of a basic dual-pressure aqua-ammonia cycle, showing the basic components of the cycle.

2.1.2 Bubble pump-driven absorption cycle (single-pressure cycle)

The basic single pressure absorption cycle consists of a generator (which includes a boiler and bubble pump), solution heat exchanger, condenser and evaporator (Marks, 1944). The first such system was patented in 1928 by von Platen and Munters, and their original patent application sketch is shown in figure 2.2. The pressure throughout the cycle is the same, bar the minute differences in pressure caused by gravity. There is no solution pump driving the fluid to raise its pressure, and because of that there can be no expansion valves since it requires too great a pressure to pass the fluid through the expansion valves. Instead, the evaporator has a third non-reactive gas (such as helium or hydrogen (Zohar *et al.*, 2005)) to lower the pressure of the fluid entering the evaporator using Dalton's law of partial pressures, causing the fluid to evaporate and absorb energy from the surroundings, reducing its temperature (Chaouachi & Gabsi, 2007).

The strong solution is heated in the generator, boiling the fluid from the absorbent which creates bubbles. The bubbles travel through a pipe and act as pistons raising columns of fluid with it. At the top of the bubble pump the weak solution is diverted to the absorber via the solution heat exchanger, where it will pre-heat the strong solution flowing from the absorber to the generator. The weak solution in the absorber will absorb the refrigerant exiting the evaporator. The bubbles at the top of the bubble pump passes through a rectifier to purify it of

any passenger particles of absorbent. From there it travels to the condenser where it dumps heat to the heat sink, causing the fluid to cool and form saturated fluid. The fluid then travels to the evaporator. The fluid is then absorbed into the weak solution, creating a strong solution which travels to the generator, and the cycle starts all over again. (Ben Ezzine *et al.*, 2010)

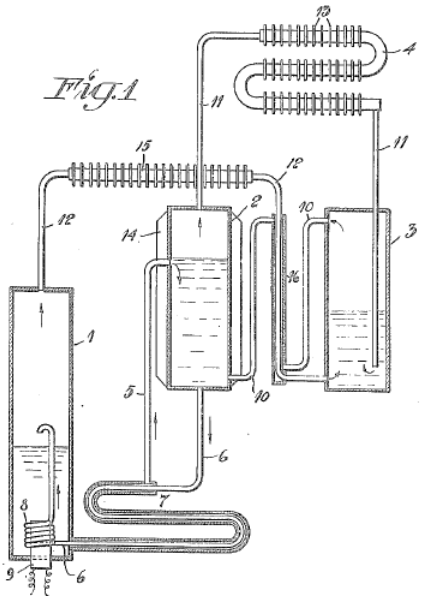

Figure 2.2 The original von Platen and Munters patent application sketch for the diffusion absorption cycle (von Platen & Munters, 1928).

According to Koyfman *et al.* (2003) the diffusion absorption cycle has many advantages over the conventional pump-driven absorption cycle. Some of these advantages include a near silent operation and enhanced reliability due to the absence of any moving parts such as pumps and fans. This makes it perfect for use at especially hotels. It can also utilise low grade energy which makes the cycle very usable even at remote places, since the heat can be applied indirectly from sources such as solar heating installations, gas flames or dumped heat from another cycle.

2.2 Purpose of the bubble pump

The bubble pump is one of the most critical components in the diffusion absorption cycle, since it's responsible for displacing the solution from the generator to the rectifier, where the solution is purified. The bubble pump's performance is directly linked to the system efficiency, relying mainly on the driving temperature, the solution head and the diameter of the pipes (Zhang *et al.*, 2006).

Besides circulating the fluid the bubble pump is also responsible for desorbing the solute refrigerant from the solution using heat added to the generator or bubble pump from a heat source. (Benhmidene *et al.*, 2010). Since the COP of the DAHP is very low, it is of utmost importance to ensure that the bubble pump is designed to desorb as much refrigerant as possible with the minimum amount of heat added (Zohar *et al.*, 2008).

One can logically conclude that a failure to describe the operation of the bubble pump accurately will result in a less efficient bubble pump model being developed and ultimately in a less efficient diffusion absorption cycle.

2.3 Basic operation of the bubble pump

A bubble pump, shown in figure 2.3, is basically a vertical cylindrical tube used to pump fluid using gas slugs as a vehicle. The fluid is heated at the bottom of the pipe in a generator, causing it to form gas bubbles as the onset of boiling occurs. These bubbles will coalesce if enough heat is added and will rise up into the pipe due to the density difference between the gas and liquid phase. The existence of both the gas and liquid phase in the bubble pump is called two-phase flow (Vicatos & Bennet, 2007).

These conglomerates of bubbles form slugs in the pipe in what is called the slug flow regime in two-phase flow terminology. This regime will only occur under certain two-phase flow conditions. These gas slugs lift segments of fluid (now a weak solution) up the pipe to the top of the cycle, at the entrance of the rectifier where the gas phase will be purified of any resident fluid particles. The fluid columns that were lifted by the gas slugs are discharged at the top of the bubble pump pipe and flow in counter current against the outside wall of the bubble pump pipe, to the absorber. (Zohar *et al.*, 2008)

It was found that the bubble pump performance could be enhanced by including a lunate channel inside the main tubes of the bubble pump. It was found that this second tube increased the motive head of the pump, which increased the solution volume flow rate and lowered the vapour mass fraction at any given driving temperature (Zhang *et al.*, 2006).

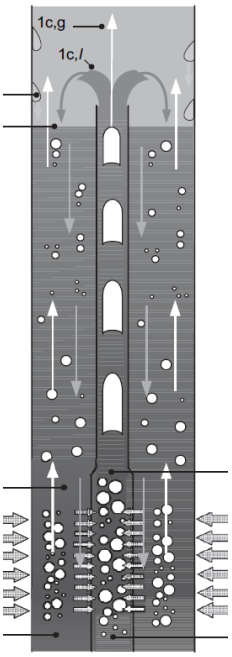

Figure 2.3 A simplified representation of the bubble pump with slug flow (Zohar *et al.*, 2008).

2.4 Previous research done on the bubble pump

2.4.1 Research done on physical modifications of the bubble pump

The first generator-bubble pump configuration of the original patented von Platen and Munters cycle (shown in figure 2.4) consisted of a pipe leaving the absorber, coiling around an element in the generator housing and straightening after that until about halfway up the total height of the cycle. The rich ammonia (or refrigerant of choice) gas leaving the pipe rises to the condenser, while the weak solution falls back into the generator tank and is drained to the absorber, where it will absorb the refrigerant again and form a strong solution (von Platen & Munters, 1928).

The above-mentioned cycle patent was filed for the Electrolux-Servel Corporation, and is still in use today under the Dometic Group with certain upgrades. The bubble pump-generator configuration was updated to its current configuration as shown in figure 2.5, taken from Zohar (2008).

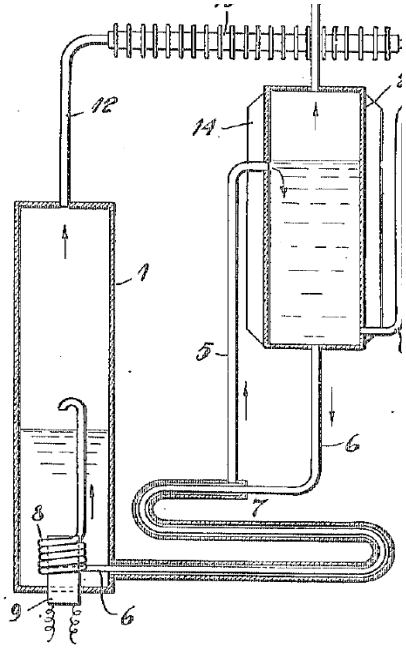

Figure 2.4 The original Platen and Munters patent application sketch showing the generator and absorber configuration (von Platen & Munters, 1928).

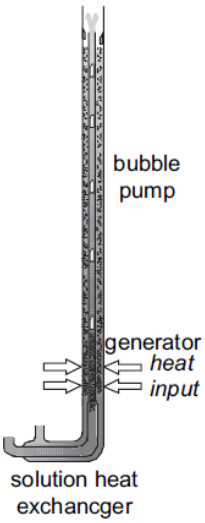

Figure 2.5 Current bubble pump configuration in use by the Dometic absorption refrigerators (Zohar *et al.*, 2007).

The modern bubble pump configuration used by Dometic was investigated and improved by Zohar, et al (2008). The original cycle configuration was analysed by Zohar *et al.* (2008) and a thermodynamic model was developed to correspond with the measured values. It was found that a partially attached bubble pump configuration desorbed more refrigerant for a fixed amount of heat input than the fully attached bubble pump configuration in use by Dometic. The improved bubble pump configuration is shown in figure 2.6. Although this research

proved better COP's were possible with an improved bubble pump design, the numerical model itself was not suited for design purposes, but rather only described mathematically what happened inside their current setup (Zohar *et al.*, 2008).

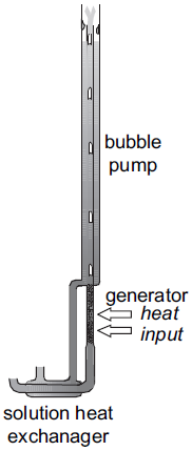

Figure 2.6 The improved partially attached bubble pump configuration as developed by Zohar *et al.* (2008).

Another type of modification done on the standard Dometic fully attached bubble pump configuration was a configuration which features a generator with a heat exchanger to reduce the heat lost through the bubble pump by using the waste heat of the rectifier to heat the strong solution coming from the absorber to the generator. This is achieved by using a counter flow tube-in-tube helical heat exchanger with the weak solution coming from the rectifier flowing upwards in the inside tube of the helical coil, while the strong solution flows downward from the absorber in the outside tube of the helical spiral. Figure 2.7 illustrates the modification (Chen *et al.*, 1996).

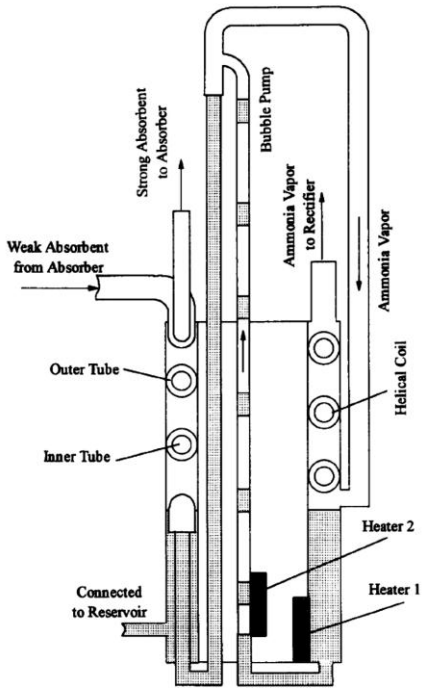

Figure 2.7 The generator with heat exchanger as developed by Chen et al (1996).

2.4.2 Research done on the mathematical modelling of the bubble pump

A mathematical model was developed by Pfaff *et al.* (1998) which incorporated important parameters like the bubble pump tube diameter, the pump lift and the driving head as variables in the model. The model is based on the manometer principle and is modelled for intermittent flow. (Pfaff *et al.*, 1998).

Another model was developed by Shelton & White Stewart (2002) which used two-phase flow as the basis for the flow modelling and incorporating the drift flux model as well as two-phase friction factors and properties of the mixture. This model also included design parameters as the bubble pump diameter, pump height and the submergence ratio defined by the height of the static head of the reservoir divided by the total pump height as independent variables (Shelton & White Stewart, 2002), (White, 2001).

Delano (1998) used the Bernoulli equation and conservation equations to model the flow and dimensional parameters, while the friction factor for the two-phase flow in the bubble pump assumed only liquid flow in the pump tube. This model was developed for use in the Einstein cycle and not for primary use in the Platen and Munters cycle.

Atkinson Schaefer (2000) improved on Delano's work by using his equation stating the dependency of the submergence ratio on the fluid properties found in the bubble pump. Schaefer also introduced the use of a flow map to determine the type of flow in the bubble pump and introduced a second law analysis to determine and consequently reduce the entropy generation in the generator and bubble pump setup.

Benhmidene *et al.* (2011) developed a model to determine the optimum heat flux for the bubble pump. The numerical model used a pipe of 1m in length, and was divided into small increments. The flow regime in the pipe was not restricted to slug flow, but it also incorporated churn and annular flow. The model used the two-fluid model for flow inside the tube. This was by far the best simulation model of the bubble pump of all the research reviewed. It incorporated aqua-ammonia's properties and it was not based on an air-lift pump model while the flow was not restricted.

2.4.3 Concluding remarks

While the research done on the configuration of the bubble pump can be directly incorporated into the current research for further analysis and development, the existing research on the mathematical model of the generator and bubble pump are far from complete and warrant further research and development.

The experimental models developed by Pfaff (1998), White (2001) and Delano (1998) are not realistic representations of the operation of the bubble pump. According to Koyfman *et al.* (2003) the experimental setups as used by Pfaff (1998) and Delano (1998) didn't operate continuously, but only intermittently. The experimental setups of Delano (1998) and White (2001) didn't use practical working fluids and the setup operated at atmosphere and not the elevated pressures which are expected in a diffusion absorption cycle.

The experimental system of White (2001) operated as an airlift pump, where pressurised air is released into the bottom of the bubble pump to induce two phase slug flow, instead of heat being added to induce two-phase flow through boiling. The mass flow of the liquid also stayed the same from the entrance of the bubble pump to its exit. In a diffusion absorption cycle the vapour would be boiled of from the liquid causing the liquid flow to decrease in

mass but increase in temperature, due to the nature of aqua-ammonia. This affected the accuracy of the derived correlation for the pressure gradient.

A number of the models discussed were developed from practical cycles, or the dimensions of the bubble pump including the submergence ratio were just chosen without reason and fixed, which means that they are by no means optimised. This includes the models from Zohar *et al.* (2008) and Chen *et al.* (1996).

None of the models reviewed could be used to determine the maximum lift height of the bubble pump under various conditions, since they were all constrained by certain parameters such as a fixed submergence ratio or a fixed pump height. The most promising model from Benhmidene *et al.* (2010) divided the pipe into increments of length which made the independent solution of the maximum pump length almost impossible.

Although various models have been presented, none has fully explored the different effects of various parameters on the bubble pump performance, while keeping the dimensions of the bubble pump unconstrained with the goal of incorporating the bubble pump model into a solar-driven absorption cycle.

3. Two-phase flow theory

In this chapter various parameters, correlations and properties necessary for developing a simulation model of a bubble pump will be discussed and explained.

3.1 Two-phase flow regimes

Two-phase flow is essentially the co-existence of both a liquid and a vapour phase in the flow through a pipe. Although there were a lot of different descriptions of essentially the same regimes as well as the definition of certain transition regimes, most researchers agreed on the characteristics of the following five basic types of flow regimes as illustrated in figure 3.1 (Samaras & Margaris, 2005):

(a) Bubble flow – Small and discrete bubbles are found scattered in the fluid, which becomes frothy with an increase in flow rates.

(b) Slug flow – With the gas flow rate increasing (either due to a higher heat input into the bubble pump or an increase in the gas flow rate in the vapour lift pump) bubbles will coalesce to form Taylor bubbles. These bubbles are almost the diameter of the pipe and are shaped like bullets. The Taylor bubbles are separated by liquid slugs.

(c) Churn flow – With an increase in gas flow rate the Taylor bubbles brake through the separating liquid slugs. It results in a unstable flow regime with the liquid flowing in an upwards and downwards oscillatory motion.

(d) Wispy annular flow – With an increase in liquid flow, the amount of droplets in the gas core also increases. This increasing amount of droplets in the core leads to the coalescence of the moisture in the core to form wisps of liquid (Spedding *et al.*, 1998) (Shelton & White Stewart, 2002) (Samaras & Margaris, 2005)

(e) Annular flow – A liquid film forms on the tube wall, while the gas phase flows in the centre of the pipe. Some liquid is also captured as small droplets in the vapour centre.

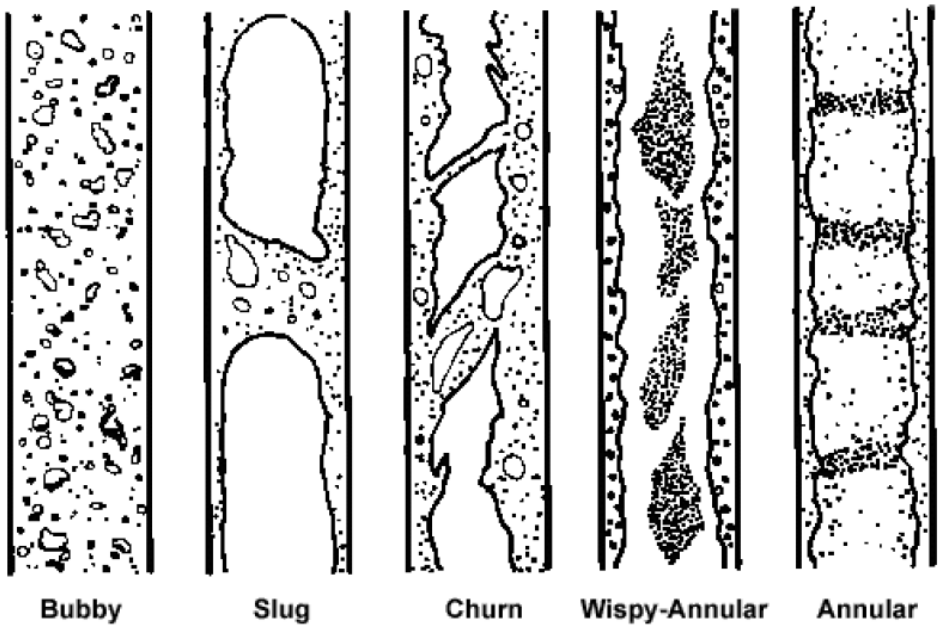

Figure 3.1 The five basic flow regimes of two-phase flow.

It has been found that the best flow regime for a bubble pump to operate in is the slug-flow regime, since it consists of a large slug of air (or vapour) almost entirely the diameter of the pipe which lifts the liquid above it to the top of the pipe (Benhmidene *et al.*, 2010).

3.2 Two-phase flow parameters

3.2.1 Void fraction

The void fraction, ϵ, exists in any gas-liquid system as the volume of space occupied by the gas. The void fraction is one of the most important parameters in two-phase flow, since it is used to calculate other important parameters such as the two-phase density and viscosity. To obtain the relative average velocity of the two phases as well as being important in predicting two-phase pressure drop, two-phase heat transfer and flow pattern transitions (Woldesemayat & Ghajar, 2006).

It is important to distinguish between quality and void fraction in two-phase flow. Quality is the percentage of mass from the fluid converted to vapour, while the void fraction is the percentage of the volume converted to vapour. (Thome, 2010).

$$quality = x = \frac{m_{vapour}}{m_{total}} \tag{3.1}$$

$$void\ \ fraction = \varepsilon = \frac{v_{vapour}}{v_{total}} \tag{3.2}$$

There are many ways to define the void fraction, which include:

- Local void fraction
- Chordal void fraction
- Volumetric void fraction
- Cross-sectional void fraction

Each of these will be explained below.

(i) *Local void fraction*

The local void fraction is defined as the small fraction of time vapour was present at a specified location (at some radius, *r*, from the channel center at time *t*) in the two-phase flow. The time-averaged local void fraction can then be defined as:

$$\varepsilon_{local}(r,t) = \frac{1}{t}\int_{t} P_k(r,t)dt \tag{3.3}$$

(ii) *Chordal void fraction*

The chordal void fraction can be defined as the chordal length the gas phase occupies (L_G) over the total chordal length ($L_{vapour} + L_{liquid}$) of the flow:

$$\varepsilon_{chordal} = \frac{L_{vapour}}{L_{vapour} + L_{liquid}} \tag{3.4}$$

(iii) *Volumetric void fraction*

The volumetric void fraction is usually determined using a pair of quick-closing valves along a tube length to trap the vapour and liquid, which can then be analysed on a volumetric basis.

$$\varepsilon_{volumetric} = \frac{v_{vapour}}{v_{vapour} + v_{liquid}} \tag{3.5}$$

(iv) *Cross-sectional void fraction*

The cross-sectional void fraction is similar to the chordal void fraction, but is based on the cross-sectional area occupied by the vapour phase rather than the chordal length. The cross-sectional average void fraction is the main void fraction used in the literature, and will be the void fraction discussed further in this dissertation. The cross-sectional void fraction can be measured by optical or electronic means. It can be summed up as:

$$\varepsilon_{cross-sectional} = \frac{A_{vapour}}{A_{vapour} + A_{liquid}} \tag{3.6}$$

Were A_{vapour} is the area of the cross-section occupied by the vapour-phase and A_{liquid} is the area occupied by the liquid phase (Thome, 2010).

The void fraction can be predicted by methods such as the homogeneous model and empirical models. The most widely used method is the basic empirical model developed by Zuber and Findlay in 1965 which has been modified numerous times. This model is also known as the drift-flux model. The basic model of Zuber and Findlay is as follows (White, 2001):

$$\varepsilon = \frac{j_{vapour}}{C_0 \cdot j_{total} + V_{vapour,j}} \tag{3.7}$$

$$with\ j_{total} = j_{vapour} + j_{liquid} \tag{3.8}$$

- j_{vapour} = Superficial velocity of the vapour phase, defined as $j_{vapour} = \frac{\dot{V}_{vapour}}{A_{total}}$, with $\dot{V}_{vapour}$ the volumetric flow rate of the vapour phase, and A_{total} the total cross-sectional area of the pipe.
- j_{liquid} = Superficial velocity of the liquid phase, defined as $j_{liquid} = \frac{\dot{V}_{liquid}}{A_{total}}$, with $\dot{V}_{Liquid}$ the volumetric flow rate of the liquid phase, and A_{total} the total cross-sectional area of the pipe.
- C_0 = A distribution parameter incorporating the non-uniformity of the flow, usually taken as 1.2.

- $V_{vapour,j}$ = Drift velocity, which is the difference between the vapour-phase velocity and the two-phase mixture velocity ,$V_{vapour,j} = V_{vapour} - j_{total}$ (Woldesemayat & Ghajar, 2006).

The drift-flux model shows that the void fraction is a function of the mass velocity, $\dot{m}_{total}$ which isn't accounted for in analytical models (Thome, 2010). All the variations of the drift-flux models vary in the terms used for the parameter, C_0, and the drift velocity, $V_{vapour,j}$ (Coddington & Macian, 2002).

During recent years there have been a few comparisons of void fraction correlations over a broad spectrum of various experimental data.

A study was done by Coddington & Macian (2002) on void fraction data taken from experiments performed at facilities in France, Japan, Switzerland, the UK and the USA on rod bundles, level swell and boil-off. The pressure ranges were from 0.1MPa to 15MPa and the mass fluxes from 1kg/m^{2}s to 2000kg/m^{2}s. Various correlations based on Zuber and Findlay's drift-flux model were compared to the experimental data.

All correlations with a mean absolute error of more than 10% or with a standard deviation of more than 15% were discarded. The 13 void fraction correlations that remained was deemed to be the most wide ranging void fractions because of their reasonable performance over the wide spectrum of experimental data. The vast number of experimental data ensured a detailed statistical comparison of all the void fraction correlations concerned.

The correlations were divided into three groups. The first group contained the correlations which were derived from tube void fraction data. The second group contained correlations with a large value for the distribution parameter, C_0, which prevented prediction of the void fraction close to one (including the original Zuber and Findlay correlation). The third group contained the predictions which gave a good prediction over the whole spectrum of data.

Table 3.1 lists 14 drift-flux void fraction correlations tested by Coddington & Macian (2002) (the 13 best correlations as well as the Maier and Coddington correlation developed from analysing the experimental data from their study), the year the correlations were first published, the data source on which it was based and the mean absolute error of the void fractions as well as the standard deviations (Coddington & Macian, 2002).

Table 3.1 Comparison of various drift-flux models in a wide variety of experimental data as done by Coddington & Macian (2002).

Correlation	Year	Data Source	Mean absolute error value	Standard deviation value
Zuber–Findlay	1965	Tube	−0.025	0.114
Ishii	1977	Tube	0.048	0.126
Gardner	1980	Tube	0.056	0.111
Liao, Parlos and Griffith	1985	Tube	0.028	0.094
Takeuchi	1992	Tube	0.04	0.083
Sun	1980	Rod bundle & Tube	−0.041	0.114
Jowitt	1981	Rod bundle	0.057	0.116
Sonnenburg	1989	Rod bundle & Tube	0.049	0.097
Toshiba	1989	Rod bundle	0.019	0.103
Dix	1971	Rod bundle	−0.010	0.092
Bestion	1985	Rod bundle & Tube	0.018	0.088
Chexal–Lellouche	1992	Rod bundle & Tube	−0.017	0.078
Inoue	1993	Rod bundle	−0.003	0.083
Maier and Coddington	1996	Rod bundle	−0.002	0.071

3.2.2 Slip

Slip is defined as the relation of the velocity of the gas-phase to the velocity of the liquid phase. In homogeneous two-phase flow models, slip does not exist since a pseudo-fluid is used with averaged values from the two phases, which means there is only one velocity for the fluid, so slip is taken as unity in homogeneous two-phase flow. In separated two-phase flow each phase is looked at separately, as if each phase flowed in its own tube (White, 2001). The slip is mathematically defined as in equation **(3.9)**. Velocities as used in equation **(3.9)** are used to calculate the superficial velocities, which in turn appear in the calculation of the lift height.

$$Slip = \frac{V_{vapour}}{V_{liquid}} \tag{3.9}$$

3.3 Two-phase pressure drop

The easiest way found to calculate the core two-phase flow parameters was to set-up a flow model using two-phase pressure drops in a vertical pipe. Accurate prediction of two-phase pressure drops in evaporators and condensers, for example, is of the utmost importance in the design of heat pumps and refrigeration systems, since inaccurate modelling of the pressure drops in the pipes can cause serious sub-cooling or inadequate evaporation of the fluid in integral parts, causing the efficiency of the cycle to suffer tremendously (Thome, 2010).

The pressure drop in a plain vertical pipe is due to the action of three factors: Wall friction force, gravitational force and momentum changes in the fluid.

Thus the total pressure drop in the pipe will be:

$$\Delta P_{total} = \Delta P_{static} + \Delta P_{momentum} + \Delta P_{friction} \tag{3.10}$$

3.3.1 Homogeneous two-phase flow pressure drop

The homogeneous model is the simplest and most convenient way to model two-phase pressure drops (Awad & Muzychka, 2008). The homogeneous fluid used is a pseudo-fluid acting as a single-phase fluid with averaged properties of the liquid and vapour phase (Thome, 2010).

For a vertical pipe the static pressure drop for a homogeneous two-phase fluid will be:

$$\Delta P_{static} = \rho_H \cdot g \cdot H \tag{3.11}$$

The homogeneous density, ρ_H, can be calculated as:

$$\rho_H = \rho_{liquid}\left(1-\varepsilon_H\right) + \rho_G \varepsilon_H \tag{3.12}$$

The homogeneous void fraction, ε_H, is determined using the quality, *x*, which results in a weighted average (Awad & Muzychka, 2008):

$$\varepsilon_H = \frac{1}{1 + \left(\frac{u_{vapour}}{u_{liquid}} \cdot \frac{(1-x)}{x} \cdot \frac{\rho_{vapour}}{\rho_{liquid}}\right)} \tag{3.13}$$

The homogeneous model implies that the vapour and liquid phases move at the same velocity, since a homogeneous fluid acts as a single-phase fluid. The result is that the velocity ratio, $\frac{u_G}{u_L}$, which is also called slip, will be unity (Awad & Muzychka, 2008). The term is called slip since in separated two-phase flow the liquid and gas phase velocities vary at the interface. The reason for this is because each phase is modelled in its own flow pipe, but this phenomenon cannot happen in reality since there is an interface separating the two phases which cannot move at different velocities, which result in the interface velocities being equal (Thome, 2010).

The momentum pressure gradient per unit length of tube is:

$$\left(\frac{dp}{dz}\right)_{mom} = \frac{d(\dot{M}_{total} / \rho_H)}{dz} \tag{3.14}$$

Where $\dot{M}_{total}$ is the mass flux, not the mass flow.

The frictional pressure drop can be seen as the most problematic term for two-phase pressure drop calculations, and can be expressed in terms of the two-phase friction factor, f_{tp}:

$$\Delta P_{friction} = \frac{2 \cdot f_{tp} \cdot H \cdot \dot{M}_{total}^2}{d_i \cdot \rho_{tp}} \tag{3.15}$$

In the case of homogeneous flows, $\rho_{tp} = \rho_H$.

In the majority of the previous research the Blasius equation is the preferred choice, since it is the only correlation for the two-phase friction dependant on the Reynolds Number. The Blasius equation will be used in calculating the two-phase friction factor:

$$f_{tp} = \frac{0.079}{Re^{0.25}} \tag{3.16}$$

The Reynolds Number, *Re*, will be calculated as follows:

$$Re = \frac{\dot{M}_{total} \cdot d_i}{\mu_{tp}} \tag{3.17}$$

The two-phase viscosity, μ_{tp}, can be calculated as follows:

$$\mu_{tp} = x \cdot \mu_{vapour} + (1-x) \cdot \mu_{liquid} \tag{3.18}$$

3.3.2 Separated two-phase flow pressure drop

The basic equation for obtaining the total pressure drop ΔP_{total} remains the same, while the methods for calculating the individual pressure drops change as well as the method for determining the void fraction, ϵ.

The static pressure drop can be calculated with the following equation:

$$\Delta P_{static} = \rho_{tp} \cdot g \cdot H \tag{3.19}$$

The two-phase density, ρ_{tp}, is calculated using the void fraction:

$$\rho_{tp} = \rho_{liquid}(1-\varepsilon) + \rho_{vapour}\varepsilon \tag{3.20}$$

The momentum pressure drop, which is the change in kinetic energy of the flow, can be calculated with the following calculation (Rousseau, 2010):

$$\Delta P_{momentum} = 0.5 \times V_{in} V_{out} (\rho_{mix,out} - \rho_{mix,in}) \tag{3.21}$$

Where V_{in} and V_{out} are the average velocities of the fluid at the inlet and outlet of the pipe section, while $\rho_{mix,out}$ and $\rho_{mix,in}$ are the average densities of the mixture at the inlet and outlet of the pipe section.

With evaporating flow in which the vapour quality, *x*, increases, which is the current case, the momentum or kinetic energy of the flow increases as the vapour quality increases, which results in a reduction of the total pressure higher up in the pipe, since the density decreases.

The frictional pressure drop for two-phase flow can be calculated with various methods, which is normally predicted using separated flow models. Lockhart and Martinelli was the first to present a model for the frictional pressure drop in 1949. The Lockhart and Martinelli method is best used for system pressures near atmospheric pressure and for fluids other than water, since it was with such data that the correlation was developed (Rohsenow *et al.*, 1985).

Other correlations include those by Friedel (1979), Grönnerud (1972), Chisholm (1973), Bankoff (1960) which is an extension of the homogeneous model, Chawla (1967) and Müller-Steinhagen & Heck (1986). All these correlations can be found in Thome (2010).

According to Thome (2010) a study was done by Tribbe & Müller-Steinhagen in 2000 and the correlation of Müller-Steinhagen & Heck from 1986 gave the best results in a study covering certain single and binary fluids. In another test conducted by Ould Didi, Kattan & Thome in 2002 compared the two-phase frictional pressure drops of various correlations to experimental data using pipes with internal diameters of 10.92mm and 12mm and a length of 3.013m. They concluded that the correlations of Grönnerud from 1972 and Müller-Steinhagen & Heck from 1986 was the most accurate (Thome, 2010).

According to Thome (2010), The Müller-Steinhagen & Heck correlation from 1986 is as follows:

The frictional pressure drop per unit length of pipe is:

$$\left(\frac{dp}{dz}\right)_{friction} = G(1-x)^{1/3} + Bx^3 \qquad (3.22)$$

And the factor G is calculated with the following equation:

$$G = A + 2(B - A)x \tag{3.23}$$

The frictional pressure gradient, *A*, for all the liquid flow $\left(dp/dz\right)_{liquid}$ is calculated as follows:

$$\left(\frac{dp}{dz}\right)_{liquid} = f_{liquid}\frac{2\dot{M}_{total}^{2}}{d_i \rho_{liquid}} \tag{3.24}$$

For laminar flows ($Re_L < 2000$) the friction factor is determined by:

$$f_{liquid} = \frac{16}{Re_{liquid}} \tag{3.25}$$

For turbulent flows ($Re_L \geq 2000$) the friction factor is determined by:

$$f_{liquid} = \frac{0.079}{Re_{liquid}^{0.25}} \tag{3.26}$$

The liquid Reynolds number is determined by:

$$Re_{liquid} = \frac{\dot{M}_{total} \cdot d_i}{\mu_{liquid}} \tag{3.27}$$

The frictional pressure gradient, *B*, for all the vapour flow $\left(dp/dz\right)_{vapour}$ is calculated as follows:

$$\left(\frac{dp}{dz}\right)_{vapour} = f_{vapour}\frac{2\dot{M}_{total}^{2}}{d_i \rho_{vapour}} \tag{3.28}$$

For laminar flows ($Re_G < 2000$) the friction factor is determined by:

$$f_{vapour} = \frac{16}{Re_{vapour}} \tag{3.29}$$

For turbulent flows ($Re_G \geq 2000$) the friction factor is determined by:

$$f_{vapour} = \frac{0.079}{Re_{vapour}^{0.25}} \tag{3.30}$$

The vapour Reynolds number is determined by:

$$Re_{vapour} = \frac{\dot{M}_{total} \cdot d_i}{\mu_{vapour}} \tag{3.31}$$

3.4 Boiling heat transfer

Boiling heat transfer in a bubble pump refers to evaporation inside a plain, vertical tube due to an external heat input. A bubble pump for a diffusion absorption refrigeration cycle uses forced convective boiling heat transfer (Jakob *et al.*, 2008).

In order to calculate the length of the bubble pump required to heat the fluid to the desired quality, correlations describing boiling heat transfer are needed.

The basic equation describing boiling heat transfer is (Riviera & Best, 1999):

$$h_{htc,tp} = \frac{Q_{flux}}{(T_{wall} - T_{sat})} \tag{3.32}$$

Q_{flux} = the local heat flux from the tube wall into the fluid in [kg/m^2].

T_{wall} = the local wall temperature at the inside of the bubble pump tube.

T_{sat} = the local saturation temperature at the local saturation pressure P_{sat} of the fluid.

$h_{htc,tp}$ = the local two-phase flow boiling heat transfer coefficient.

There are different flow models that can be used to determine the local heat transfer coefficient, of which the Chen-, Shah- and Gungor-Winterton correlations as well as the Steiner Taborek asymptotic model is the most noteworthy (Thome, 2010).

A study was done to derive correlations for determining the boiling heat transfer coefficients for aqua-ammonia and ammonia-lithium nitrate mixtures from experimental data over a range of conditions. The proposed correlations had a mean deviation of ±16% for the ammonia-lithium nitrate mixtures and ±25% for the ammonia-water mixtures. The aqua-ammonia mixture's concentration was varied from 38 to 48% (on a weight basis), with the pressure varying between 9.4 to 12.4 bar. It was concluded that the local heat transfer coefficients were strongly dependant on both the quality of the mixture and $\frac{1}{X_{tt}}$ (the inverse of the Lockhard-Martinelli parameter) for the aqua-ammonia mixture (Riviera & Best, 1999).

The derived correlation from their experimental results for the heat transfer coefficient of aqua-ammonia was:

$$h_{htc,tp} = 65(1/X_{tt})^{0.5}(Bo)^{0.15} \tag{3.33}$$

X_{tt} = Lockhard-Martinelli parameter.

Bo = Boiling number, with:

$$Bo = \frac{Q_{flux}}{\dot{M}_{total} \bullet h_{LG}} \tag{3.34}$$

3.5 Flow regime map for a vertical pipe

Flow regime maps are a very important tool for evaluating in which flow regime the current flow is. This is necessary in order to ensure that the flow is in its optimised state (as chosen by the researcher), but must be verified experimentally as well. No two-phase flow regime map can be accepted as an absolute, since there is no consensus in the research over various modelling parameters since most prove difficult to predict theoretically (Spedding *et al.*, 1998).

Flow regime maps are mostly developed for airlift pumps, which is an adiabatic type of bubble pump, otherwise known as a vapour lift pump. But both bubble pumps and airlift pumps work on the same principles, and since there is much more information on airlift pumps, it is a good place to start. Since both bubble pumps and airlift pumps are essentially two-phase flow in a vertical pipe, both can be modelled by two-phase flow theories (Shelton & White Stewart, 2002).

The model used in Samaras et al. (2005) represents the transition lines as a function of the gas void fraction and the gas superficial velocity as shown in figure 3.2, which is very handy to use if there is only experimental data available with the amount of gas pumped into the air-lift pump, and which enables the researcher to see the development of the flow regime with the increasing void fraction in forced convective boiling two-phase flow. This configuration easier to interpret than most of the standard flow regime maps which uses complex functions and correlations to plot the flow regime map.

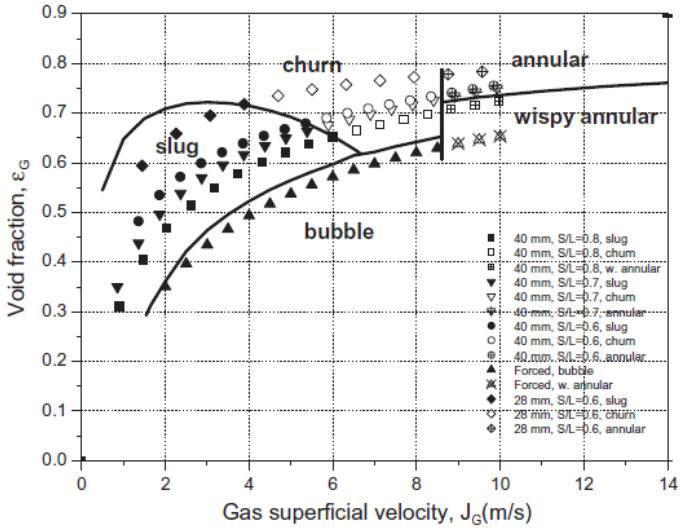

Figure 3.2 Flow regime map showing void fraction as a function of the gas superficial velocity (Samaras & Margaris, 2005).

3.6 Conclusion

In this chapter the main parameters and correlations needed in developing a simulation model for a solar-driven bubble pump were explained. These parameters and correlations will be applied to the mathematical model in the next chapter and will be discussed in more detail relating to their application.

4. Mathematical model

4.1 Conservation equations

The three laws of conservation need to be applied to any simulation model in order to formulate the model clearly and correctly. These laws describe the flow of mass and energy across the system boundaries and are essential in solving the model analytically. It can be seen as the governing equations for the simulation model (Rousseau, 2010). The three laws are:

(a) Conservation of mass

(b) Conservation of momentum

(c) Conservation of energy

The conservation equations will be applied to sections of a pipe, each of unequal and unknown length, but known fluid quality. The reasons for this is to generate a table with thermo-physical properties for aqua-ammonia at a given pressure, varying the quality as desired, and making the height of the generator and lift tube a variable that is fully dependant on the flow. Figure 4.1 and table 4.1 illustrate this.

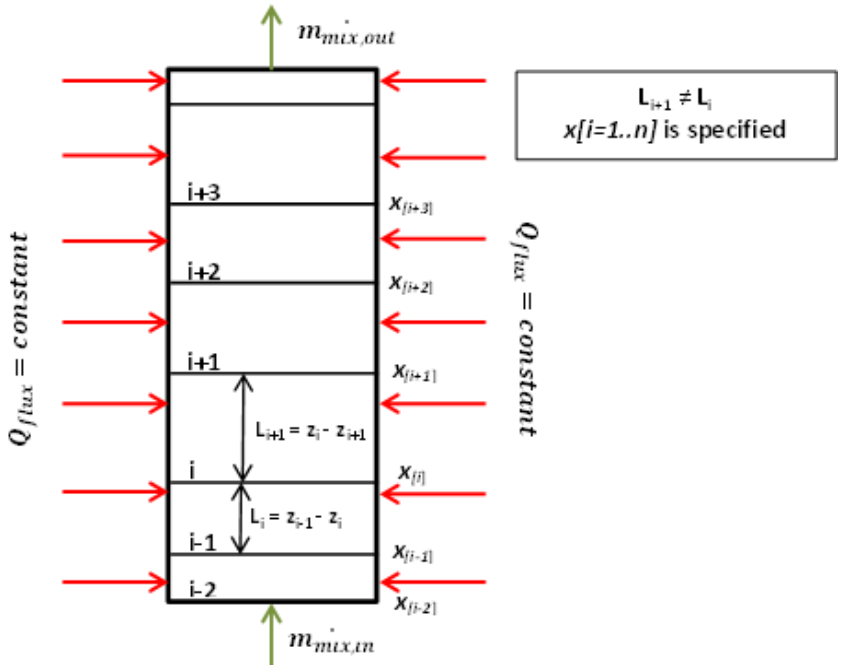

Figure 4.1 Generator tube segment showing arbitrary divisions of known quality.

Table 4.1 Example of data retrieved from REFPROP, with the quality varied at a constant pressure of 1MPa

Quality [kg/kg]	Temp [K]	Enthalpy [kJ/kg]	Liquid phase enthalpy [kJ/kg]	Vapour phase enthalpy [kJ/kg]	Liquid phase mass fraction, NH_3 [kg/kg]	Vapour phase mass fraction, H_2O [kg/kg]
0	353.66	262.07	262.07	1797.6	0.40000	0.60000
0.1	366.33	465.81	312.16	1848.6	0.33906	0.66094
0.2	380.65	685.59	376.64	1921.4	0.27514	0.72486
0.3	394.16	913.42	443.09	2010.9	0.21757	0.78243
0.4	405.02	1140.4	499.61	2101.7	0.17244	0.82756
0.5	413.16	1363.1	543.40	2182.8	0.13925	0.86075
0.6	419.22	1581.5	576.61	2251.4	0.11504	0.88496
0.7	423.82	1796.3	602.01	2308.2	0.097112	0.90289
0.8	427.38	2008.6	621.77	2355.3	0.083542	0.91646
0.9	430.21	2218.8	637.45	2394.5	0.073037	0.92696
1	432.50	2427.6	650.13	2427.6	0.064728	0.93527

The bubble pump will consist of a generator area where the heat input is applied to achieve two-phase flow and a lift-tube area, which will be an adiabatic lift pipe to pump the fluid and gas upwards. This is in-line with the design from Zohar *et al.* (2008) who stated that a bubble pump is more efficient if the heating area of the pump is directly applied to the pipe section in which the aqua-ammonia mixture is flowing, and not indirectly through an outer pipe in which the weak solution flows. The height of the generator section of the pipe will be the height to which the bubble pump will be filled before pumping commences (submergence height). A basic representation of the bubble pump is given in figure 4.2.

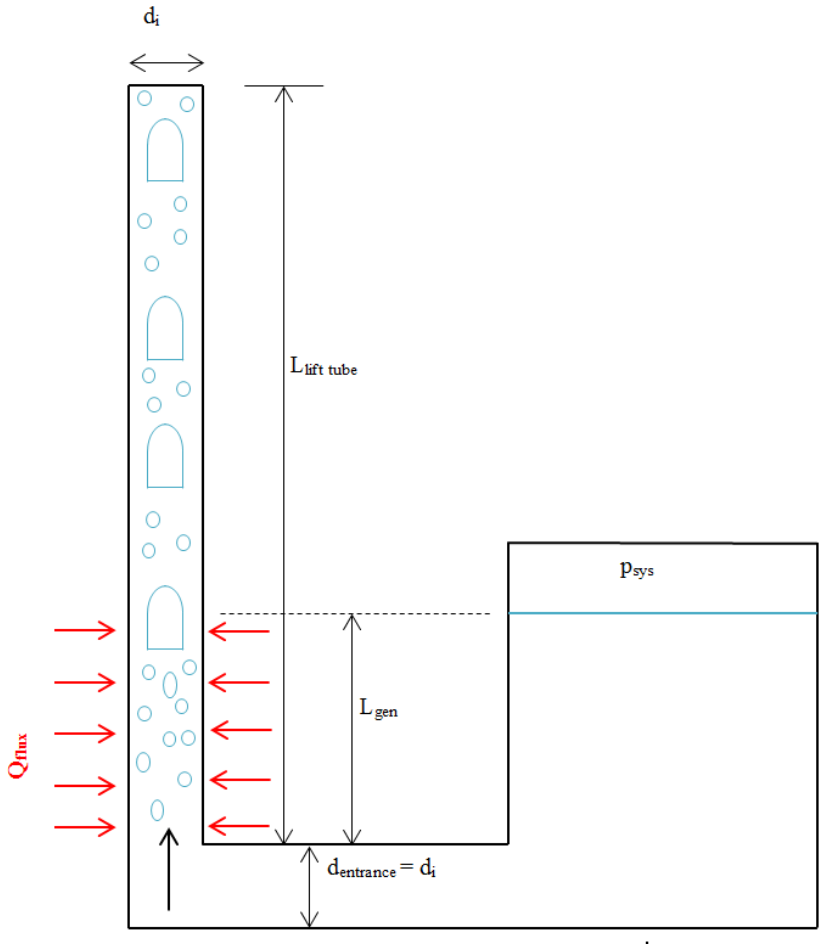

Figure 4.2 Basic representation of the bubble pump setup.

4.1.2 Conservation of mass

This law describes the total mass flow across the system boundaries. For the generator and bubble pump setup, there is only one inlet and one outlet, thus the mass balance will be for each node:

$$\dot{m}_{mix,in} = \dot{m}_{mix,out} \tag{4.1}$$

4.1.3 Conservation of momentum

The conservation of momentum relates to pressure losses in vertical flow. The total pressure drop can either be calculated by applying a homogeneous flow model to the intube flow or by assuming separated two-phase flow. Since the latter is a more accurate prediction of reality, separated two-phase flow will be used (Rohsenow *et al.*, 1985). Pressure loss in upward flow usually consists of three terms (Thome, 2010):

(i) *Static pressure loss*

This term (ΔP_{static}) is the pressure loss due to a change in the potential energy of the fluid in the generator. This is caused by the change in position of the fluid in the pipe over time, which changes the pressure of the aqua-ammonia fluid mixture due to gravity as the fluid rises in the tube.

$$\Delta P_{static} = \rho_{mix} g(z_{out} - z_{out}) \tag{4.2}$$

(ii) *Momentum pressure loss*

The momentum pressure loss occurs due to the change in kinetic energy as the fluid flows up the pipe. In order to model the flow correctly for each node, the density of the node's inlets and outlets are averaged to give a description of what happens between the inlet and outlet. It can thus be modelled as (Rousseau, 2010):

$$\Delta P_{momentum} = 0.5 \times V_{in} V_{out} (\rho_{mix,out} - \rho_{mix,in}) \tag{4.3}$$

(iii) *Frictional pressure loss*

Frictional pressure loss in the generator occurs due to viscous effects of the fluid on the wall of the tube and is a function of the Reynolds number. It is important to know whether the flow is laminar or turbulent, since it determines whether there forms a viscous layer near the tube wall or not. It was found that the correlation of Muller-Steinhagen and Heck was one of the most reliable over various databases (Thome, 2010). The correlation is given by:

$$\left(\frac{dp}{dz}\right)_{frictional} = G(1-x)^{1/3} + Bx^3 \tag{4.4}$$

With:

$$G = A + 2(B - A)x \tag{4.5}$$

$$A = \left(\frac{dp}{dz}\right)_{liquid} = f_{liquid} \frac{2\dot{m}_{mix}^2}{d_i \rho_{liquid}} \tag{4.6}$$

$$B = \left(\frac{dp}{dz}\right)_{vapour} = f_{vapour} \frac{2\dot{m}_{mix}^2}{d_i \rho_{vapour}} \tag{4.7}$$

$$f = \frac{16}{\mathrm{Re}} \tag{4.8}$$

For Turbulent flow the friction factor is calculated using equation (3.26) for liquid flow and equation (3.30) for vapour flow. For laminar flow the friction factor is calculated using equation (3.25) for liquid flow and equation (3.29) for vapour flow. The Reynolds numbers can be calculated using equation (3.27) for liquid flow and equation (3.31) for vapour flow.

(iv) *Complete conservation equation*

The complete equation for the conservation of momentum for the generator, with the above equations applied, will then be:

$$p_{total,out} = p_{total,in} + 0.5 \times V_{in} V_{out} (\rho_{out} - \rho_{in}) - (\frac{\rho_{in} + \rho_{out}}{2})(z_{out} - z_{in}) + \left(\frac{dp}{dz}\right)_{friction} (z_{out} - z_{in}) \tag{4.9}$$

4.1.4 Conservation of energy

The energy that is applied to the generator of the bubble pump should equal the difference in potential energy as the fluid rises in the pipe as well as the change in enthalpy from heating the fluid in the generator. The energy equation will then be:

$$\dot{Q}_{in} = (\dot{m}_{out} \cdot g \cdot z_{out} - \dot{m}_{in} \cdot g \cdot z_{in}) + (\dot{m}_{out} \cdot h_{0,out} - \dot{m}_{in} \cdot h_{0,in}) \tag{4.10}$$

It is known that the energy input should equal the heat flux from the inner tube wall over the area of the segment evaluated:

$$\dot{Q}_{in} = Q_{flux} \cdot d_i \pi (z_{out} - z_{in}) \tag{4.11}$$

4.2 Void fraction

The void fraction that was recommended by Thome (2010) for use in separated two-phase flow was the one by Rouhani-Axelsson (Rouhani I). It was also recommended by Woldesemayat (2006) along with the Toshiba correlation for vertical upward flow. The Rouhani-Axelsson (Rouhani I) correlation is given by Woldesemayat (2006) as:

$$\varepsilon = \frac{x}{\rho_{vapour}}\left[C_0\left(\frac{x}{\rho_{vapour}} + \frac{1-x}{\rho_{liquid}}\right) + \frac{U_{GM}}{\dot{m}_{flux}}\right]^{-1} \tag{4.12}$$

With:

$$U_{GM} = \frac{1.18}{\sqrt{\rho_{liquid}}}\left[g \cdot \sigma(\rho_{liquid} - \rho_{vapour})\right]^{0.25} \tag{4.13}$$

$$C_0 = 1 + 0.2 \cdot (1-x) \tag{4.14}$$

And the Toshiba correlation as given by Coddington & Macian (2002) as:

$$\varepsilon = \frac{j_{vapour}}{C_0 j_{tot} + v_{gj}} \tag{4.15}$$

With:

$$C_0 = 1.08$$

$$v_{gj} = 0.45$$

The definition of j_{tot} will be given in the next section, in equation (4.19).

4.3 Two-phase velocity and mass flow

As was mentioned earlier, the void fraction is very important in determining other parameters. This includes one of the most important parameters in two-phase flow namely the flow velocity. In separated two-phase flow the two phases can be seen as if each phase flow in a separate tube, which means the equations for the different phase flow velocities will be:

$$V_{liquid} = (m_{liquid,NH_3} + m_{liquid,water}) \cdot \frac{\dot{m}_{mix}}{\rho_{liquid}(1-\varepsilon)A_{c-s}} \tag{4.16}$$

$$V_{vapour} = (m_{vapour,NH_3} + m_{vapour,water}) \cdot \frac{\dot{m}_{mix}}{\rho_{vapour}\varepsilon A_{c-s}} \tag{4.17}$$

$$Slip = \frac{V_{vapour}}{V_{liquid}} \tag{4.18}$$

The superficial velocity is the velocity of the fluid without being a function of the void fraction. It can be calculated as:

$$j_{tot} = j_{liquid} + j_{vapour} \tag{4.19}$$

$$j_{liquid} = V_{liquid}(1-\varepsilon) \tag{4.20}$$

$$j_{vapour} = V_{vapour}\varepsilon \tag{4.21}$$

The mass flow can be calculated from the quality of the fluid:

$$\dot{m}_{liquid} = \dot{m}_{mix} \quad (for\ x = 0) \tag{4.22}$$

$$\dot{m}_{vapour} = \dot{m}_{mix} \quad (for\ x = 1) \tag{4.23}$$

$$\dot{m}_{liquid} = (1-x)\cdot\dot{m}_{mix} \tag{4.24}$$

$$\dot{m}_{vapour} = x\cdot\dot{m}_{mix} \tag{4.25}$$

4.4 Two-phase heat transfer coefficient

The heat transfer coefficient is necessary to calculate the tube wall temperature, which is required in calculating both the conduction loss through the tube wall as well as the minimum tube wall superheat required for nucleation to take place. The basic equation for the two-phase heat transfer is given as:

$$h_{htc,tp} = \frac{Q_{flux}}{T_{wall} - T_{sat}} \tag{4.26}$$

The methods used in the current simulation of the bubble pump are the new Gungor & Winterton correlation as found in Thome (2010) and Shah (2006), the Shah correlation (Shah, 1982) and the correlation by Riviera & Best (1999). According to a study conducted by Shah (2006), six of the most verified correlations were tested for horizontal and vertical boiling heat transfer in tubes and annuli. The data covered a wide variety of fluids, pressure ranges

and mass fluxes. The new Gungor-Winterton and the Shah correlations were found to be the most accurate in the study by Shah (2006), but the correlation from Riviera & Best (1999) was not included since it was developed especially for aqua-ammonia and was not a generalised correlation. The correlation from Riviera & Best (1999) will then be compared alongside the generalised correlations from Shah and Gungor-Winterton.

4.4.1 Gungor-Winterton correlation

The new Gungor-Winterton correlation is defined as:

$$h_{htc,tp} = E_{new} h_{htc,liquid} \tag{4.27}$$

The term $h_{htc,liquid}$ is the well-known Dittus-Boelter correlation used to calculate the convective heat-transfer coefficient of the liquid phase (Rousseau, 2010), while the term E_{new} is the new two-phase convection multiplier:

$$h_{htc,liquid} = 0.023 \frac{k_{liquid}}{d_i} \mathrm{Re}_{liquid}^{\ 0.8} \mathrm{Pr}_{liquid}^{\ 0.4} \tag{4.28}$$

$$E_{new} = 1 + 3000 Bo^{0.86} + 1.12 \left(\frac{x}{1-x} \right)^{0.75} \left(\frac{\rho_{liquid}}{\rho_{vapour}} \right)^{0.41} \tag{4.29}$$

The boiling number, Bo, which defines the effect of heat flux on nucleate boiling, is defined as:

$$Bo = \frac{Q_{flux}}{\dot{m}_{flux} (h_{vapour} - h_{liquid})} \tag{4.30}$$

4.4.2 Shah correlation

Shah considered both nucleate and convective boiling in his heat transfer correlation, and chose the bigger of the two for his two-phase heat transfer coefficient (Thome, 2010).

The Shah correlation starts with a dimensionless parameter, *N*, which is for vertical pipes:

$$N = C_0 \tag{4.31}$$

The factor C_0 is determined as follows:

$$C_0 = \left(\frac{1-x}{x}\right)^{0.8}\left(\frac{\rho_{vapour}}{\rho_{liquid}}\right)^{0.5} \tag{4.32}$$

The liquid Froude number, Fr_{liquid}, is defined as:

$$Fr_{liquid} = \frac{m_{flux}^2}{\rho_{liquid}^2 g d_i} \tag{4.33}$$

His convective boiling heat transfer coefficient is calculated as shown, using the Dittus-Boelter correlation for the liquid-only convective heat transfer coefficient:

$$\frac{h_{htc,cb}}{h_{htc,liquid}} = \frac{1.8}{N^{0.8}} \tag{4.34}$$

The appropriate equation for calculating the nucleate boiling heat transfer correlation is chosen by using the parameter N. When $N > 1$ and $Bo > 0.0003$, the equation will be:

$$\frac{h_{htc,nb}}{h_{htc,liquid}} = 230 Bo^{0.5} \tag{4.35}$$

When $N > 1$ and $Bo < 0.0003$, the equation will be:

$$\frac{h_{htc,nb}}{h_{htc,liquid}} = 1 + 46 Bo^{0.5} \tag{4.36}$$

When $1 > N > 0.1$, the equation for the nucleate boiling heat transfer coefficient will be:

$$\frac{h_{htc,nb}}{h_{htc,liquid}} = F_S Bo^{0.5} e^{(2.74N - 0.1)} \tag{4.37}$$

When $N < 0.1$, the nucleate boiling heat transfer coefficient in the bubble suppression regime is calculated as:

$$\frac{h_{htc,nb}}{h_{htc,liquid}} = F_S Bo^{0.5} e^{(2.74N - 0.15)} \tag{4.38}$$

The Shah constant, F_S, will be:

$$F_S = 14.7 \quad when\ Bo > 0.0011$$
$$F_S = 15.43 \quad when\ Bo < 0.0011$$

4.4.3 Riviera and Best correlation

The correlation by Riviera and Best were developed from a practical setup that consisted of a vertical pipe that was heated uniformly along its length, with aqua-ammonia as its fluid. The experimental data was correlated with a model proposed by Mishra et al. The ammonia concentration of the strong solution was varied between 38% and 48%, the pressure range from 9.4 to 12.4 bar and the tube was 1.48m long with a diameter of 25.8 mm (Riviera & Best, 1999). Their correlation for aqua-ammonia was found to be:

$$h_{htc,tp} = 65\left(\frac{1}{X_{tt}}\right)^{0.5}(Bo)^{0.15} \tag{4.39}$$

With X_{tt} the Lockhart-Martinelli parameter which is given as:

$$X_{tt} = \left(\frac{1-x}{x}\right)^{0.9}\left(\frac{\rho_{vapour}}{\rho_{liquid}}\right)^{0.5}\left(\frac{\mu_{liquid}}{\mu_{vapour}}\right)^{0.1} \tag{4.40}$$

4.4.4 Critical wall superheat

The wall temperature is calculated from the basic equation for the two-phase heat transfer coefficient given in equation (4.26). This reflects the temperature difference between the inner wall of the lift tube and the saturation temperature of the fluid at the bulk fluid pressure. The wall superheat achieved during operation is calculated as:

$$\left(\Delta T_{sat}\right)_{wall} = T_{wall} - T_{sat} \tag{4.41}$$

A correlation for the minimum wall superheat required to initiate nucleation was developed by Davis and Anderson and is defined as (Rousseau, 2010):

$$\left(\Delta T_{sat}\right)_{wall,crit} = \frac{8\sigma T_{sat} Q_{flux}}{\rho_{vapour}(h_{vapour} - h_{liquid})k_f} \tag{4.42}$$

4.5 Flow regime transitions

One of the most important factors in two-phase flow is knowing in which flow regime you are, since this determines the flow characteristics that influences a number of things. Since the bubble pump operates most efficiently in the slug flow regime, it is of utmost importance to know exactly in which flow regime the fluid currently is. A recent study done by Samaras & Margaris (2005) on flow regime maps attempted to create a more universally applicable flow regime map, which is also easier to interpret. The study concluded with a map that plotted the gas superficial velocity, j_{vapour}, against the gas void fraction, ε.

From the definition of the gas void fraction for the slug and churn regimes by Wallis (1969), the following correlations were derived for the transition lines between bubbly and slug flow, slug and churn flow and churn and annular flow.

For the transition line between bubbly and slug flow, the correlation is:

$$\varepsilon_{vapour} = \frac{j_{vapour}}{1.2\left(j_{vapour} + 2.17 + 35.45e^{\frac{-j_{vapour}}{0.4}} \right) + 0.345\sqrt{gd_i\left(\rho_{liquid} - \rho_{vapour}\right)/\rho_{liquid}}} \quad (4.43)$$

For the transition line between slug and churn flow, the correlation is:

$$\varepsilon_{vapour} = \frac{j_{vapour}}{1.2\left(j_{vapour} + 0.047e^{\frac{j_{vapour}}{1.75295}} \right) + 0.345\sqrt{gd_i\left(\rho_{liquid} - \rho_{vapour}\right)/\rho_{liquid}}} \quad (4.44)$$

For the transition line between churn and annular flow, the correlation is:

$$\varepsilon_{vapour} = \frac{j_{vapour}}{1.2\left(j_{vapour} + 0.1385 + 2.085\times10^{47}e^{\frac{-j_{vapour}}{0.07853}} \right) + 0.345\sqrt{gd_i\left(\rho_{liquid} - \rho_{vapour}\right)/\rho_{liquid}}} \quad (4.45)$$

The void fraction correlation by Wallis (1969) from which the above correlations were derived, is not valid for the annular regime. Another correlation by Wallis (1969) is used which calculates the void fraction in upwards annular flow (Samaras & Margaris, 2005). The resulting correlation is defined as:

$$\varepsilon = 1 - \left(\frac{-B + (B^2 - 4AC)^{0.5}}{2A} \right) \tag{4.46}$$

Where:

$$A = 6.295 \left[g d_i \left(\rho_{liquid} - \rho_{vapour} \right) \right]^{0.5} \tag{4.47}$$

And:

$$B = 2.85 \left[j_{vapour} \rho_{vapour}^2 + j_{liquid} \rho_{liquid}^2 - 0.775 \left[g d_i \left(\rho_{liquid} - \rho_{vapour} \right) \right]^{0.5} \right] \tag{4.48}$$

$$C = -j_{liquid} \rho_{liquid}^{0.5} \tag{4.49}$$

4.6 Pressure gradient along the lift tube height

The lift tube itself can be considered an adiabatic vertical tube in its simplest form, in which a certain flow regime of two-phase flow moves upward. A study was done by White (2001) on air-lift pump theory where an adiabatic air-lift pump was built and tested at atmospheric pressure using compressed air and water. The correlation developed was based on the base case of Delano (1998). The correlation describes the average pressure gradient along the lift tube, which makes it possible to predict the maximum attainable pump height for a given generator height (taken as the height of submergence) and specified velocities (calculated from the governing equations). The correlation of Shelton and White-Stewart (2002) is given as:

$$Ratio_{submergence} = Term1 + Term2 + Term3 + Term4 \tag{4.50}$$

$$Term1 = \frac{f_{tp} (\rho_{liquid} j_{liquid} + \rho_{vapour} j_{vapour})^2}{2 g d_i \rho_{liquid} \rho_{tp}} \tag{4.51}$$

$$Term2 = \frac{j_{liquid}^2 \left[\frac{d_i}{d_{entrance}} \right]^4}{2 g L_{lift\,tube}} \tag{4.52}$$

$$Term3 = \frac{j_{liquid}\rho_H\left[\frac{d_i}{d_{entrance}}\right]^2\left[\left(j_{liquid}+j_{vapour}\right)-j_{liquid}\left(\frac{d_i}{d_{entrance}}\right)^2\right]}{\rho_{liquid}gL_{lift\,tube}} \quad (4.53)$$

$$Term4 = 1-\varepsilon \quad (4.54)$$

$$Ratio_{submergence} = \frac{L_{generator}}{L_{lift\,tube}} \quad (4.55)$$

This equation was modified to incorporate the differences in density, velocity and temperature during the boiling process in the generator tube, which was not accounted for in the model by Shelton and White-Stewart (2002). The reason for this was because the model was developed from an adiabatic air-lift pump setup at atmospheric pressure. Such an air-lift pump assumes the liquid mass flowing into the lift tube is the same as the liquid mass flowing out of the tube, while the gas is injected from an external source. This causes the slug flow to occur almost immediately. In a bubble pump, however, the liquid flows into the tube and is heated inside the tube over a certain length dictated by the heat flux. Vapour is released from the liquid which causes the temperature of the mixture to increase (aqua-ammonia is a zeotrope). The liquid mass flow at the exit of the bubble pump is then less than the liquid mass flow at the start.

The modified correlation becomes:

$$Term1 = \frac{f_{tp}\left(\rho_{liquid,out}j_{liquid,out}+\rho_{vapour,out}j_{vapour,out}\right)^2}{2gd_i\rho_{liquid,out}\rho_{tp}} \quad (4.56)$$

$$Term2 = \frac{j_{liquid,out}^2\left[\frac{d_i}{d_{entrance}}\right]^4}{2gL_{lift\,tube}} \quad (4.57)$$

$$Term3 = \frac{j_{liquid,out}\rho_H\left[\frac{d_i}{d_{entrance}}\right]^2\left[\left(j_{liquid,out}+j_{vapour,out}\right)-j_{liquid,out}\left(\frac{d_i}{d_{entrance}}\right)^2\right]}{\rho_{liquid,out}gL_{lift\,tube}} \quad (4.58)$$

$$Term4 = 1 - \varepsilon \tag{4.59}$$

$$Ratio_{submergence} = \frac{L_{generator}}{L_{lift\,tube}} \tag{4.60}$$

The subscript *out* refers to the parameters at the outlet of the generator, after the heat addition occurred.

The main difference in the application of equations (4.56) - (4.60) in the simulation model, shown in Appendix A – Simuation model on page 90, is that White (2001) used a fixed length for the lift tube (0.5m) and varied the submergence ratio to calculate the bubble pump efficiencies at these different ratios. It was found that the higher the submergence ratio, the higher the efficiency, which is logical since the higher the starting point, the less energy is needed to lift the fluid out of the tube. In the current study, the height of the generator is fixed for a certain quality which is determined by the flow regime, diameter and heat flux input into the generator. The height of the lift pump is then calculated from these values for the slug-flow regime, which usually has a low submergence ratio, since it can be seen as the maximum height attainable with the current conditions.

5. Results and discussion

5.1 Range of pressures for the test

The temperature at which the condenser must exchange heat in order to condense the ammonia inside the condenser will dictate the system pressure of the diffusion absorption refrigeration system. Since the condenser will have to exchange heat with the environment, it may be subject to temperature extremes which vary from sub-zero temperatures in winter to scorching summer temperatures. Theses temperature differences can have serious consequences for the cycle efficiency since it can cause the condenser to sub-cool the fluid too much or even cause it to not condense everything completely (Theunissen, 2011).

A study was conducted by Theunissen (2011) in order to minimise these temperature differences. It was found that a radiative cooling system can minimise the temperature difference significantly. It shows, for example, the ambient temperature difference for Pretoria, South Africa, in 2010 as 43ºC (a winter minimum of -9ºC and a summer high of 34ºC). According to Tillner-Roth & Friend (1998) this corresponds with pressure of approximately between 300 kPa and 1300 kPa needed to condense the vapour ammonia in the condenser. The study showed that the temperature difference was reduced to 22ºC (a minimum temperature of 3ºC and a maximum temperature of 19ºC). This corresponds to a condenser pressure of between roughly 480 kPa and 830 kPa. The study also showed that the temperature fluctuations happened more gradually (Theunissen, 2011).

A lower system pressure is vital if solar radiation is used to heat (either directly or indirectly) the generator of the bubble pump since it lowers the saturation temperature of the aqua-ammonia solution that exits the absorber. A lower saturation pressure equates to less energy needed to boil off the ammonia from the solution, which raises the COP of the cycle (Chaouachi & Gabsi, 2007).

Table 5.1 illustrates the effect of system pressure on the liquid saturation temperature of a 40% ammonia rich aqua-ammonia mixture. Keep in mind that aqua-ammonia is a zeotropic mixture, which means that the saturation temperature changes as the composition changes with an increase in quality.

Table 5.1 Table illustrating the effect of system pressure on the fluid and vapour saturation temperatures

System Pressure [MPa]	Saturated fluid temperature [K] x = 0	Saturated vapour temperature [K] x = 1
0.4	320.90	399.75
0.6	334.44	413.55
0.8	344.94	423.99
1	353.66	432.50
1.2	361.19	439.72
1.4	367.87	446.03
1.6	373.91	451.65
1.8	379.43	456.73

5.2 Selection of void fraction correlation

As stated previously, the void fraction is one of the most important parameters in two-phase flow. One of the main purposes of the void fraction correlation is to determine the flow regime of the two-phase flow. It is very important to determine the current flow regime in the pipe as accurately as possible, because the bubble pump operates most efficiently in the slug flow regime (Benhmidene *et al.*, 2011). The void fraction correlations from Rouhani-Axelsson (Rouhani I) and Toshiba are compared in the figure 5.1 below.

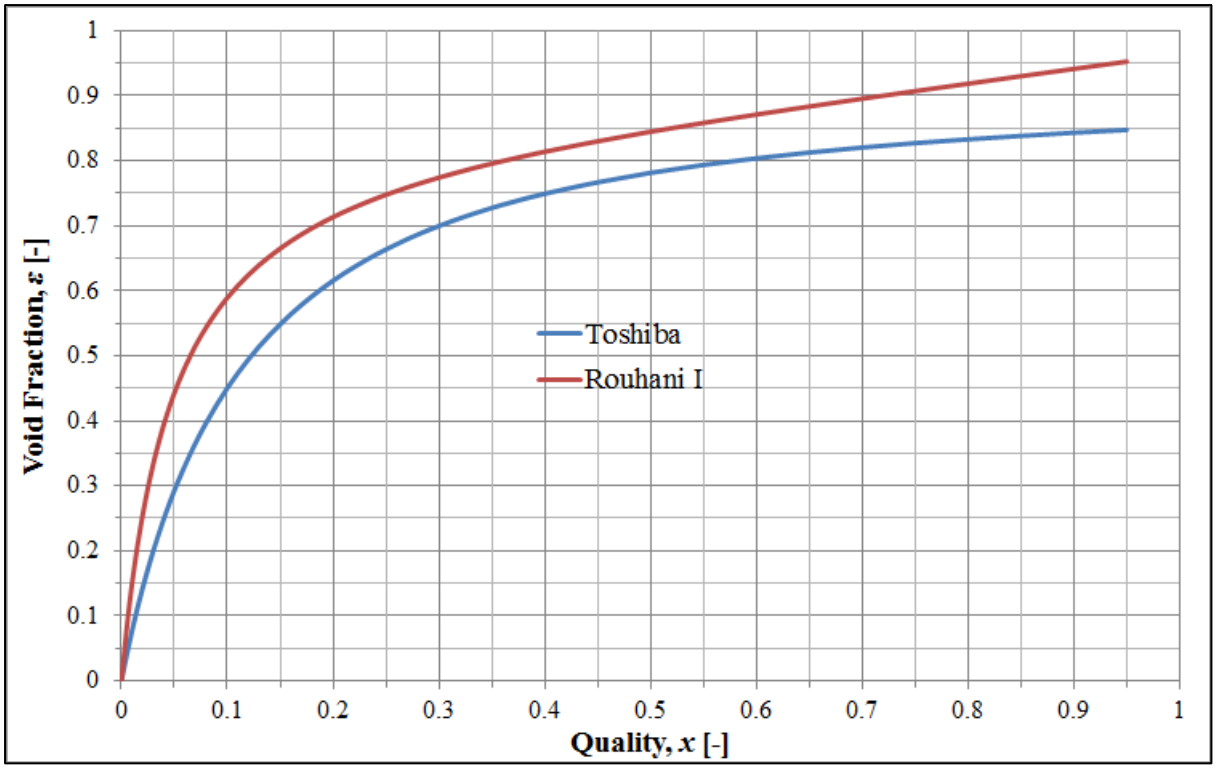

Figure 5.1 Comparison between the Rouhani-Axelsson (Rouhani I) void fraction correlation and the Toshiba void fraction correlation for a system pressure of 8 [bar], mass flux of 20 [kg/m^{2}s] and a tube diameter of 10 [mm].

It can be seen that the Toshiba correlation isn't nearing a void fraction of 1 for a quality of 1 (according to the definition of the void fraction, it must be 1 for a quality of 1), rather it seems to flatten out at just above 85% void fraction.

The Rouhani-Axelsson (Rouhani I) void fraction correlation seems to be nearing 1 for higher void fraction, and would thus be a better choice in the current study. The reason for this is because the Rouhani-Axelsson (Rouhani I) correlation uses vapour mass fraction (quality), surface tension, density and the mass flux of the fluid to calculate the void fraction. All of these properties, excluding the mass flux, are inherent to the fluid while the mass flux is an input, which will result in a more realistic calculation of the void fraction. The Toshiba correlation instead uses pre-determined constants for C_0 and v_{gj} in the drift-flux model which is based on empirical studies for mostly azeotropic mixtures and adiabatic air-water systems.

Both the Rouhani-Axelsson (Rouhani I) and the Toshiba correlation are superimposed on the Samaras et al (2005) flow regime map in figure 5.2 and figure 5.3. It can be seen that because

of the above-mentioned factors that the Toshiba correlation group the different mass-fluxes almost indistinguishably close to each other, while the Rouhani-axelsson (Rouhani I) correlation spreads the different mass flux curves further apart.

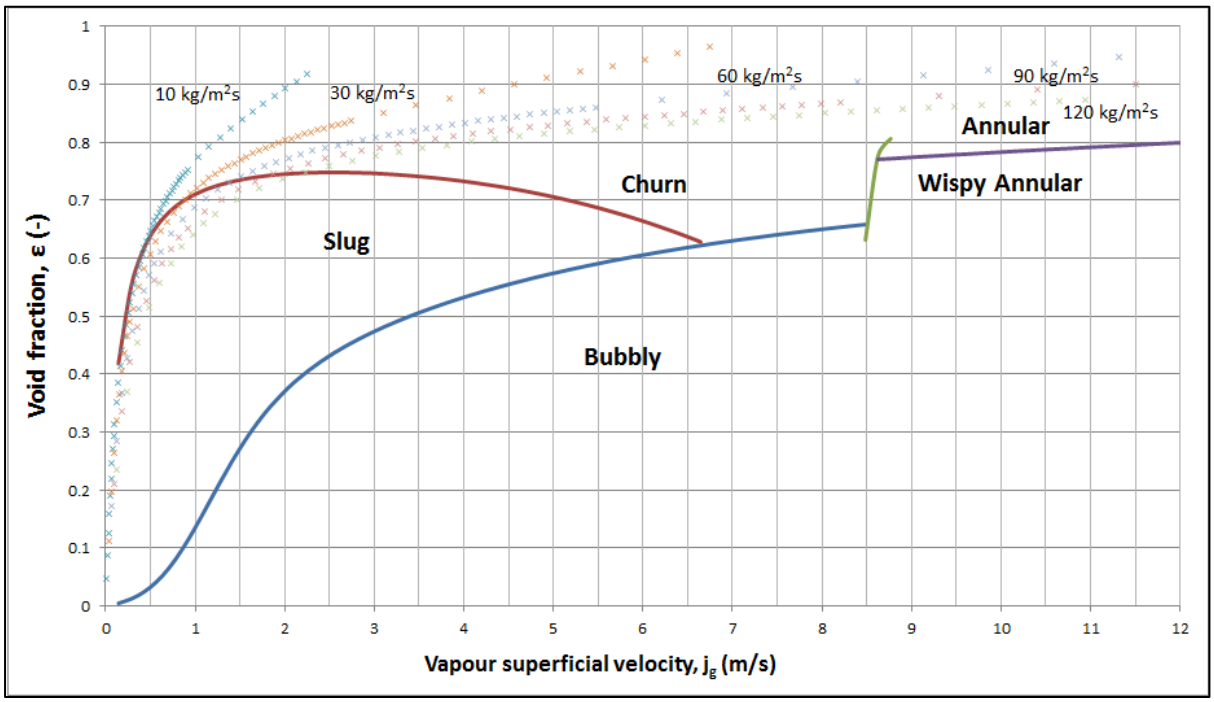

Figure 5.2 Rouhani-Axelsson void fraction correlation for massfluxes ranging from 10 – 120 [kg/m^2], system pressure of 8[bar] and a tube diameter of 20[mm].

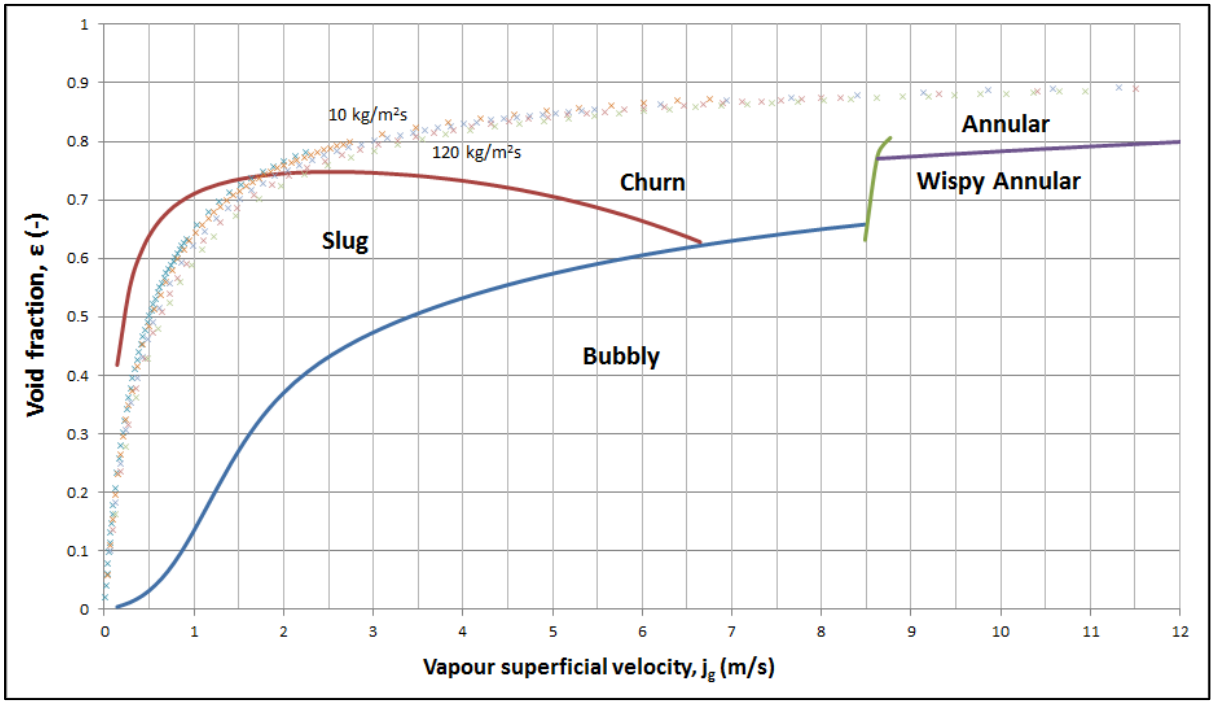

Figure 5.3 Toshiba void fraction correlation for massfluxes ranging from 10 – 120 [kg/m^2], system pressure of 8[bar] and a tube diameter of 20[mm].

Because of the above-mentioned factors, The Rouhani-Axelsson (Rouhani I) correlation will be used for the remainder of the study unless otherwise stated.

5.3 Discussion and modification of two-phase heat transfer correlation

The heat transfer coefficient is used to calculate the wall temperature in the tube of the generator. This wall temperature is then used to calculate the achieved wall superheat to determine if it is sufficient to induce nucleate boiling. If not, there will only be convective boiling which is insufficient to cause further nucleation (Rousseau, 2010).

The two-phase heat transfer correlation from Riviera & Best (1999) was given as:

$$h_{htc,tp} = 65\left(\frac{1}{X_{tt}}\right)^{0.5}(Bo)^{0.15} \qquad (5.1)$$

It is interesting to note that the above equation is dimensionless, since the Lockhart - Martinelli parameter $1/X_{tt}$ and the boiling number Bo are both dimensionless. The equation used to correlate the experimental data is in generic form, and is given by:

$$h_{tp} = \text{Constant}\, h_L \left(\frac{1}{X_{tt}}\right)^{m} (Bo)^{n} \qquad (5.2)$$

This generic equation for the two-phase heat transfer coefficient contains also the liquid-only heat transfer coefficient, given by the Dittus-Boelter equation. If the heat transfer coefficient is added to the published equation, then the modified equation will be:

$$h_{htc,tp} = 65 h_L \left(\frac{1}{X_{tt}}\right)^{0.5}(Bo)^{0.15} \qquad (5.3)$$

This modification now has the correct dimensions and correlate to the generic equation. The results obtained can also be correlated to the experimental results obtained during the tests conducted by Riviera & Best (1999). The reason for the difference in results obtained using the original published equation can be simply because of an error in typing the report. The

fact of the matter is that the correct results are obtained with the modified equations, while the published equation's values are nowhere near the experimental results.

The original published test results are given below in figure 5.4 with the modification to the equation added in red. The results obtained using the published equation as well as the results obtained using the modification are tabulated in table 5.2 and table 5.3. The heat transfer coefficients were obtained calculating the average heat transfer coefficient from the local heat transfer coefficients at the same locations along the lift tube as in the experimental study.

Table 5.2 Comparison of results obtained using the original published equation and the modified equation. Results are for a mass flux of 5 [kg/m^{2}s], a system pressure of 10 [bar] and a concentration of 40% ammonia.

Heat flux, Q_{flux}	$h_{htc,tp}$ (original)	$h_{htc,tp}$ (modified)
[kW/m^2]	[kW/m^{2}K]	[kW/m^{2}K]
12	25.551	3.458
14	28.374	3.736
16	30.833	3.98

Table 5.3 Comparison of results obtained using the original published equation and the modified equation. Results are for a mass flux of 8 [kg/m^{2}s], a system pressure of 10 [bar] and a concentration of 40% ammonia.

Heat flux, Q_{flux}	$h_{htc,tp}$ (original)	$h_{htc,tp}$ (modified)
[kW/m^2]	[kW/m^{2}K]	[kW/m^{2}K]
12	19.147	3.95
14	21.009	4.244
16	22.832	4.528

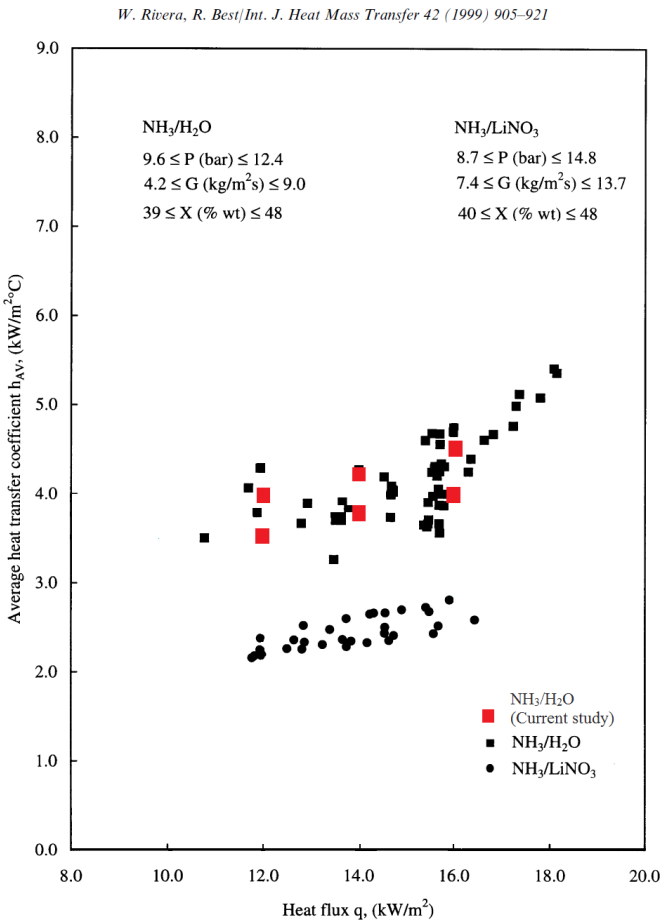

Figure 5.4 Results from the modified equation (in red) superimposed on the experimental results from Riviera & Best (1999).

Although the difference in values between the published equation and the modified equation, the effect of the change is not that large, as illustrated in figure 5.5 and figure 5.6. The difference between the original and modified equations is just large enough to predict the achieved wall superheat ($\Delta T_{wall,achieved}$) sufficient for nucleation at the heat fluxes used in this study. This is illustrated in figure 5.5 and figure 5.6. It is interesting to note that the difference in the wall superheat between the original and modified equations almost vanishes with the higher heat flux (as seen in figure 5.6).

The authors Riviera & Best (1999) were contacted about the possible printing error, but no feedback was received at the time of print. Because of this, the original correlation is used further in the study. The only effect this will have on the study is on the wall temperature and in the determination of whether or not the critical wall superheat necessary to achieve nucleation is reached.

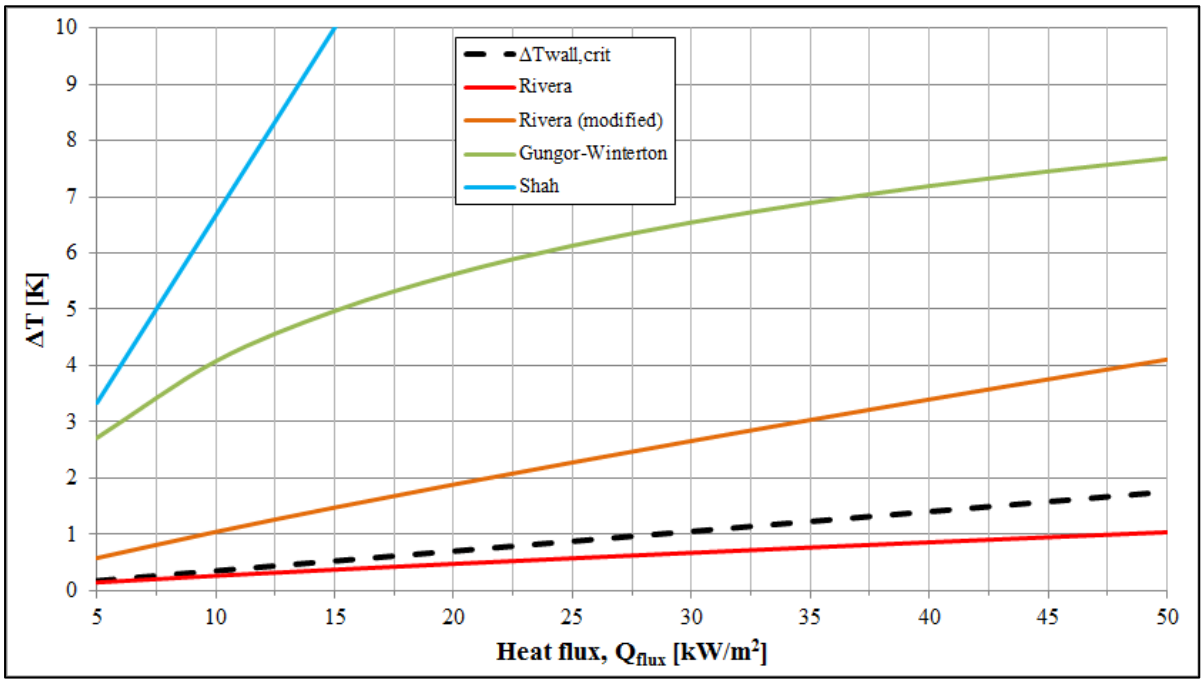

Figure 5.5 **Comparison between the different heat transfer coefficient correlations, including the modified Riviera and Best (1999) correlation, and the critical heat flux needed for nucleation. Mass flux of 10 [kg/m^{2}s], a system pressure of 8 [bar] and a tube diameter of 10 [mm].**

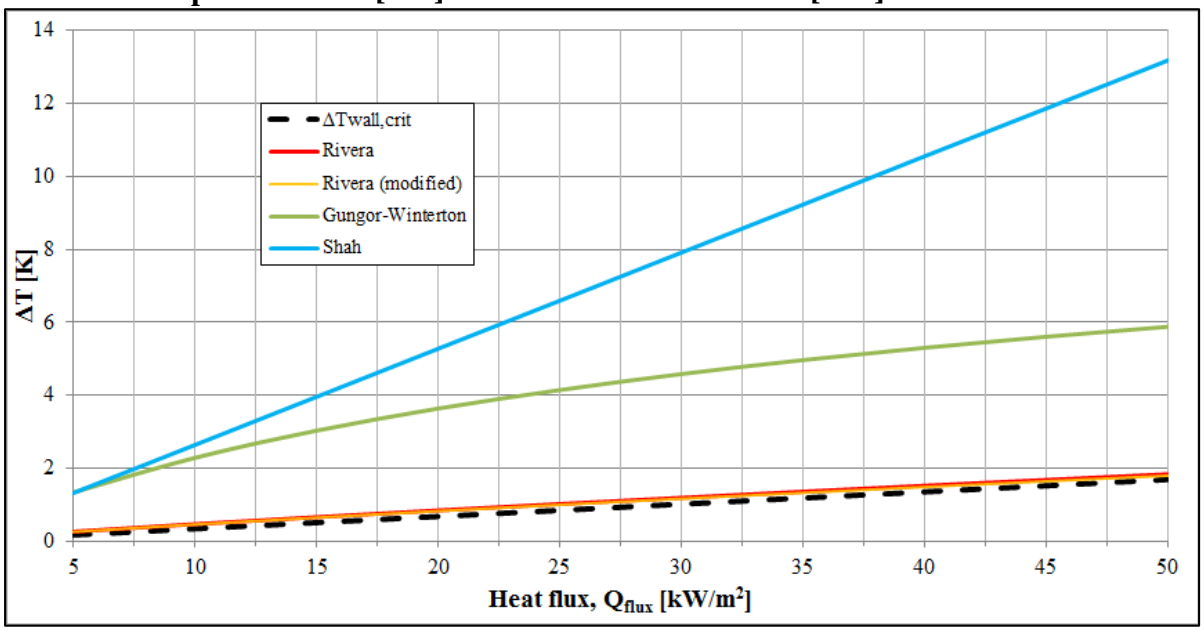

Figure 5.6 **Comparison between the different heat transfer coefficient correlations, including the modified Riviera and Best (1999) correlation, and the critical heat flux needed for nucleation. Mass flux of 50 [kg/m^{2}s], a system pressure of 8 [bar] and a tube diameter of 10 [mm].**

5.4 Heat transfer coefficient correlations

The heat transfer correlation of Riviera & Best (1999) predicts that the wall superheat becomes insufficient in the slug flow region, which limits the length of the lift tube significantly. The wall superheat is predicted by both the correlations of Gungor & Winterton (as found in Shah (2006)) and Shah (1982) to be more than sufficient for the entire slug flow regime and the applied heat flux range. Figure 5.7 below illustrates the three correlations' prediction of the wall superheat at the slug-to-churn transition, together with the wall superheat required for nucleation.

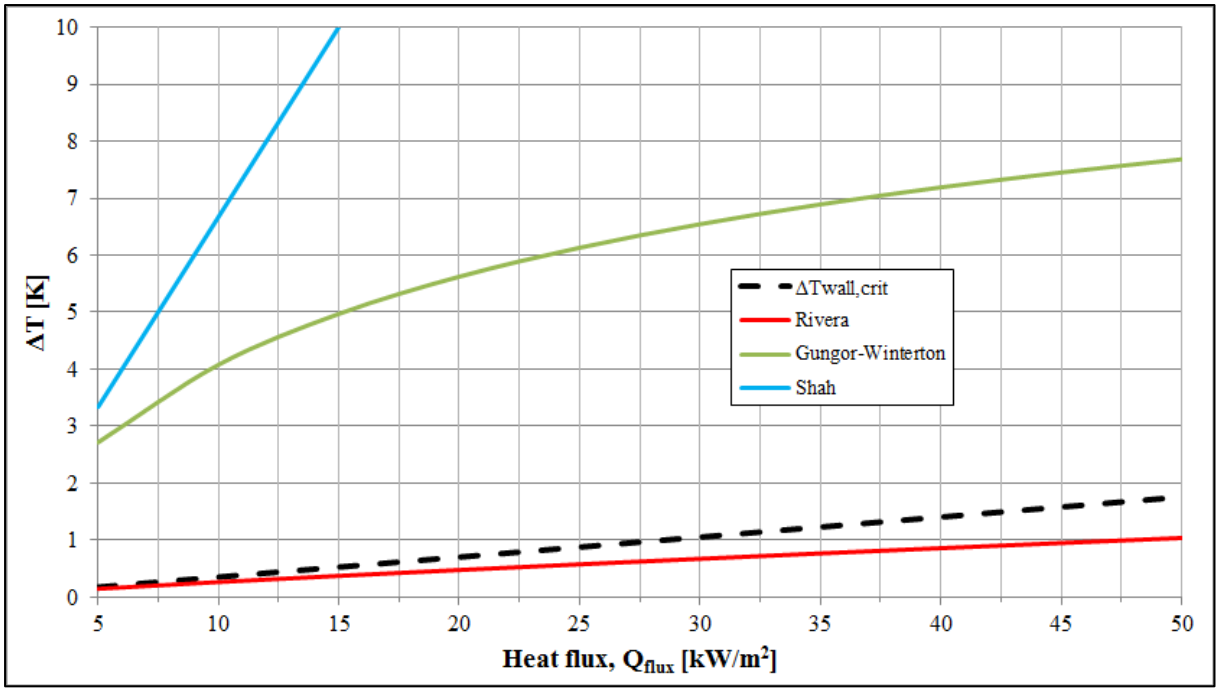

Figure 5.7 Comparison of the achieved wall superheat ($T_{wall} - T_{sat}$) against the critical wall superheat at different heat flux values, for a massflux of 10 kg/m^{2}s, a system pressure of 8 [bar] and a tube diameter of 10 [mm].

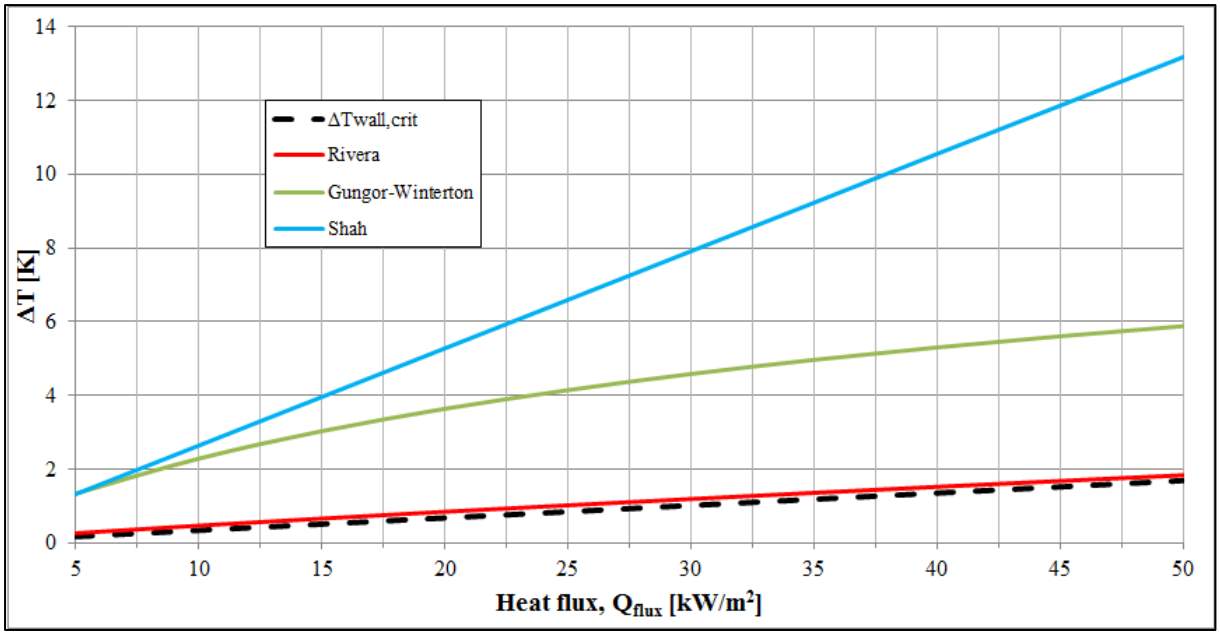

Figure 5.8 Comparison of the achieved wall superheat ($T_{wall} - T_{sat}$) against the critical wall at different heat flux values, for a massflux of 50 kg/m^{2}s, a system pressure of 8 [bar] and a tube diameter of 10 [mm].

It can be observed that the two general heat transfer correlations from Gungor-Winterton and Shah have a much higher prediction of the wall superheat than the specific correlation of River and Best.

Since the main purpose of the heat transfer coefficient is to calculate the achieved wall temperatures along the tube length, it will be interesting to compare the three selected heat transfer correlations in terms of the wall temperature. Figure 5.9 illustrates this comparison. The values for figure 5.9 was taken from a numerical study from Benhmidene *et al.* (2011) where it predicted the optimum heat flux under certain conditions. These conditions were for a cycle with a system pressure of 18 [bar], a mass flux of 50 [kg/m^{2}s] and a tube diameter of 10 [mm].

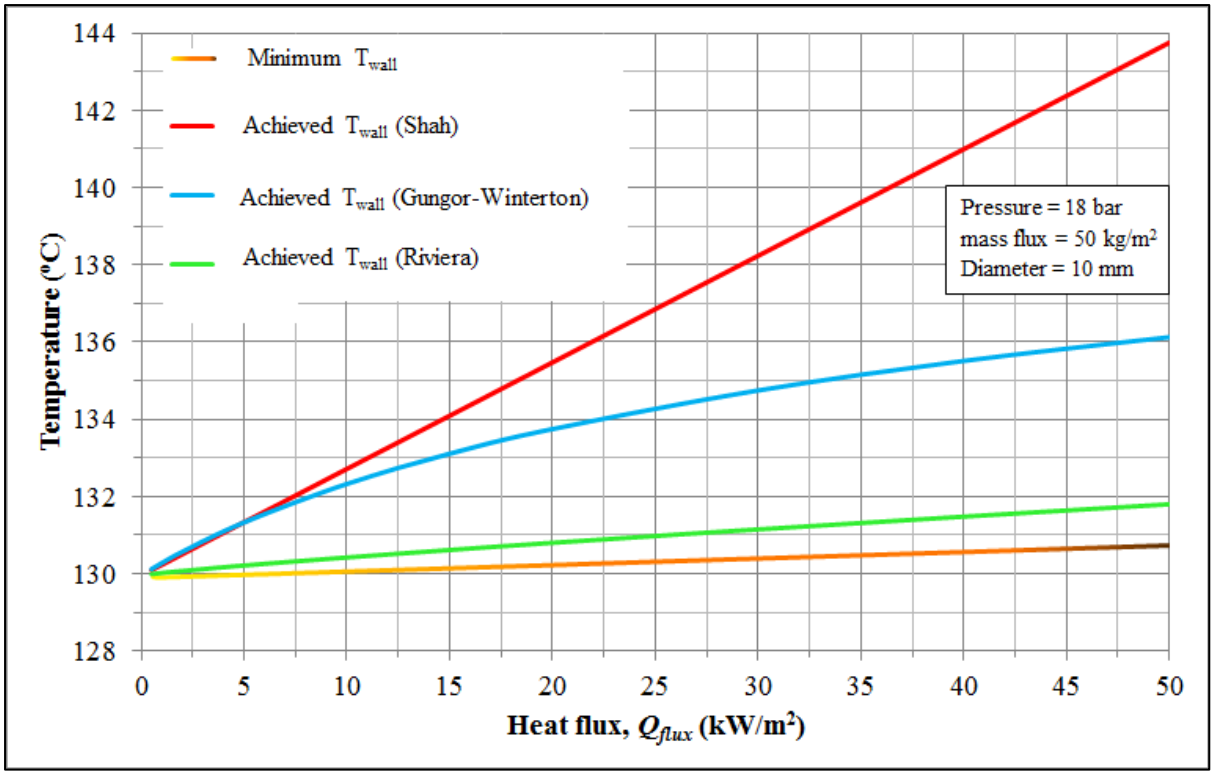

Figure 5.9 Comparison of heat transfer correlations for the achieved wall temperature against the minimum required temperature to achieve nucleation for the values in Benhmidene *et al.* (2011).

It can be seen that the correlations by Shah and Gungor-Winterton predict the wall temperature a lot higher than necessary. This can become a problem in solar-driven cycles since the heat storage device used for heating the fluid used in the generator to boil the aqua-ammonia mixture can't produce high temperatures continually due to energy constraints, and if the prediction of the required wall temperature is too high then it can cause the design to be discarded unfairly. The predicted wall temperature from the correlation of Riviera and Best is much more moderate.

Since the correlation of River and Best is the only correlation developed specifically for aqua-ammonia, it can be assumed that the correlations by Gungor-Winterton and Shah overpredict the wall superheat and thus the wall temperature, probably since both have been developed and verified mainly on azeotropic mixtures, while aqua-ammonia is a zeotropic mixture. The correlation of Rivera and Best (1999) will thus be the appropriate choice for the design of a bubble pump in cycle using aqua-ammonia as the fluid.

5.5 Length of bubble pump

The main design criteria set forth at the beginning of the research, was to ascertain the maximum height attainable at the lowest possible heat input while maintaining a decent flow rate of refrigerant. The generator will be designed according to the flow regime transition from slug to churn flow. The generator length will thus be calculated as the area of heated pipe needed in order to heat the fluid until just before it transitions to churn flow. The bubble pump length will be the length of the generator plus the length of the lift tube.

5.5.1 Effect of tube diameter on bubble pump length

The diameter of the lift tube is a very important design parameter since it is fixed once the bubble pump is installed and the diameter can't be changed like the heat flux by varying certain inputs. Unlike the heat input or system pressure which can vary under certain conditions. It must therefore be chosen at an optimum (or near optimum) for a range of pressures and heat inputs. Figure 5.10 illustrates the effect of varying the tube diameter on the height of the bubble pump.

It can clearly be seen in figure 5.10 that there is an optimum diameter for the bubble pump where it would reach a maximum pumping height, after which it would decline again. It can also be seen that the generator heat input as well as the generator height required reaches a maximum value after which it declines, however the optimum diameter differs for all three the parameters compared. Figure 5.11 shows the effect that an increase in mass flux has on the optimum tube diameter. The optimum tube diameter seems to increase with an increase in the mass flux for a constant heat flux and system pressure.

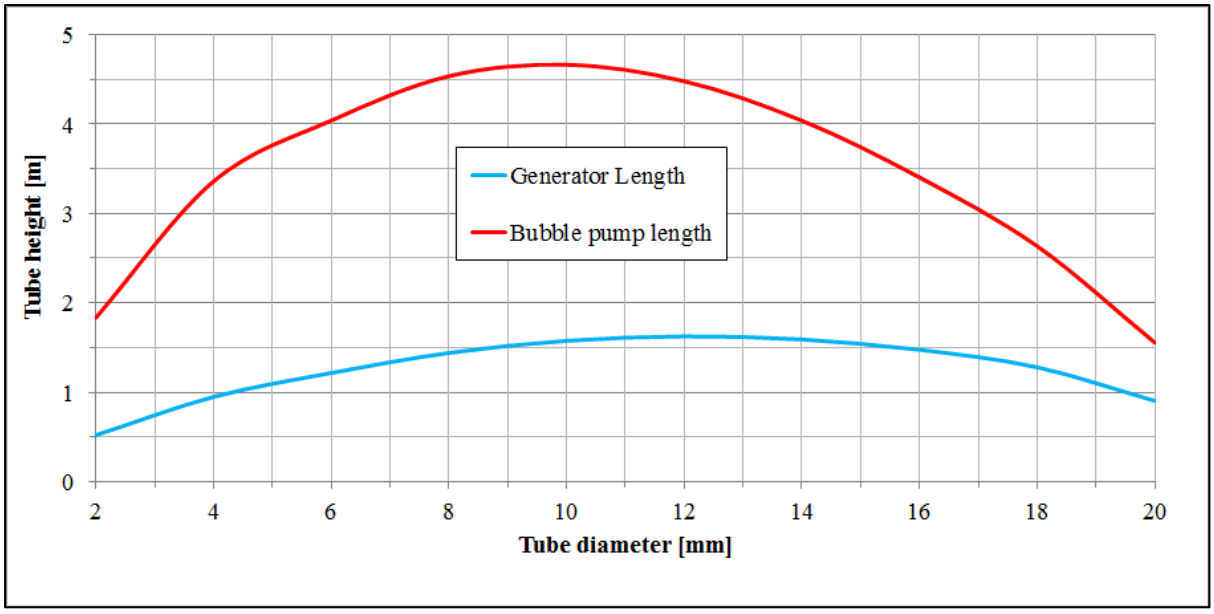

Figure 5.10 Influence of different tube diameters on the maximum lift height of the bubble pump and the generator height for a system pressure of 8 [bar], mass flux of 20 [kg/m^{2}s] and a heat flux of 10 [kW/m^2].

Figure 5.11 illustrates the effect that mass flux has on the optimum tube diameter. Where flow is throttled in the cycle, some of the bubble pumps in the cascade should rather be turned off than the flow in each lift tube be reduced or increased. If the flow is increased or reduced in individual tubes, then the tubes will not operate at an optimum.

Both Benhmidene *et al.* (2011) and Shelton & White Stewart (2002) have shown that there exists an optimum operating point for a bubble pump under certain operating conditions. Benhmidene *et al.* (2011) searched for the optimum heatflux for a certain diameter and mass flux, while Shelton & White Stewart (2002) showed that there existed an optimum diameter for a certain mass flux.

It is difficult to compare the results of the current study to Benhmidene *et al.* (2010) since they kept the total length of their test section at a fixed length of 1m in which all the flow regimes occur, while the current study searched for the bubble pump length achievable at the slug to churn transition. Benhmidene *et al.* (2010) defined the optimum operating point as the point where the velocity of the weak solution at the pump outlet is a maximum, while the current study defines it as the maximum lift height of the pump at the slug to churn transition.

A comparison of the current study to the results of Shelton & White Stewart (2002) is done in section 5.8.

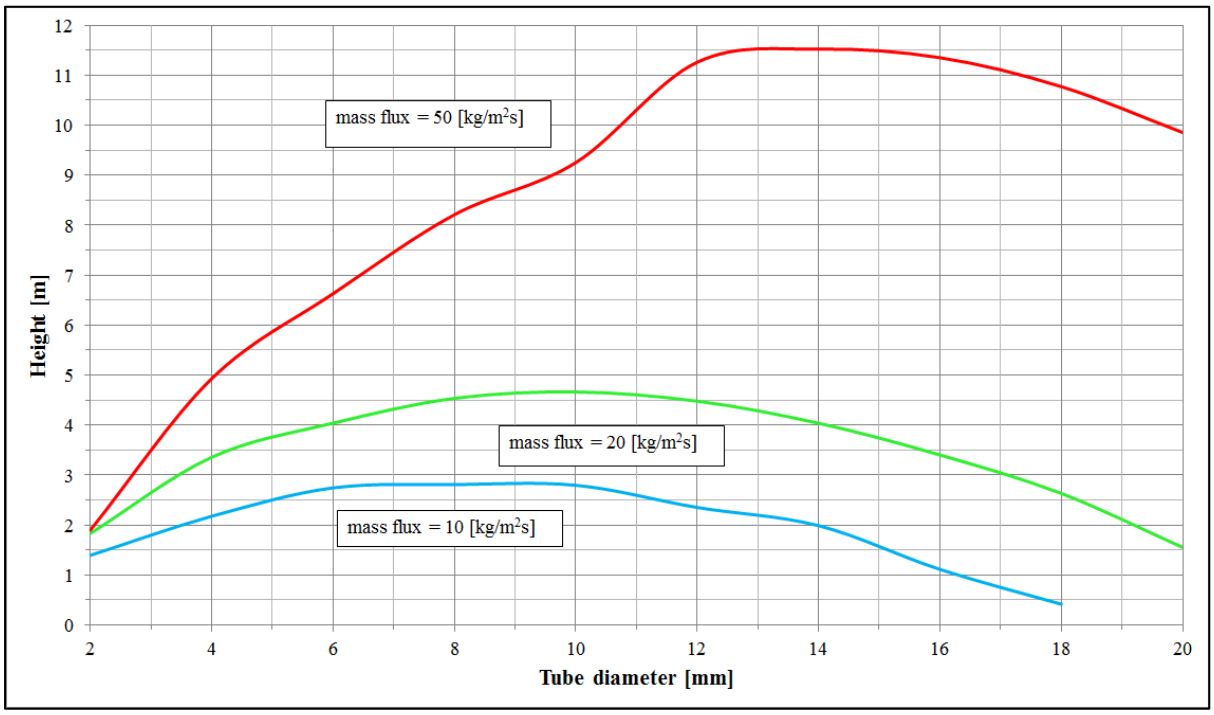

Figure 5.11 The influence of the mass flux on lift height and on the optimum diameter, for a system pressure of 8 [bar] and a heat flux of 10 [kW/m^2].

5.5.2 Effect of heat flux on bubble pump length

The heat flux is determined by the intensity at which the generator heat is applied over the generator tube surface. This intensity will be a function of the heating fluid used in the heat exchanger to transfer the heat to the generator, but generally this will be limited by the area the heat exchanger's pipe occupies around the generator. This dimensional constraint together with the physical properties of the heating fluid prevents the heat flux from being excessively high compared to an open flame (Jakob *et al.*, 2008). The effect of the heat flux on the length of the bubble pump tube is shown in figure 5.12.

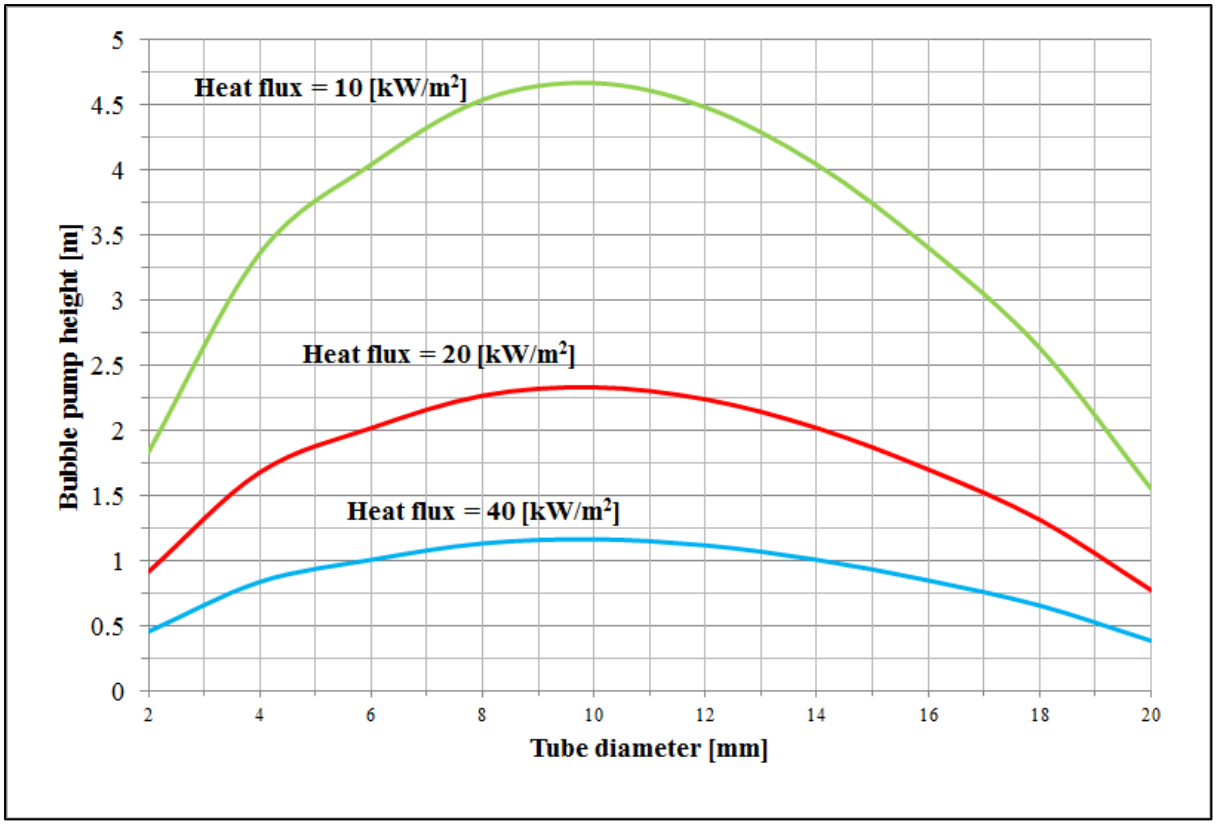

Figure 5.12 Effect of heat flux on the bubble pump length for a mass flux of 20 [kg/m^{2}s] and a system pressure of 8 [bar].

The height of the generator doubles each time the heat flux is halved, and because the submergence ratio stays the same with a change in the heat flux, the total bubble pump length also doubles as a result. Since the simulation model of the pump uses increments of vapour mass fraction (quality) to divide the pipe in sections and not equal length increments, the fluid parameters remain the same at the slug-to-churn transition and the only thing that changes due to the change in heat flux is the length of the increments of the bubble pump tube where these fluid parameters are.

It seems logical to increase the submergence height (which is equal to the generator height) to raise the bubble pump height as high as possible, but the pressure drop along the tube also has to be kept in mind, since this is not accounted for entirely in the equation used for predicting the pump height from White (2001) and Shelton & White Stewart (2002). The differences in the fluid properties brought on by the change in temperature in the generator are not incorporated. Figure 5.13 below illustrates the pressure loss in the pipe, which can be seen to

increase significantly for a heat flux smaller than 10 [kW/m^2] and drastically for a heat flux smaller than 5-6 [kW/m^2].

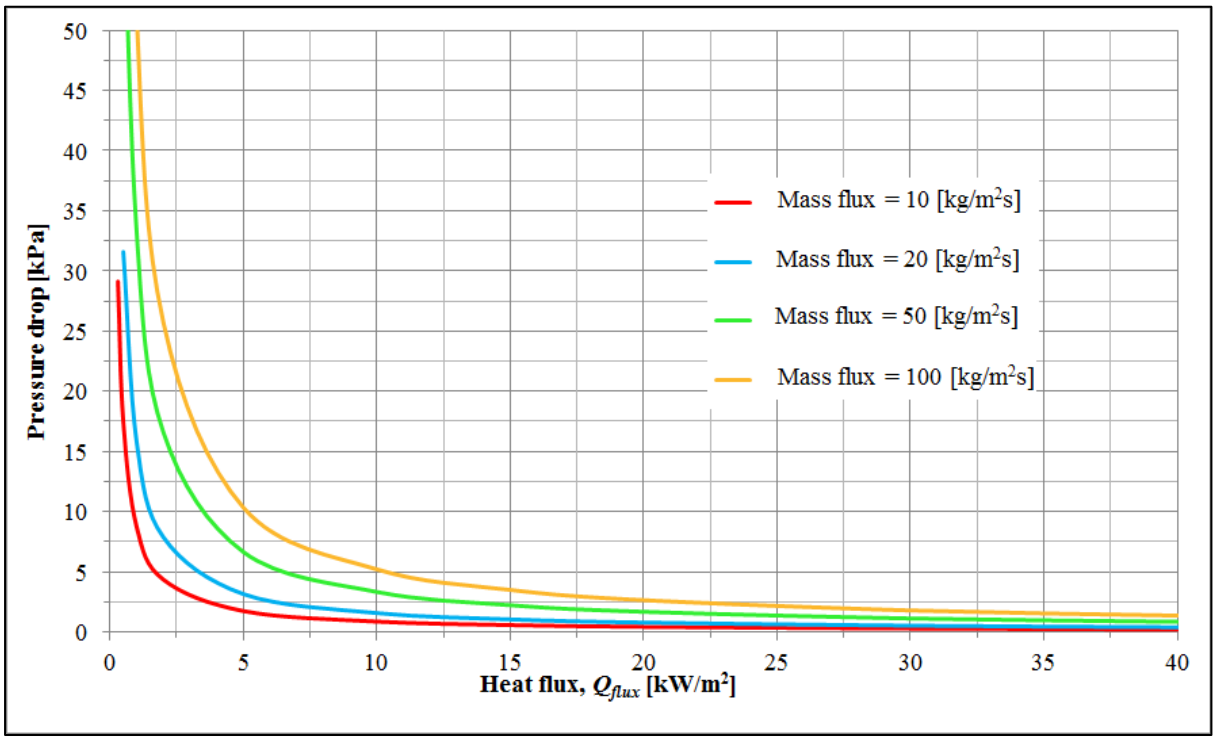

Figure 5.13 Influence of heat flux on the pressure drop at the slug-churn transition, for a mass flux of 10, 20, 50 and 100 [kg/m^{2}s], tube diameter of 10 [mm] and a system pressure of 8 [bar].

5.5.3 Effect of mass flux on bubble pump length

The mass flux, which is the mass flow per unit of cross-sectional area of the tube pipe, determines the mass flow through a certain diameter tube. It can be seen from figure 5.11 that an increase in mass flux not only increases the lift height of the tube, but it also increases the optimum diameter of the tube. The optimum diameter for a mass flux of 10 [kg/m^2] is 8 [mm], the optimum diameter for a mass flux of 20 [kg/m^2] is 10 [mm] and the optimum diameter for a mass flux of 50 [kg/m^2] is 14 [mm].

While it will seem that it is clear that a higher mass flux will produce a higher lift height, it must also be kept in mind that the fluid quality at the transition of slug to churn flow reduces with higher mass fluxes. This result in more fluid pumped with the ammonia vapour as well, which equates in more energy necessary to pump a lot of fluid for only a small gain in ammonia vapour pumped. It is thus better to choose lower mass fluxes and put in more tubes

into the bubble pump cascade than to put in fewer pumps but boost the mass flux. This will result in a smaller bubble pump tube diameter of around 10 [mm] which will be a safe choice since most heat fluxes from 10 – 50 [kg/m^{2}s] still have excellent performance for this diameter tube.

5.6 Bubble pump heat input

The bubble pump heat input is one of the most important parameters, since the heat is acquired either directly from the solar collectors or through a heat storage device which obtains its energy from solar collectors. This means that the lowest possible amount of heat must be used since the source of energy, the sun, can only be usefully tapped for about 6 hours per day in the summer, if it's not overcast. Below is a graph showing the influence of mass flux on the bubble pump heat input required and the bubble pump length, all at the slug to churn transition.

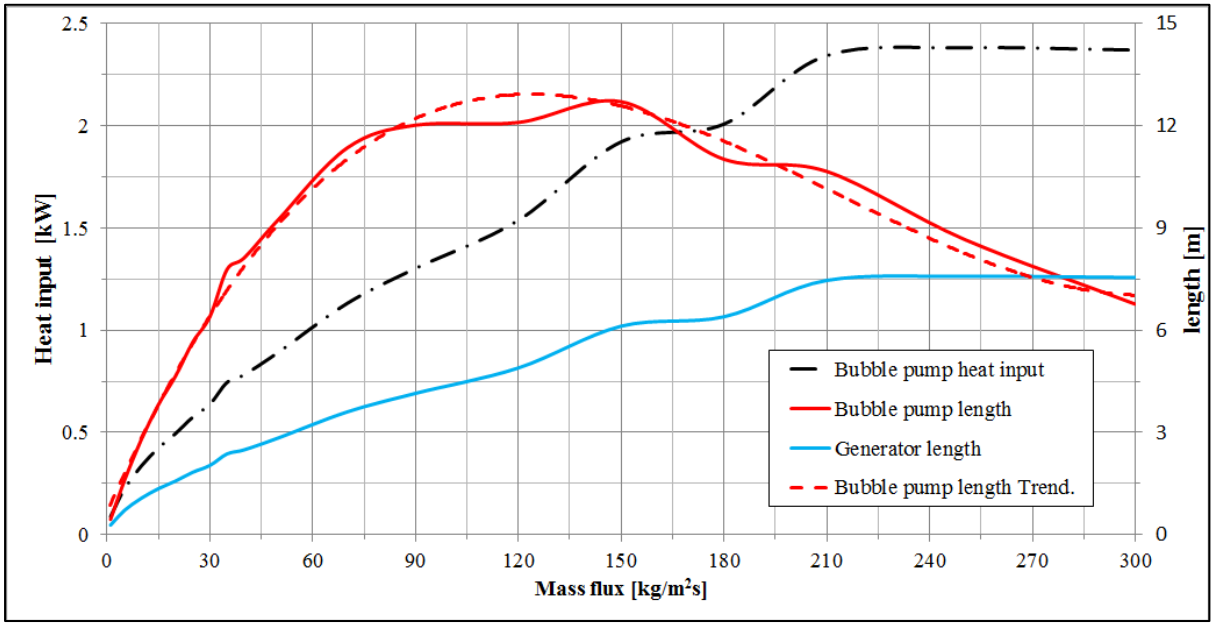

Figure 5.14 Heat input, generator length and total length of the bubble pump at various mass flux values at the slug-churn transition, for a tube diameter of 10 [mm], at a pressure of 8 [bar].

It can be seen that there is an optimum point for the bubble pump length for the given diameter, heat flux and system pressure, while the generator heat input required and the generator length reach an optimum simultaneously. For the height in the current study, the

optimum mass flux will be 20 – 30 [kg/m^{2}s] for the required height of between 4.5 [m] and 6 [m] needed for a suburban two-storey A-frame house.

It was already shown in figure 5.10 and figure 5.11 that there was an optimum tube diameter for a given mass flux, while it was shown that the heat flux only varied the tube height at the optimum tube diameter and had no effect on the optimum tube diameter. Figure 5.15 shows the effect that the tube diameter has on the generator heat input, and it can be seen that the turning point for the heat input required is well after the maximum bubble pump height is reached. This means that a smaller rather than a larger diameter tube needs to be used, since there are two diameters which can be reached for example 3 [m] in tube height: 3.5 [mm] and 17 [mm]. The 3.5 [mm] tube would require only about 0.12 [kW] of heat input, while the 17 [mm] diameter tube would require 0.75 [kW] of heat to achieve the same height.

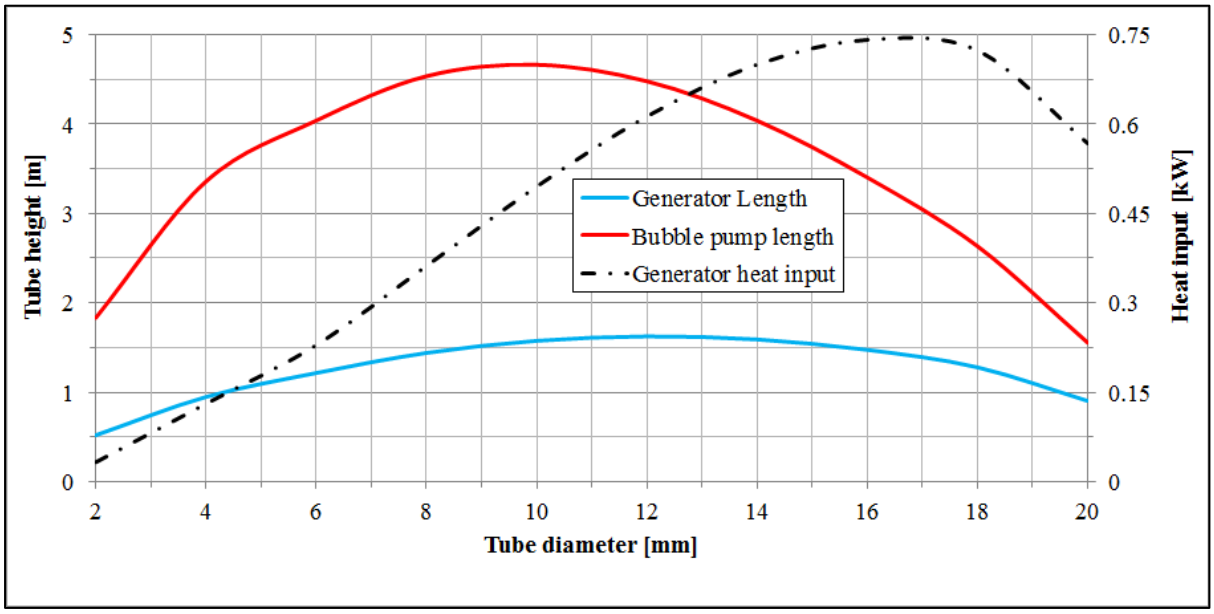

Figure 5.15 Influence of different tube diameters on the maximum lift height of the bubble pump, the generator height and the generator heat input required for a system pressure of 8 [bar], mass flux of 20 [kg/m^{2}s] and a heat flux of 10 [kW/m^2].

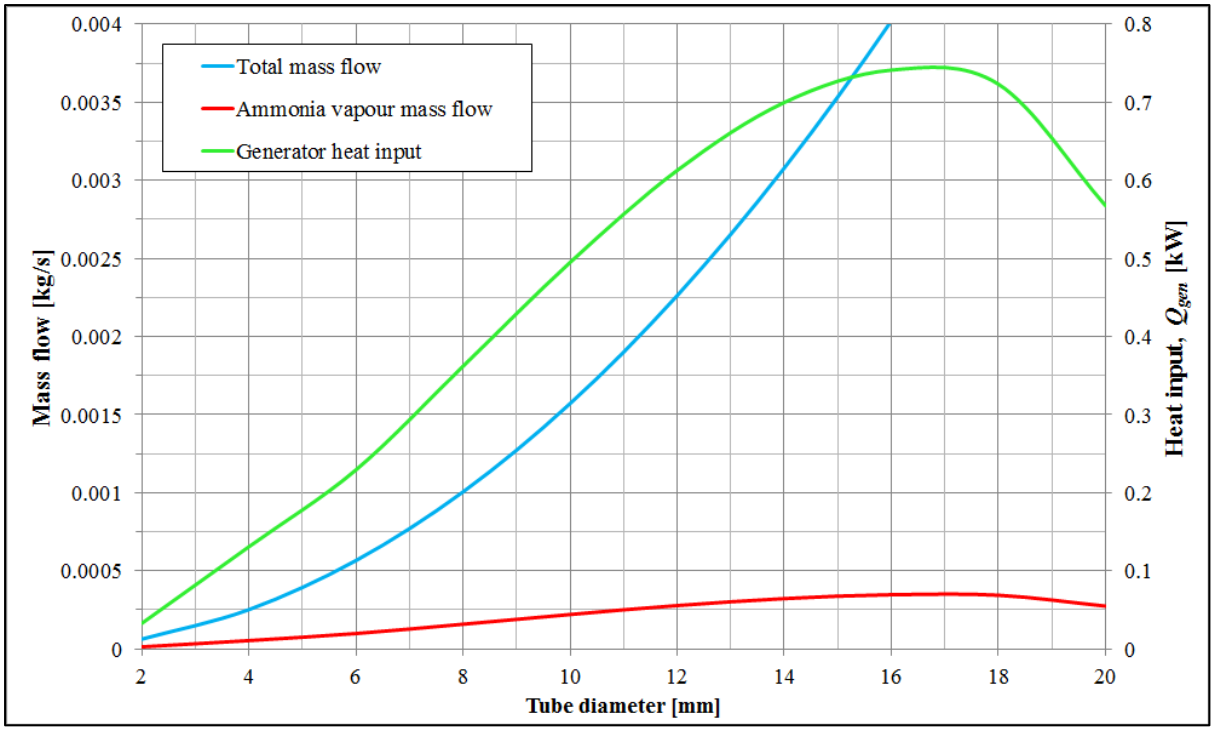

Figure 5.16 Influence of different tube diameters on the total fluid pumped and the ammonia vapour at the outlet of the pump tube for a system pressure of 8 [bar], mass flux of 20 [kg/m^{2}s] and a heat flux of 10 [kW/m^2].

Figure 5.16 shows that the 17 [mm] tube pumps a lot more total fluid than the 3.5 [mm] tube, the increase in the total ammonia vapour pumped is not so great. The ammonia vapour pumped is of more significance than the total fluid pumped, since it is the refrigerant that is needed in the condenser and the evaporator. The more total fluid is pumped with the ammonia vapour, the more energy is wasted on unnecessary pumping.

5.7 System pressure influence

If the environmental conditions change, it can affect the system pressure. Figure 5.17 shows the effect a change in system pressure has on the bubble pump lift height. A higher pressure increases the lift height of the pump, but the generator heat input required also increases, as shown in figure 5.18. While a higher system pressure produces a higher pump height, it also causes less ammonia vapour to be pump out of the tube, as seen in figure 5.19, which means that less refrigerant will circulate through the system.

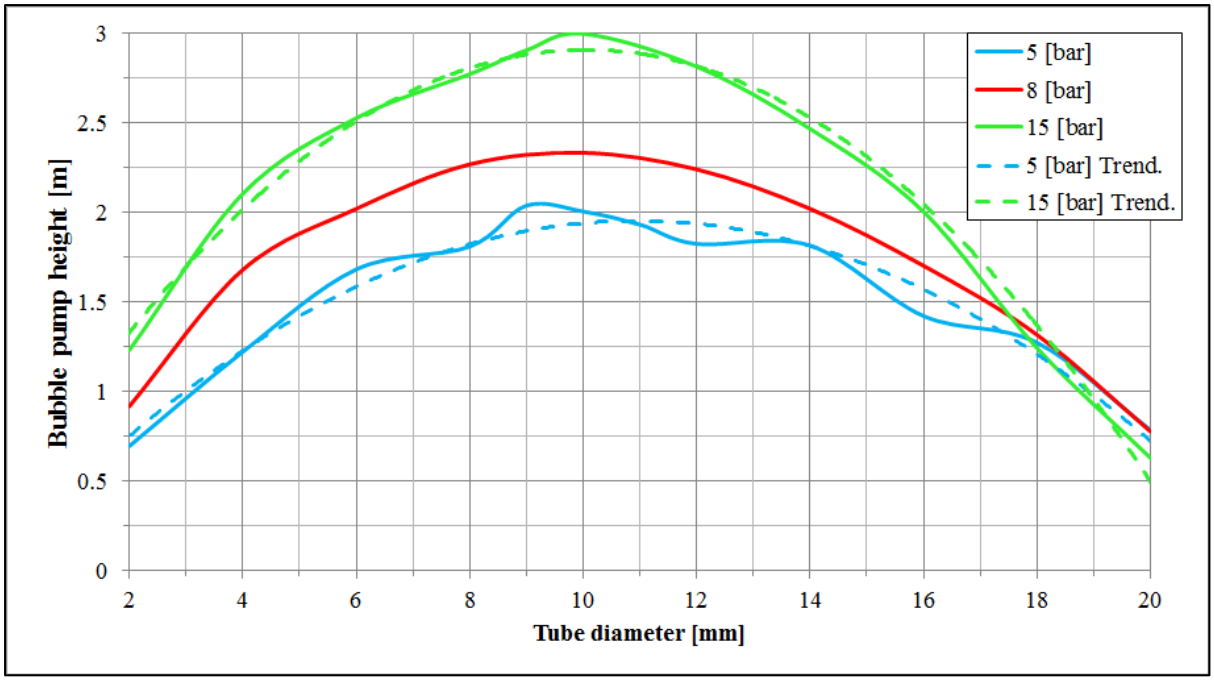

Figure 5.17 System pressure influence on the bubble pump height with varying tube diameter, for a mass flux of 20 [kg/m^{2}s] and a heat flux of 20 [kW/m^2].

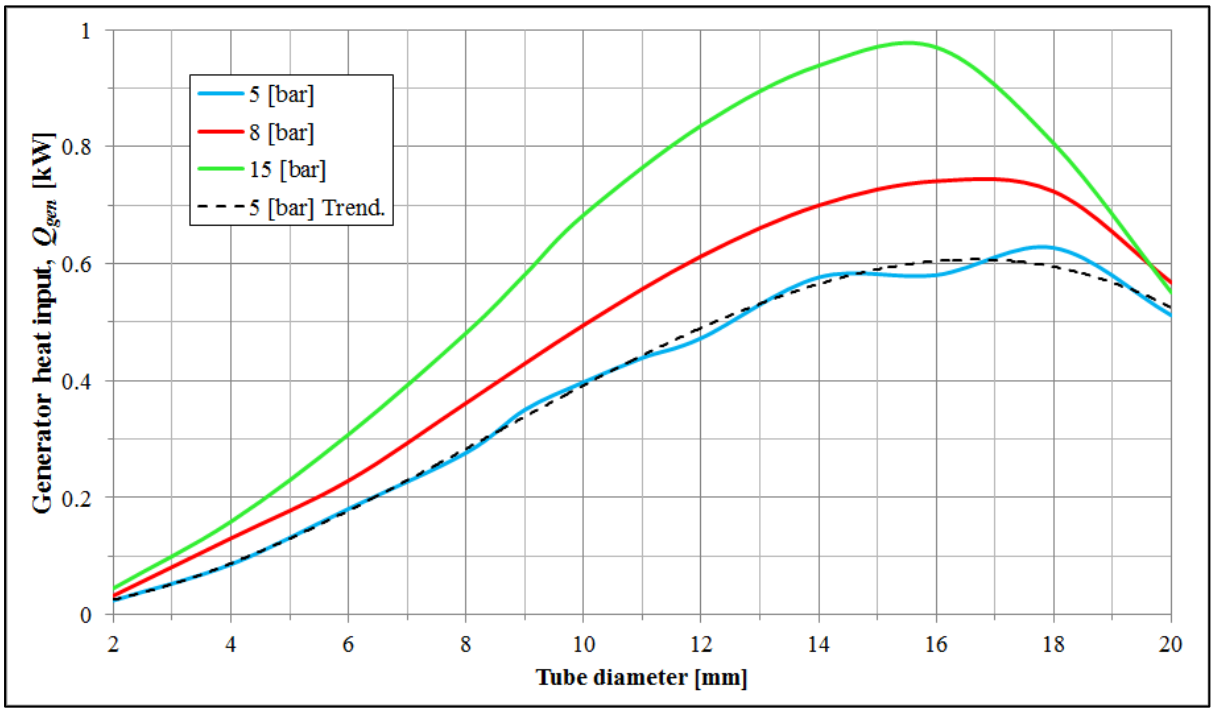

Figure 5.18 System pressure influence on the bubble pump heat input required with varying tube diameter, for a mass flux of 20 [kg/m^{2}s] and a heat flux of 20 [kW/m^2].

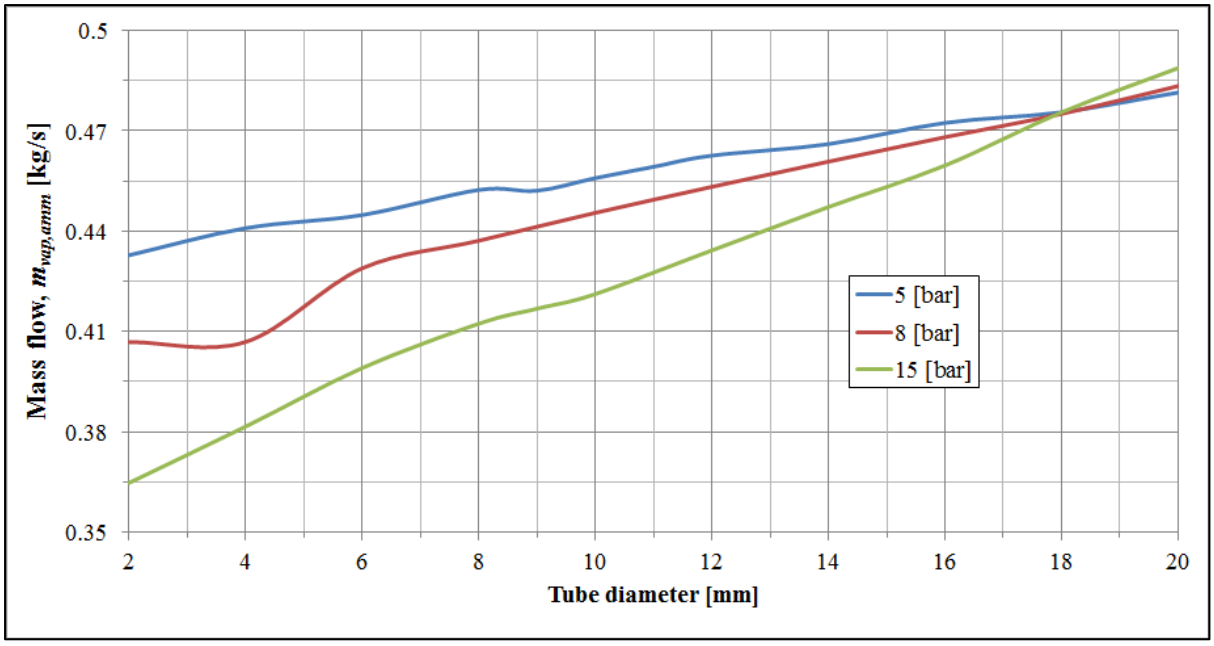

Figure 5.19 System pressure influence on the ammonia vapour produced with varying tube diameter, for a mass flux of 20 [kg/m^{2}s] and a heat flux of 20 [kW/m^2].

An increase in pressure causes the lift height of the tube to increase, it causes the mass flow of the ammonia vapour which is desorbed in the generator to decrease. This means that with an increase in pressure you need an increase in generator heat input, an increase in the saturation temperature of the aqua-ammonia mixture (as illustrated in table 5.1), an increase in the pump lift height but a decrease in the refrigerant released from the bubble pump at the optimum diameter.

5.8 Comparison of results to Shelton & White-Stewart (2002)

The research done by Shelton & White-Stewart (2002) and White (2001) showed that there was an optimum diameter for certain flow conditions, which was also shown by the current model (see figure 5.12 and figure 5.17). There was however some concern on the results of the research of Shelton & White-Stewart (2002) and White (2001). Some of their results are shown in figure 5.20.

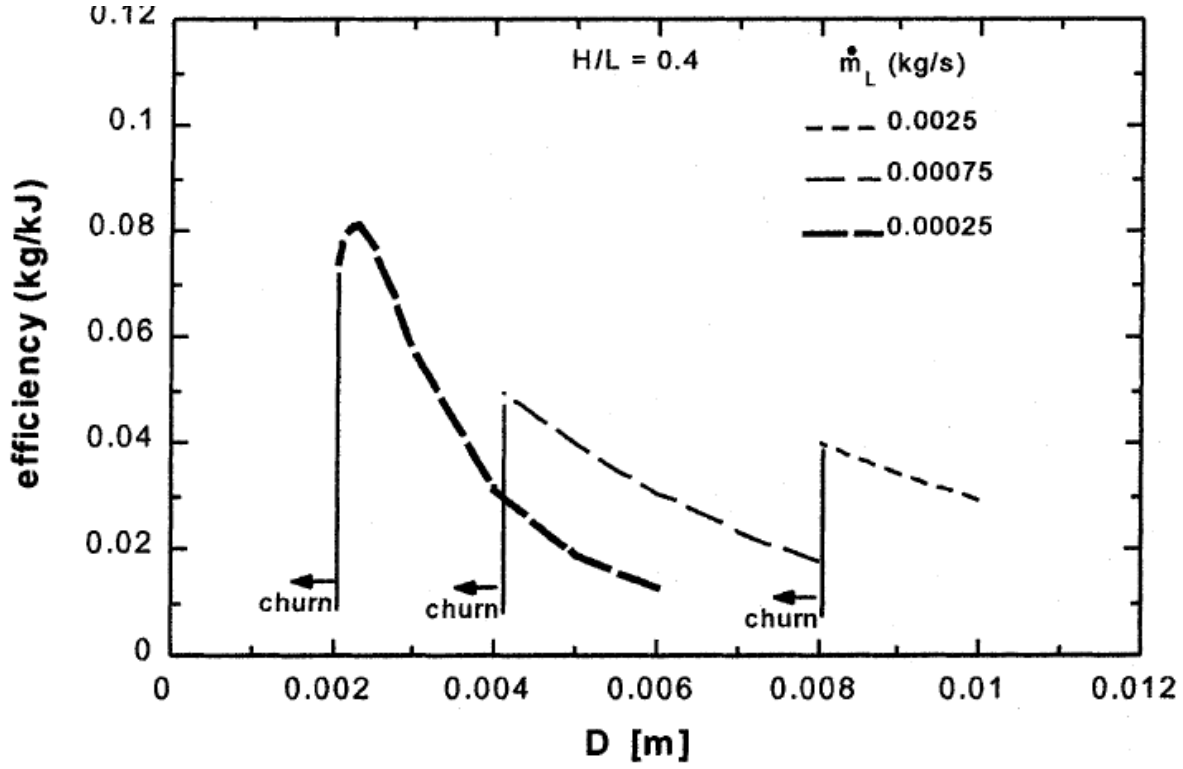

Figure 5.20 Results for the bubble pump efficiency of Shelton & White-Stewart (2002) for a ratio of 0.4, with a mixture concentration of 15.5% ammonia and a system pressure of 4 [bar].

Their results show an optimum diameter achieved at or close to the slug to churn transition, but their heat input required for the generator seemed a little low compared to the minimum heat required to heat a saturated aqua-ammonia fluid to the required two-phase conditions for slug flow as was done in the current study. The current study uses thermodynamic data from Tillner-Roth & Friend (1998) which is incorporated into the computer program REFPROP (reference fluid properties). Some of their results will be compared with the current model utilising this data at the optimum diameter. The efficiency as seen in figure 5.20 is defined as the liquid mass flow rate pumped per unit of heat input to the bubble pump.

The equation for this is given by:

$$\eta_{bp} = \frac{\dot{m}_{liquid}}{\dot{Q}_{bubblepump}} \tag{5.4}$$

The heat input to the generator can easily be calculated by manipulating the above equation:

$$\dot{Q}_{bubblepump} = \frac{\dot{m}_{liquid}}{\eta_{bp}} \qquad (5.5)$$

Table 5.4 Comparison of current model to Shelton & White-Stewart (2002).

Diameter	Mass flow	Shelton et al. (2002) heat input	Current model heat input	Shelton et al. (2002) Submergence ratio	Current model Submergence ratio	Shelton et al. (2002) Temp	Current model Temp
[mm]	[g/s]	[W]	[W]	[-]	[-]	[K]	[K]
2	0.25	3.333	37.16	0.4	0.6225	375	381.3
4.1	0.75	15	129.9	0.4	0.3287	375	382.5
8	2.5	62.5	371.6	0.4	0.2984	375	381.3
2.75	0.75	3.95	83.71	0.6	0.8931	375	379.4
5.1	2.5	14	279	0.6	0.5398	375	379.4

Table 5.5 Percentage differences between the current model and the model of Shelton & White-Stewart (2002).

Diameter	Mass flow	Current model heat input difference	Current model Submergence ratio difference	Current model Temperature difference
[mm]	[g/s]	[%]	[%]	[%]
2	0.25	1014	55.6	1.68
4.1	0.75	766	-17.8	2
8	2.5	494	-25.4	1.68
2.75	0.75	2019	48.85	1.17
5.1	2.5	182	-10.0	1.17

Table 5.4 and table 5.5 show that the calculated temperatures correlate quite well, although there are some significant differences between the submergence ratios. The calculated values of the heat input required by the bubble pump for the current study are far higher than the values obtained by Shelton & White-Stewart (2002), the differences range from 766% to 2019% as reported in table 5.5. The diameter at the transition for a submergence ratio of 0.6

for a mass flow of 0.25 [g/s] was too small for the flow rate to achieve any lift. The same was true for all the diameters at the transitions for a submergence ratio of 0.8.

According to Saisorn & Wongwises (2008) mini-channels and micro-channels can be generally classified as a channel smaller than 3 [mm] in inner diameter. The difference between a conventional channel and a micro channel is that there can be different flow patterns, void fractions deviate from general correlations used for conventional channels and velocity slip can become small. This is mainly due to the fact that surface tension and viscosity dominate due to the scale of the flow, which affects the hydrodynamics of the flow (Triplett *et al.*, 1999), (Kawahara *et al.*, 2009).

The main concern in the data from Shelton & White-Stewart (2002) was the heat input of the bubble pump needed to achieve the given flow. Since the simulation from the current study simulates the minimum energy needed for evaporation of the fluid using correlations from Tillner-Roth & Friend (1998), the values as calculated by Shelton & White-Stewart (2002) compared far too low.

5.9 Summary

A mathematical model for a single tube bubble pump for a solar-driven aqua-ammonia diffusion absorption heat pump was evaluated under various operating conditions to determine its behaviour. Below is a summary of the different observations made while testing the mathematical model which can be used as design guidelines for an optimised bubble pump design.

(a) The Rouhani-Axelsson (Rouhani I) void fraction correlation seemed better suited to the model than the Toshiba correlation, since it gave the most realistic void fractions especially at higher qualities. This probably was due to the fact that the Rouhani-Axelsson correlation used only quality and the corresponding thermophysical properties of the fluid, rather than superficial velocities and pre-determined constants.

(b) Three different heat transfer correlations were tested against each other. Only the Riviera & Best (1999) correlation was developed with aqua-ammonia in mind. This was also the only correlation to give realistic values for the heat transfer coefficient and for the predicted wall temperature over a wide range of operating conditions. The other two correlations predicted a wall temperature that could be too high for the solar heat storage system to deliver. The Riviera and Best correlation was therefore recommended.

(c) The published equation for the Riviera and Best correlation seemed to have no dimensions, and the values of the calculated heat transfer coefficients using this equation produced values far higher than the published experimental values. It was found that the addition of the liquid-only heat transfer coefficient (approximated by the Dittus-Boelter equation) produced the correct dimensions and the correct values, as shown on Figure 5.4. The authors were contacted about the potential error, but no feedback was received at the time of print.

(d) An optimum diameter was found that produced a maximum lift height for a certain mass flux and heat flux (figure 5.10 and figure 5.11).

(e) It was found that a decrease in heat flux increased the lift height, but also increased the pressure loss (figure 5.12 and figure 5.13).

(f) An increase in heat flux was found to increase the wall temperature, which could limit the design due to a maximum delivery temperature constraint caused by the solar-driven heat storage facility's maximum temperature deliverable (figure 5.9).

(g) There was an optimum diameter for a certain mass flux, heat flux and system pressure which produced the highest lift for the bubble pump (figure 5.10).

(h) It was found that an increase in mass flux resulted in an increase in the optimum diameter for a fixed system pressure and heat flux (figure 5.11). But it also resulted in a reduction of the vapour quality at the slug-churn transition, which resulted in a lot more fluid pumped for only a small increase of ammonia vapour.

(i) It was shown that there was an absolute maximum height that the bubble pump could pump at an optimum mass flux, for a fixed tube diameter, system pressure and heat flux (figure 5.14). This limits the variation in mass flux that can be applied when throttling the bubble pump.

(j) Although a larger diameter tube was shown to require more heat input, it also pumped a lot more fluid in total than a smaller diameter pipe. But the increase in ammonia vapour pumped increased only a small fraction compared to the large increase in total pumped fluid. This meant that a lot of heat input was wasted on pumping more fluid, with only small increase in refrigerant.

(k) An increase in system pressure was shown to result in an increase in generator temperature (table 5.1), bubble pump lift height and generator input required, but gave a lower mass flow of ammonia vapour (the refrigerant) pumped than at lower pressures at and around the optimum diameter (figure 5.17, figure 5.18 and figure 5.19).

Since the current bubble pump model is intended as a general design model, no specific optimised design values are given for a single set of conditions, but rather recommendations and guidelines on making certain choices under different operating conditions. This will ensure that the bubble pump will be optimised for various conditions, rather than just one optimised condition. This bubble pump model needs to be used in conjunction with a mathematical model for the entire cycle, to observe the complete impact of the varying parameters. The pump is intended to be cascaded in a bundle of multiple bubble pumps for an increased output.

6. Conclusions and recommendations

6.1 Introduction

Higher electricity demands and the inability of the electricity suppliers to satisfy the growing demand have caused researchers to explore alternative means of energy, especially energy that is utilised in heating and refrigeration. The most attractive prospect is the development in solar energy in South Africa because of its high annual solar radiation and light influx. If the solar energy could be coupled with a heating and cooling device for domestic use, it would reduce the load on the electricity suppliers.

The objective was to design a model for a bubble pump for a domestic solar-driven aqua-ammonia diffusion absorption heat pump and determine the height that the bubble pump could deliver. The minimum height should be the height of a general suburban home in South Africa.

6.2 The model in general

A simulation model for a bubble pump was developed using separated two-phase flow theory. This model incorporated thermophysical data from Tillner-Roth & Friend (1998) and the pump tube was divided into segments of known quality and unknown length to ensure the calculation was strictly only from saturated liquid to saturated vapour. The model also incorporated a two-phase heat transfer coefficient especially developed by Riviera & Best (1999) for aqua-ammonia under the conditions similar to the simulated conditions instead of the older heat transfer coefficient from Chen which is normally used. Flow regime correlations from Samaras & Margaris (2005) were also introduced to ensure that flow remained in the optimum slug flow region.

The model used the bubble pump tube diameter, total mass flux of the strong solution (strong in ammonia) and the heat flux as inputs to produce the outputs. The main outputs were the required generator heat input to produce slug flow, the required height of the generator, the maximum length of the bubble pump, the flow regime in each segment of pipe and the mass flows, especially the vapour mass flow of ammonia.

This model's approach was unique in that it calculated the generator height, submergence ratio necessary and the lift tube height as functions of the tube diameter, total mass flux and heat flux. Other models used the submergence ratio, generator tube and lift tube height as inputs to calculate the heat input necessary. This model proved more useful as a design model for a bubble pump since it calculated the optimum heights of the lift tube, generator tube and the submergence ratio necessary for the given conditions. This ensured optimised values for the tube heights and heat inputs. If it was done the other way round like most other models, the relationship of the lift and generator tubes, the submergence ratio and the generator heat input could prove not ideal for the conditions.

The use of quality rather than length to divide the segments of pipe was also unique in a bubble pump model, which assisted in the optimisation of the bubble pump tube height. Since the height was calculated according to the flow development, and not the other way around. This ensured that no presuppositions on pump height hindered the investigation. This method also ensured the accuracy of the flow data since it was always known at the segment, and it was never necessary to extrapolate or interpolate the thermophysical properties.

6.3 Comparison with other models

Since this model is unique in its approach to the different parameters (e.g. calculating the generator heat input, generator length, lift tube length and especially submergence ratio, rather than specifying a fixed submergence ratio) it was impossible to completely verify or compare this model with other models.

The model was compared with the bubble pump model from Shelton & White-Stewart (2002). The temperature, submergence ratio and generator heat input were compared at a specified mass flow and tube diameter at the slug-churn transition. It was found (see table 5.5) that the temperature was within a 2% of each other, the submergence ratios had a difference of 10% at larger diameters but was inaccurate at very small diameters with a difference of 55.6% at 2mm diameter. The heat input necessary to produce their flow was unrealistically low, shown to be at least 7.5 times smaller and up to 20 times smaller than the minimum heat input necessary obtained from Tillner-Roth & Friend (1998) thermodynamic correlations.

It was also observed that the optimum diameters proposed for the bubble pump was too small for conventional two-phase flow which meant that it was classified as mini- and micro tubes. The flow in these tubes was known to be different from conventional two-phase flow as the viscosity and the surface tension of the fluid dominated the flow.

The heat transfer coefficient was calculated at exactly the same tube heights and input parameters as was done in the experimental setup of Riviera & Best (1999). It was found that the heat transfer coefficient was almost ten times higher than the measured heat transfer coefficient at the low heat fluxes as done in the experiments. It was found that the published equation of the heat transfer correlation was dimensionless. It was only after the equation was modified and the liquid-only heat transfer coefficient (approximated by the Dittus-Boelter equation) was added that the simulated heat transfer coefficients correlated almost perfectly with the published experimental values. This was also a testament to how accurate the thermophysical data from Tillner-Roth & Friend (1998) was.

6.4 Results and general remarks from the simulation model

The simulation model was intended as a general design model to ensure that it can be used under a variety of design conditions, rather than an optimised model catering only for a single set of conditions. The model proved flexible in the wide variety of parameters it could give as outputs.

It was found that the void fraction correlation from Rouhani-Axelsson (Rouhani I) was more suited than the Toshiba correlation due in part to the zeotropic nature of the aqua-ammonia fluid under pressure and the thermophysical properties the Rouhani-Axelsson (Rouhani I) correlation used to determine the void fractions, rather than velocities and general constants.

The heat transfer correlation of Riveira and Best (1999) was shown to be better suited to the cycle's design and optimisation, while the correlations of Gungor-Winterton and Shah (as given in Thome (2010)) seemed to over-predict the wall temperatures, which would cause the solar-driven heat storage device to produce the heating fluid at a higher temperature than necessary. One of the results from Benhmidene *et al.* (2011) was used as a case study to illustrate this point (see figure 5.9).

It was shown that there existed an optimum point where a certain diameter would yield a maximum lift height for the bubble pump. Studies by Shelton & White-Stewart (2002) and Benhmidene *et al.* (2011) also came to the conclusion that there was an optimum diameter for a certain set of conditions.

Parameters such as heat flux and mass flux was shown that it also affected the maximum lift height of the bubble pump tube. Mass flux in particular also affected the optimum diameter.

An absolute maximum lift height for a certain mass flux was shown to exist for a system with a fixed tube diameter, a fixed system pressure and a fixed heat flux.

It was found that a larger diameter bubble pump pipe as well as a larger mass flux pumped more total fluid, but the increase in vapour ammonia (the refrigerant) desorbed was minimal compared to the total fluid pumped. This meant that energy would be wasted with higher diameters and mass fluxes by pumping a higher percentage of unwanted fluid compared to refrigerant pumped.

An increase in system pressure caused an increase in the generator temperature, the pump height and the generator heat input needed, but it resulted in a higher total fluid pumped. The refrigerant (ammonia vapour) that was desorbed at higher pressures, however, was less than at lower pressures.

This model introduced another unique approach, by dividing the bubble pump tube into segments of known quality, rather than known length. This approach made it easier to design for and interpret the flow parameters. It was also easier to see the effect of varying certain parameters (like the mass flux) on the length of the tube, since you do not constrain the tube length by specifying the length increments.

6.5 Recommendations for further study

The current bubble pump model needs to be used in conjunction with a simulation of the full solar-driven aqua-ammonia diffusion absorption cycle. It is only then that the full impact of the varying parameters can be evaluated in a meaningful way.

This model is by no means complete, and will benefit a lot by developing it further alongside a practical test model, although it would be extremely expensive. But this model would hopefully lay the groundwork for further study in this field, by showing that it is better to specify less data in order to optimise more parameters, than constraining the model by specifying too much data. This was the problem in recent studies, where the tube length, the submergence ratio and the generator heat input was specified (among others) as a design input, which rather should be output parameters affected by certain other input parameters.

The model can be expanded on by including detailed conduction (when a certain material is selected for the assembly) as well as sub-cooled boiling effects, if it is found that the bubble pump pre-heater(s) cannot produce saturated liquid strong solution at the bubble pump inlet.

A more detailed correlation for determining the lift tube height needs to be developed. The current correlation used for determining the lift tube height from the generator height and certain other inputs, is one adapted from White (2001) and Shelton & White Stewart (2002). Although they developed the model especially for aqua ammonia in a bubble pump, it has certain shortcomings:

- This correlation was developed from test data obtained from an air-lift pump operating at adiabatic conditions under room temperature. One of the problems with this was that the liquid mass flow entering the bubble pump was the same as the liquid mass flow exiting the bubble pump. This is true for an air-lift pump, where external air is pumped into the tube to induce two-phase flow, but it is not true for a bubble pump, where the liquid entering the bubble pump is heated and the vapour is released from the fluid, reducing the liquid mass flow.
- Another problem was the assumption that the heat transfer area on the tube was minimal, almost not existent, since in an air-lift pump the amount of air needed for a certain flow regime is pumped in and the desired flow regime is achieved almost instantly. In a bubble-pump setup the boiling of the fluid requires a certain area to increase the quality and flow velocity enough to induce the desired flow, this is especially important in a solar-driven cycle where the heat flux is not as high, and a

larger area (which equates to a longer section of pipe) is needed to boil off the vapour and induce the two-phase flow.

- Another very important factor that wasn't accounted for, was the fact that aqua-ammonia is a zeotropic fluid, which means that its saturation temperature increase with an increase in vapour quality. The correlation assumes that the temperature stays constant. This was accounted for in a way by including the thermophysical properties of the fluid at slug flow conditions into the correlation, and not just the inlet conditions of the bubble pump.

The current model needs to be developed further to accommodate multiple bubble pumps and its effects. Such a bubble pump cascade was found by Vicatos & Bennet (2007) to increase heating and refrigeration capacity, which is essential if it is to be incorporated into a larger-scale cycle for domestic use.

7. Bibliography

ATKINSON SCHAEFER, L. 2000. *Single pressure absorption heat pump analysis*. Atlanta: Georgia Institute of Technology.

AWAD, M.M. & MUZYCHKA, S.Y. 2008. Effective property models for homogeneous two-phase flows. *Experimental Thermal and Fluid Science*

BEN EZZINE, N., GARMA, R., BOUROUIS, M. & BELLAGI, A. 2010. Experimental studies on bubble pump operated diffusion absorption machine based on light hydrocarbons for solar cooling. *Renewable Energy*:464-470.

BENHMIDENE, A., CHAOUACHI, B. & GABSI, S. 2010. A Review of Bubble Pump Technologies. *Journal of Applied Sciences*:1806-1813.

BENHMIDENE, A, CHAOUACHI, B, GABSI, S & BOUROUIS, M. 2011. Modelling of heat flux received by a bubble pump of absorption-diffusion refrigeration cycles. *Heat Mass Transfer*:1341–1347.

BHAGWAT, S.M. & GHAJAR, A.J. 2012. Similarities and differences in the flow patterns and void fraction in vertical upward and downward two phase flow. *Experimental Thermal and Fluid Science*:213-227.

CHAOUACHI, B. & GABSI, S. 2007. Design and Simulation of an Absorption Diffusion Solar Refrigeration Unit. *American journal of applied sciences*, 4(2):85-88.

CHEN, J., KIM, K.J. & HEROLD, K.E. 1996. Performance enhancement of a diffusion-absorption refrigerator. *International Journal of Refrigeration*, 19:208-218.

CODDINGTON, P. & MACIAN, R. 2002. A study of the performance of void fraction correlations used in the context of drift-flux two-phase flow models. *Nuclear Engineering and Design*:199-216.

DALKILIC, A.S. & WONGWISES, S. 2010. New experimental approach on the determination of condensation heat transfer coefficient using frictional pressure drop and void fraction models in a vertical tube. *Energy Conversion and Management*:2535-2547.

DELANO, A.D. 1998. *Design analysis of the Einstein refrigeration cycle*. Atlanta: Georgia Institute of Technology.

HEROLD, K.E., RADERMACHER, R. & KLEIN, S.A. 1996. Absorption Chillers and Heat Pumps. Boca Raton: CRC Press.

JAKOB, U., EICKER, U., SCHNEIDER, D., TAKI, A.H. & COOK, M.J. 2008. Simulation and Experimental Investigation into Diffusion Absorption Cooling Machines for Air-Conditioning Applications. *Applied Thermal Engineering*:1138-1150.

KAWAHARA, A., MICHIO, S., NEI, K. & MATSUO, H. 2009. Experimental study on bubble velocity, void fraction and pressure drop for gas–liquid two-phase flow in a circular microchannel. *International Journal of Heat and Fluid Flow*, 30:831–841.

KOYFMAN, A., JELINEK, M., LEVY, A. & BORDE, I. 2003. An experimental investigation of bubble pump performance for diffusion absorption refrigeration system with organic fluids. *Applied Thermal Engineering*:1881-1894.

MARKS, L.S. 1944. Mechanical Engineers' Handbook. New York: McGraw-Hill Book Company.

MENYAH, K. & WOLDE-RUFAEL, Y. 2010. Energy Consumption, Pollutant Emissions and Economic Growth in South Africa. *Energy Economics*:1374-1382.

PFAFF, M., SARAVANAN, R., M.M., Prakash & SRINIVASA MURTHY, S. 1998. Studies on bubble pump for a water-lithium bromide vapour absorption refrigerator. *International Journal of Refrigeration*:452-462.

RIVIERA, W. & BEST, R. 1999. Boiling heat transfer coefficients inside a vertical smooth tube for water/ammonia and ammonia/lithium nitrate mixtures. *Interantional Journal of Heat and Mass Transfer*:905-921.

ROHSENOW, W.M., HARTNETT, J.P. & GANIC, E.N. 1985. Handbook of heat transfer fundamentals. New-York: McGraw-Hill Book Company.

ROUSSEAU, P.G. 2010. Thermal-fluid systems modelling II. Potchefstroom: North-West University.

SAISORN, S. & WONGWISES, S. 2008. A review of two-phase gas–liquid adiabatic flow characteristics in micro-channels. *Renewable and Sustainable Energy Reviews*, 12(3):824-838. April.

SAMARAS, V.C. & MARGARIS, D.P. 2005. Two-phase flow regime maps for air-lift pump vertical upward gas–liquid flow. *International Journal of Multiphase Flow*:757-766.

SHAH, M.M. 1982. Chart Correlation for Saturated Boiling Heat Transfer: Equations and Further Study. *ASHRAE Transactions*, 88(1):185-196.

SHAH, M.M. 2006. Evaluation of general correlations for heat transfer during boiling of saturated liquids in tubes and annuli. *HVAC&R Research*, 12(4):1047-1063. October.

SHELTON, S.V. & WHITE-STEWART, S.J. 2002. Bubble pump design for single pressure absorption refrigeration cycles. *ASHRAE Transactions*, 108

SONNTAG, R.E., BORGNAKKE, C. & VAN WYLEN, G.J. 2003. Fundamentals of Thermodynamics. Hoboken: John Wiley & Sons.

SÖZEN, A., ALTIPARMAK, D. & USTA, H. 2002. Development and testing of a prototype of absorption heat pump system operated by solar energy. *Applied Thermal Engineering*:1847-1859.

SPEDDING, J.L., WOODS, G.S., RAGHUNATHAN, R.S. & WATTERSON, J.K. 1998. Vertical two-phase flow - Part 1: Flow regimes. *Trans IChemE*, 76

THEUNISSEN, R. 2011. *Investigation of a radiative cooling system with natural circulation for regulating a heat sink.* Potchefstroom.

THOME, J.R. 2010. Wolverine Heat Transfer Engineering Data book III. Decatur: Wolverine Tube, Inc.

TILLNER-ROTH, R. & FRIEND, D.G. 1998. A Helmholtz free energy formulation of the thermodynamic properties of the mixture (water + ammonia). *J. Phys. Chem. Ref. Data*, 27(1):63-96.

TRIPLETT, K.A., GHIAASIAAN, S.M., ABDEL-KHALIK, S.I., LEMOUEL, A. & MCCORD, B.N. 1999. Gas±liquid two-phase flow in microchannels Part II: void fraction and pressure drop. *International Journal of Multiphase Flow*, 25:395±410.

VICATOS, G. & BENNET, A. 2007. Multiple lift tubes boost refrigeration capacity in absorption plants. *Journal of Energy in Southern Africa*:49-57.

VON PLATEN, B.C. & MUNTERS, C.G. 1928. *Refrigerator*. 1,685,764.

WHITE, S.J. 2001. *Bubble Pump Design and Performance*. Atlanta.

WOLDESEMAYAT, M.A & GHAJAR, A.J. 2006. Comparison of void fraction correlations for different flow patterns in horizontal and upward inclined pipes. *International journal of multiphase flow*, 33:347-370.

ZHANG, L., WU, Y., ZHENG, H., GUO, J. & CHEN, D. 2006. An experimental investigation on performance of bubble pump with lunate channel for absorption refrigeration system. *International Journal of Refrigeration*:815-822.

ZIEGLER, F. 1999. Recent developments and future prospects of sorption heat pump systems. *International Journal of Thermal Science*:191-208.

ZOHAR, A., JELINEK, M., LEVY, A. & BORDE, I. 2005. Numerical investigation of a diffusion absorption refrigeration cycle. *International Journal of Refridgeration*, 28:515-525.

ZOHAR, A., JELINEK, M., LEVY, A. & BORDE, I. 2007. The Influence of Diffusion Absorption Refrigeration Cycle Configuration on the Performance. *Applied Thermal Engineering*:2213-2219.

ZOHAR, A., JELINEK, M., LEVY, A. & BORDE, I. 2008. The influence of the generator and bubble pump configuration on the performance of diffusion absorption refrigeration (DAR) system. *International Journal of Refrigeration*:962-969.

8. Appendix A – Simuation model

```
"!FUNCTIONS BEFORE MAIN PROGRAM"
Function Constant(D, L)                    "Function to determine the constant needed in
                                            the function for determining the slug to churn flow
                                            transiton"

    If (L / D) > 120 then
                                                        m = 0.96
                                            Else
                                                        m = 0.1928 +
0.01089 * (L / D) - 3.754 * 10^(-5) * (L / D) ^2
    Endif

    Constant = m

End
"-----------------------------------------------------------------------------------------------------------------------
---------------"
Function Pressure_wall(T_wall)  "Function to determine the corresponding liquid saturation pressure
                                 for T_wall"
    Duplicate i = 1,31
                                            T_function[i] = 330 + (i-1)*5
    End

j=0
    repeat
                                            j=j+1
    Until (T_wall<T_function[j])

T_interpolate1 = T_function[j-1]
T_interpolate2 = T_function[j]
P_interpolate1 = Lookup('Lookup 3', 1,(j-1))
P_interpolate2 = Lookup('Lookup 3', 1,j)
P_wall = (P_interpolate2 - P_interpolate1) / (T_interpolate2 - T_interpolate1) * (T_wall -
T_interpolate1) + P_interpolate1

Pressure_wall = P_wall
"-----------------------------------------------------------------------------------------------------------------------
---------------"
End

Function Pressure_sat(T_sat)
    Duplicate i = 1,31
                                            T_function[i] = 330 + (i-1)*5
    End

j=0
    repeat
                                            j=j+1
    Until (T_sat<T_function[j])

T_interpolate1 = T_function[j-1]
T_interpolate2 = T_function[j]
P_interpolate1 = Lookup('Lookup 3', 1,(j-1))
P_interpolate2 = Lookup('Lookup 3', 1,j)
P_sat = (P_interpolate2 - P_interpolate1) / (T_interpolate2 - T_interpolate1) * (T_sat - T_interpolate1)
+ P_interpolate1
```

```
Pressure_sat = P_sat
End
"-------------------------------------------------------------------------------------------------------------------------------"
Function SHAH(N, Bo, h_htc_liq, h_htc_CB)
      If (Bo>0.0011) Then
                                                F_s = 14.7
                                                Else
      If (Bo<0.0011) Then
                                                F_s = 15.43
                                                Endif
      Endif


      If (N>1) and (Bo>0.0003) Then
                                                h_htc_NB = h_htc_liq * 230 * Bo^0.5
                                                Else
      If (N>1) and (Bo<0.0003) Then
                                                h_htc_NB = h_htc_liq * (1+46 * Bo^0.5)
                                                Else
      If (N<1) and (N>0.1) Then
                                                h_htc_NB = h_htc_liq * F_s * Bo^0.5*exp(2.74*N-
0.1)
                                                Else
      If (N<0.1) Then
                                                h_htc_NB = h_htc_liq * F_s * Bo^0.5*exp(2.74*N-
0.15)
                                                                Endif
                                                Endif
      Endif
Endif

      If (h_htc_NB > h_htc_CB) Then
                                                h_htc_tp = h_htc_NB
                                                Else
      h_htc_tp = h_htc_CB
Endif

SHAH = h_htc_tp
"-------------------------------------------------------------------------------------------------------------------------------"
End

Function f_liquid (Re)

If    (Re < 2000) and (Re > 0) then
      f = 16 / Re
                                                Else
If    (Re >= 2000) then
      f = 0.079 / Re^0.25
                                                Else
      f = 0
      Endif
Endif
f_liquid = f

End
"-------------------------------------------------------------------------------------------------------------------------------"
```

```
Function f_vapour (Re)

If    (Re < 2000) and (Re > 0) then
      f = 16 / Re
                                                    Else
If    (Re >= 2000) then
      f = 0.079 / Re^0.25
                                                    Else
      f = 0
      Endif
Endif
f_vapour = f

End
"-------------------------------------------------------------------------------------------------------------------------------"
Function FLOWREGIME$(epsilon, epsilon_BubSlug, epsilon_SlugChurn, epsilon_ChurnAnn,
epsilon_AnnWispy)

      If (epsilon < epsilon_BubSlug) Then
                                                    A$ = 'Bubbly'
                                                    Else
      If (epsilon > epsilon_BubSlug) and (epsilon < epsilon_SlugChurn) Then
                                                    A$ = 'Slug'
                                                    Else
      If (epsilon > epsilon_SlugChurn) and (epsilon > epsilon_BubSlug) and (epsilon_ChurnAnn <0.2)
Then
                                                    A$ = 'Churn'
                                                    Else
      If (epsilon < epsilon_ChurnAnn) and (epsilon > epsilon_AnnWispy) Then
                                                    A$ = 'Wispy Annular'
                                                    Else
      A$ = 'Annular'

                                                                Endif
                                                    Endif
      Endif
Endif

FLOWREGIME$ = A$
End
"-------------------------------------------------------------------------------------------------------------------------------"
"-------------------------------------------------------------------------------------------------------------------------------"
"!MAIN PROGRAM"

"General parameters - Inputs"

g = 9.81                                  [m/s^2]          "Gravitational
constant"
p_atm = 85                                [kPa]            "Atmospheric
pressure"
material$ = '318 Stainless Steel'                          "Pipe material"
d_i = 0.01                                [m]              "Pipe inside
diameter"
A_cross = pi / 4 * d_i^2                                   "Pipe cross
sectional flow area"
M_molar_ammonia = 17.03026                [kg/kmol]        "Molar mass NH3"
```

```
M_molar_water = 18.015268                    [kg/kmol]          "Molar mass H2O"
M_dot_flux = 50                              [kg/(m^2·s)]
m_dot_mix = M_dot_flux * A_cross
Q_flux = 10       [kW/m^2]                   "Heat-flux over total length of internal
                                             Pipe."
slug = 17                                    "First solve the program, and check in arrays if
slug flow is obtained, if indeed, use the array number of the last slugflow entry for the variable slug
here"

"System pressure is used for determination of thermo-physical properties of a 40% mixture in"
"the corresponding lookup table. There is currently tables for 5bar, 8bar, 10bar, 15bar and 18bar"
concentration$ = '40% Mixture 8bar'

"-------------------------------------------------------------------------------------------------------------------------
------------"
"Divide pipe into 58 increments for quality from 0 to 1"
n = 58                                                                   "Counter end"
p_sys = Lookup('concentration$',1,1)                                     "Pre-defined
system pressure"

"Lookup of fluid properties for node in and outlets"
Duplicate i = 1,n
    T_mix[i] = Lookup('concentration$',i,2)          "Temperature"
    x[i] = Lookup('concentration$',i,15)             "Quality of mixture"
    m_dot_mix[i] = m_dot_mix                         "Conservation of mass"
    Velocity[i] = m_dot_mix[i] / (rho[i]*A_cross)    "Calculation of mixture velocity"
    rho[i] = Lookup('concentration$',i,3)
    rho_liq[i] = Lookup('concentration$',i,4)
    rho_vap[i] = Lookup('concentration$',i,5)
    v_liq[i] = Lookup('concentration$',i,7)
    v_vap[i] = Lookup('concentration$',i,8)
    h_0[i] =  Lookup('concentration$',i,9)
    h_liq[i] = Lookup('concentration$',i,10)
    h_vap[i] = Lookup('concentration$',i,11)
    sigma[i] = Lookup('concentration$',i,25) * Convert(mN/m,N/m)
    m_liq_ammonia[i] = Lookup('concentration$',i,21)
    m_liq_water[i] = Lookup('concentration$',i,22)
    m_vap_ammonia[i] = Lookup('concentration$',i,23)
    m_vap_water[i] = Lookup('concentration$',i,24)
    c_p_liq[i] = lookup('concentration$',i,27)
End

"Solution Properties in the vapour and liquid phases"
T_crit_ammonia = T_crit(Ammonia)
T_crit_water = T_crit(Water)
T_crit_mix = 570.27                          [K]                "From REFPROP
for mixture"

"-------------------------------------------------------------------------------------------------------------------------
------------"
"!Flow equations"

p[1] = p_sys * Convert(MPa,kPa)
z[1] = 0                                     [m]                "Bottom of pipe"

Duplicate i = 2,n
    Length[i] = z[i] - z[i-1]
    "Conservation of momentum"
    rho_avg[i] = Average(rho[i-1],rho[i])
```

```
    p[i] = p[i-1] + 0.5 * Velocity[i-1] * Velocity[i] * (rho[i] - rho[i-1]) * Convert(m^2*kg/s^2*m^3,kPa) -
rho_avg[i] * g * (z[i] - z[i-1]) * Convert(kg*m*m/m^3*s^2,kPa) + (DELTAP_friction[i]*(z[i] - z[i-1])) *
Convert(kg/m*s^2,kPa)
    "Conservation of energy"
    Q_dot[i] = m_dot_mix[i] * h_0[i] - m_dot_mix[i-1] * h_0[i-1] + m_dot_mix[i] * g * z[i] *
Convert(kg*m^2/s^3,kW) - m_dot_mix[i-1] * g * z[i-1] * Convert(kg*m^2/s^3,kW)
    Q_dot[i] = Q_flux * (d_i * pi * Length[i])
    d_max_slug[i] = 19 * ((sigma[i] * v_liq[i]) / (g * (1 - v_liq[i] / v_vap[i])))^(0.5)
End

Q_dot = Sum(Q_dot[i],i=2,n)
Length = Sum(Length[i],i=2,n)

epsilon[1] = 0
epsilon[n] = 1

"Void fraction calculation - Rouhani Axelsson version of drift-flux model"
Duplicate i = 2,(n-1)
    epsilon[i] = x[i] / rho_vap[i] * (C_0[i] * (x[i] / rho_vap[i] + (1-x[i]) / rho_liq[i]) + U_GM[i] /
M_dot_flux)^(-1)
    U_GM[i] = (1.18 / sqrt(rho_liq[i])) * (g * sigma[i] * (rho_liq[i] - rho_vap[i]))^(0.25)
    C_0[i] = 1 + 0.2 * (1 - x[i])                    "C_0 defined for Rouhani I, not Rouhani II"
End

"Toshiba void fraction model"
C_0 = 1.08                                    "Values as chosen by Toshiba for their model"
v_gj = 0.45
Duplicate i = 2,n-1
    epsilon[i] = j_vap[i] / (C_0 * j_tot[i] + v_gj)    "Generic version of the drift flux model as developed
                                                        by Zuber and Findlay"
End

m_dot_liq[1] = m_dot_mix
m_dot_vap[n] = m_dot_mix

Velocity_liq[1] = m_dot_mix / (rho_liq[1] * A_cross)
Velocity_liq[n] = 0
Velocity_vap[1] = 0
Velocity_vap[n] = m_dot_mix / (rho_vap[n] * A_cross)

Duplicate i = 2,(n-1)
    "Mass flow for liquid and vapour phases of mixture"
    Velocity_liq[i] = (1-x[i]) * m_dot_mix[i] / (rho_liq[i] * (1 - epsilon[i]) * A_cross)
    Velocity_vap[i] = x[i] * m_dot_mix[i] / (rho_vap[i] * epsilon[i] * A_cross)
    m_dot_liq[i] = (1 - x[i]) * m_dot_mix
    m_dot_vap[i] = x[i] * m_dot_mix
    m_dot_vap_ammonia[i] = m_dot_vap[i] * m_vap_ammonia[i]
    Slip[i] = Velocity_vap[i] / Velocity_liq[i]
End


C_m = Constant(d_i, Length)

Duplicate i = 1,n
    "Superficial velocities for liquid and vapour phases of mixture"
    j_tot[i] = j_liq[i] + j_vap[i]
    j_liq[i] = Velocity_liq[i] * (1 - epsilon[i])
    j_vap[i] = Velocity_vap[i] * epsilon[i]
```

```
    "Jayanti and Hewitt prediction of flooding velocity for bubble to churn transition"
    sqrt(j_star_vap[i]) + C_m * sqrt( j_star_liq[i]) = C_SlugChurn[i]
    j_star_liq[i] = j_liq[i] * sqrt(rho_liq[i]) / sqrt(g * d_i * (rho_liq[i] - rho_vap[i]))
    j_star_vap[i] = j_vap[i] * sqrt(rho_vap[i]) / sqrt(g * d_i * (rho_liq[i] - rho_vap[i]))

End

h_htc_tp[1] = 0.023 * k_liq_mix[1]  / d_i * Re_liq[1]^0.8 * Pr_liq[1]^0.4

Duplicate i = 2, n-1
    "General Equations for Heat transfer coefficient"
    Q_dot[i] = h_htc_tp[i] * (T_wall_inner[i] - T_mix[i]) * (d_i * pi * Length[i])
    h_htc_liq[i] = 0.023 * (k_liq_mix[i])  / d_i * Re_liq[i]^0.8 * Pr_liq[i]^0.4        "Dittus-Boelter
    correlation for liquid-phase only heat transfer coefficient"
    X_tt[i] = ((1 - x[i]) / x[i])^0.9 * (rho_vap[i] / rho_liq[i])^0.5 * (mu_liq_mix[i] / mu_vap_mix[i])^0.1
    Bo[i] = Q_flux / (M_dot_flux * (h_vap[i] - h_liq[i]))

    "Wall superheat required to initiate nucleation"
    DELTAT_sat_w_crit[i] = (8 * sigma[i] * T_mix[i] * Q_flux) / (rho_vap[i] * ((h_vap[i] - h_liq[i]) *
Convert(kJ/kg, J/kg)) * k_liq_mix[i])
    DELTAT_sat_w_achieved[i] = T_wall_inner[i] - T_mix[i]
End

"Rivera and Best 1999 correlation for Heat transfer coefficient"
h_constant = 65        "h_constant is actually (Constant * h_L_dittusboelter) as found in Rivera et al
                       for aqua-ammonia"

Duplicate i = 2, n-1
    h_htc_tp[i] = h_constant * h_htc_liq[i] * (1 / X_tt[i])^0.5 * (Bo[i])^0.15
END

Duplicate i = 2, n-1
    "Gungor-Winterton for Heat transfer coefficient"
    h_htc_tp[i] = E_new[i] * h_htc_liq[i]
    E_new[i] = 1 + 3000 * Bo[i]^0.86 + 1.12 * (x[i] / (1 - x[i]))^0.75 * (rho_liq[i] / rho_vap[i])^0.41
END

Duplicate i = 2, n-1
    "Shah Correlation for Heat transfer coefficient"
    N[i] = C_SHAH[i]
    C_SHAH[i] = ((1 - x[i]) / x[i])^0.8 * (rho_vap[i] / rho_liq[i])^0.5
    Fr_liq[i] = M_dot_flux^2 / (rho_liq[i]^2 * g * d_i)        "Liquid Froude number"
    h_htc_CB[i] = h_htc_liq[i] * 1.8 / N[i]^0.8
    h_htc_tp[i] = SHAH(N[i], Bo[i], h_htc_liq[i], h_htc_CB[i])
End


LOWER = (8 * (1 + M_molar_ammonia / M_molar_water))

Duplicate i = 1, n
    "Viscosity of liquid and vapour solutions"
    ln(mu_liq_mix[i]) = c_liq_amm[i] * ln(mu_amm_T_star_liq[i]) + (1 - c_liq_amm[i]) *
ln(mu_water_T_star_liq[i]) + DELTAmu_T_mix_liq[i]
    mu_vap_mix[i] = c_vap_amm[i] * mu_amm_T_star_vap[i] / (c_vap_amm[i] + (1 - c_vap_amm[i]) *
PHI_12[i]) + ((1 - c_vap_amm[i]) * mu_water_T_star_vap[i]) / ((1 - c_vap_amm[i]) + c_vap_amm[i] *
PHI_21[i])

    mu_amm_T_star_liq[i] = Viscosity(Ammonia,T = T_star_ammonia[i], x=0)      "EES gebruik ook
fenghour se vgl's soos voorgeskryf deur M.Conde"
```

```
    mu_water_T_star_liq[i] = Viscosity(Water,T = T_star_water[i], x=0)
    mu_amm_T_star_vap[i] = Viscosity(Ammonia,T = T_star_ammonia[i], x=1)
    mu_water_T_star_vap[i] = Viscosity(Water,T = T_star_water[i], x=1)
    DELTAmu_T_mix_liq[i]  = (0.534 - 0.815 * (T_mix[i] / T_crit_water)) * F_mu_x[i]
    F_mu_x[i] = 6.38 * (1 - c_liq_amm[i])^(1.125 * c_liq_amm[i]) * (1 - exp(-0.585 * c_liq_amm[i] * (1 -
c_liq_amm[i])^0.18)) * ln(mu_amm_T_star_liq[i]^(0.5) * mu_water_T_star_liq[i]^(0.5))
    PHI_12[i] = UPPER[i]^2 / LOWER^(0.5)
    UPPER[i] = (1 + (mu_amm_T_star_vap[i] / mu_water_T_star_vap[i])^(0.5) * (M_molar_water /
M_molar_ammonia)^(0.25))
    PHI_21[i] = PHI_12[i] * (mu_water_T_star_vap[i] / mu_amm_T_star_vap[i]) * (M_molar_ammonia
/ M_molar_water)

    m_molar_liq_amm[i] = m_liq_ammonia[i] * M_molar_ammonia        "Molar mass of ammonia in
                                                                   liquid phase"
    m_molar_liq_water[i] = m_liq_water[i] * M_molar_water      "Molar mass of water in liquid
                                                               phase"
    m_molar_liq_mix[i] = m_molar_liq_amm[i] + m_molar_liq_water[i]   "Total Molar mass of liquid
                                                                     phase"
    c_liq_amm[i] = m_molar_liq_amm[i] / m_molar_liq_mix[i]     "Liquid ammonia molar
                                                               concentration"

    m_molar_vap_amm[i] = m_vap_ammonia[i] * M_molar_ammonia        "Molar mass of ammonia in
                                                                   liquid phase"
    m_molar_vap_water[i] = m_vap_water[i] * M_molar_water    "Molar mass of water inliquid phase"
    m_molar_vap_mix[i] = m_molar_vap_amm[i] + m_molar_vap_water[i]       "Total Molar mass
                                                                         of liquid phase"
    c_vap_amm[i] = m_molar_liq_amm[i]/ m_molar_vap_mix[i]          "Liquid ammonia molar
                                                                   concentration"

    THETA[i] = T_mix[i] / T_crit_mix
    tau[i] = 1 - THETA[i]
    T_star_ammonia[i] = THETA[i] * T_crit_ammonia
    T_star_water[i] = THETA[i] * T_crit_water

    "Liquid conductivity of ammonia-water solution"
    k_liq_amm_Tstar[i] = (8.902275*10^2 * T_star_ammonia[i]^0 +(-
0.69235)*T_star_ammonia[i]^1+(-2.4010*10^(-3))*T_star_ammonia[i]^2+0
*T_star_ammonia[i]^3)*Convert(milliW/m-K,kW/m-K)"MConde book is in" "milliW/m-K"
    k_liq_water_Tstar[i] = Conductivity(water,T=T_star_water[i], x = 0) * Convert(W/m-K,kW/m-K)
    k_liq_mix[i] =  c_liq_amm[i] * k_liq_amm_Tstar[i] + (1 - c_liq_amm[i]) * k_liq_water_Tstar[i]

    "Reynolds numbers"
    Re_liq[i] = ((1-x[i]) * M_dot_flux * d_i) / mu_liq_mix[i]
    Re_vap[i] = (x[i] * M_dot_flux * d_i) / mu_vap_mix[i]

    "Prandtl liquid number"
    Pr_liq[i] = (c_p_liq[i]*Convert(kJ/kg-K,J/kg-K)) * mu_liq_mix[i] / (k_liq_mix[i]*Convert(kW/m-
K,W/m-K))
End

"Muller Steinhagen - Correlation calculates the frictional pressure drop gradien (Pa/m) "
Duplicate i = 1,n
    DELTAP_friction[i] = (G[i] * (1 - x[i])^(1/3) + B[i] * x[i]^3)
    A[i] = f_liq[i] * (2 * (M_dot_flux)^2) / (d_i * rho_liq[i])
    B[i] = f_vap[i] * (2 * (M_dot_flux)^2) / (d_i * rho_vap[i])
    f_liq[i] = f_liquid(Re_liq[i])
    f_vap[i] = f_vapour(Re_vap[i])
    G[i] = A[i] + 2 * (B[i] - A[i]) * x[i]
End
```

"Flow transitions according to samaras"

"The flow transition equations for the parametric table"
count = 50
epsilon_BubSlug[count] = j_vap_tester / (1.2 * (j_vap_tester + 2.17 + 35.45 * exp(- j_vap_tester / 0.4)) + 0.345 * sqrt(g * d_i * (rho_liq[count] - rho_vap[count]) / rho_liq[count]))
epsilon_SlugChurn[count] = j_vap_tester / (1.2 * (j_vap_tester + 0.047 * exp(j_vap_tester / 1.75295)) + 0.345 * sqrt(g * d_i * (rho_liq[count] - rho_vap[count]) / rho_liq[count]))
epsilon_ChurnAnn[count] = j_vap_tester / (1.2 * (j_vap_tester + 0.1385 + 2.085 * 10^(47) * exp(- j_vap_tester / 0.07853)) + 0.345 * sqrt(g * d_i * (rho_liq[count] - rho_vap[count]) / rho_liq[count]))
epsilon_AnnWispy = 1 - ((-Term_B + (Term_B^2 - 4*Term_A * Term_C)^(1/2))) / (2 * Term_A)
Term_A = 6.295 * (g * d_i * (rho_liq[count] - rho_vap[count]))^(1/2)
Term_B = 2.85 * (j_vap_tester*rho_vap[count]^(1/2) + j_liq_tester*rho_liq[count]^(1/2) - 0.775 * (g*d_i*(rho_liq[count] - rho_vap[count]))^(1/2))
Term_C = - j_liq_tester * rho_liq[count]^(1/2)
j_liq_tester = 1.12 "According to samaras flow map, fig 1, and page 762, eq.14"

"The flow transition equations for determining transitions in the main program"
Duplicate i =1, n
epsilon_BubSlug[i] = j_vap[i] / (1.2 * (j_vap[i] + 2.17 + 35.45 * exp(- j_vap[i] / 0.4)) + 0.345 * sqrt(g * d_i * (rho_liq[i] - rho_vap[i]) / rho_liq[i]))
epsilon_SlugChurn[i] = j_vap[i] / (1.2 * (j_vap[i] + 0.047 * exp(j_vap[i] / 1.75295)) + 0.345 * sqrt(g * d_i * (rho_liq[i] - rho_vap[i]) / rho_liq[i]))
epsilon_ChurnAnn[i] = j_vap[i] / (1.2 * (j_vap[i] + 0.1385 + 2.085 * 10^(47) * exp(- j_vap[i] / 0.07853)) + 0.345 * sqrt(g * d_i * (rho_liq[i] - rho_vap[i]) / rho_liq[i]))
epsilon_AnnWispy[i] = 1 - ((-Term_B[i] + (Term_B[i]^2 - 4*Term_A[i] * Term_C[i])^(1/2))) / (2 * Term_A[i])
Term_A[i] = 6.295 * (g * d_i * (rho_liq[i] - rho_vap[i]))^(1/2)
Term_B[i] = 2.85 * (j_vap[i]*rho_vap[i]^(1/2) + j_liq[i]*rho_liq[i]^(1/2) - 0.775 * (g*d_i*(rho_liq[i] - rho_vap[i]))^(1/2))
Term_C[i] = - 1.12 * rho_liq[i]^(1/2) "j_liq[i] is put equal to 1.12m/s according to Samaras, page 762 eq.14"
End

Duplicate i = 2, n-1
"Determination of flow regime"
FlowRegime$[i] = FLOWREGIME$(epsilon[i], epsilon_BubSlug[i], epsilon_SlugChurn[i], epsilon_ChurnAnn[i], epsilon_AnnWispy[i])
End

"Susan White Stewart-model to determine maximum height for lift tube"
RATIO_submergence = Term1 + Term2 + Term3 + Term4
Term1 = (f_tp * (rho_liq[slug]*j_liq[slug] + rho_vap[slug]*j_vap[slug])^2) / (2*g*d_i*rho_liq[slug]*rho_tp)
Term2 = (j_liq[slug]^2 * (d_i/d_entrance)^4) / (2 * g * L_bubblepump)
Term3 = (j_liq[slug]*rho_homogeneous*(d_i/d_entrance)^2 * ((j_liq[slug]+j_vap[slug])-j_liq[slug]*(d_i/d_entrance)^2)) / (rho_liq[slug] * g * L_bubblepump)
Term4 = 1 - epsilon[slug]
d_entrance = d_i
A_entrance = pi / 4 * d_entrance^2
f_tp = 4*f_star_tp
1/f_star_tp = 3.48 - 4*log10(2*epsilon_roughness/d_i + 9.35/(Re_tp * sqrt(f_star_tp)))
epsilon_roughness = 0.05*10^(-3)
Re_tp = (rho_vap[slug] * j_vap[slug] + rho_liq[slug] * j_liq[slug]) / mu_tp_mix
mu_tp_mix = epsilon_homogeneous*mu_vap_mix[slug] + mu_liq_mix[slug]*(1-epsilon_homogeneous)*(1+2.5*epsilon_homogeneous)
epsilon_homogeneous = x[slug] / (x[slug] + (rho_liq[slug] / rho_vap[slug]) * (1-x[slug]))
rho_homogeneous = rho_liq[slug] * d_entrance^2*V_1 / (d_i^2*Velocity[slug])
rho_tp = rho_vap[slug] * epsilon[slug] + rho_liq[slug]*(1 - epsilon[slug])

```
V_1 = j_liq[1] * A_cross / A_entrance
RATIO_submergence = z[slug] / L_bubblepump
L_generator = z[slug]
eta_bubblepump = m_dot_liq[slug] / Q_dot_bubblepump
Q_dot_bubblepump = sum(Q_dot[2..slug])
p_drop = p_sys * convert(MPa, kPa) - p[slug]
m_dot_vap_ammonia = m_vap_ammonia[slug] * m_dot_vap[slug]
m_dot_vap = m_dot_vap[slug]
quality = x[slug]
"-------------------------------------------------------------------------------------------------------------------------------------------"
```